Interconversion and Interception of Reactive Intermediates using H_2

by

Lillian V. A. Hale

A dissertation submitted in partial fulfillment
of the requirements for the degree of
Doctor of Philosophy
(Chemistry)
in the University of Michigan
2018

Doctoral Committee:

Associate Professor Nathaniel K. Szymczak, Chair
Professor John Montgomery
Professor Melanie Sanford
Professor Levi Thompson

Lillian V. A. Hale

lilhale@umich.edu

ORCID iD: 0000-0001-9951-4180

Dedication

To my family and friends, especially Mitch, Stout, Danger and Buttercup

Acknowledgements

This work would not be possible without support and guidance from my research advisor, Nate Szymczak. Nate encouraged me to be an independent scientist from the very beginning, and as a result I am extremely proud of the work in this dissertation. I was able to pursue many of my own ideas throughout the past five years, and Nate helped me focus them into valuable scientific contributions. He was always supportive during the times I struggled with tunnel vision or scattered thoughts about a project, and I would not be successful without those helpful discussions. I'm also grateful for the many learning opportunities he provided me with. I could go on, but I don't want to be too verbose, or vague. In short, thank you for helping me become the chemist I am today.

I am also very thankful to my undergraduate research advisor, Tim Clark, who introduced me to chemistry research and catalysis. Tim encouraged me to pursue graduate studies and gave me many opportunities to grow at WWU and USD, and he continues to be a great mentor to me.

I would also like to thank my committee members: Prof. Melanie Sanford, Prof. John Montgomery, and Prof. Levi Thompson for their helpful advice throughout graduate school. I am also thankful to Ruben Martin for hosting me at ICIQ, and John Montgomery for providing the opportunity. Working on a new project in a different lab was a big turning point for me during graduate school. It gave me a new perspective on catalysis research, a new set of problem solving skills, and confidence as an independent scientist.

The Szymczak lab has been a wonderful crew to work with. I am thankful to Tim Tseng, who took me under his wing so I could carry on the Ru-bMepi torch. I had many good times relieving the stress of graduate school with Eric Dahl, my chemistry brother. Jacob Geri always pushed me to think about the practical aspects of my chemistry. I was lucky to have the incredibly smart Grayson Ritch to sit next to for 5 years. Jim Shanahan is a genuinely kind and calming person to chat with, and we had many good conversations while we were working in gbox 3 and 4. Thanks for the beer, Jim. I'm glad to have worked with John Kiernicki, and I've learned a ton from having him around lab. John also helped me eat my leftovers, even if it was questionable

looking yogurt. I am very proud to have worked with Jessi Wilson and Marianne Sykes, and I am very excited to see where they both end up in the future. I especially want to thank Marianne for taking over my Ru-ketenimine chemistry, all the other bits and pieces I left behind, and Janet (my glovebox). My undergraduates Michael Keating and Anna-Li contributed to this work by synthesizing many of the ligands and complexes, as well as testing out wacky ideas of mine. Mike, thank you for being my first mentee. Anna-Li, thank you for being my extra pair of hands during the last few months. Outside of the Szymczak crew, the "hardcore wheelers", Eric, Alonso, and Jordan, were wonderful friends to spend time with in Spain. Also, from my time in Spain, I am grateful to have met and worked with Rosie Somerville. After battling 10 weeks of Ni-chemistry, Rosie has become a great friend and collaborator.

Most of all, I am thankful to my family. Mom, Dad, Zack, and Mitch have given never-ending patience and support throughout the past 5+ years. My greatest thanks go to Mitch. I am so lucky to have you and the doggies in my life.

Table of Contents

List of Figures

List of Tables

Abstract

This dissertation describes the advances in hydrogen transfer catalysis with nitrogen-based substrates using ruthenium pincer catalysts. Compared to C–O bonds, amines, imines, and nitriles are difficult substrates for (de)hydrogenation reactions. The high Lewis basicity of nitrogen often encourages the deactivation or inhibition of a transition-metal catalyst and can promote undesirable side reactions between the organic intermediates. Because of these challenges, the mechanistic details and catalyst requirements for hydrogen transfer across C–N bonds are not well-understood.

The ruthenium-pincer catalyst, $HRu(bMepi)(PPh_3)_2$ (**1**, bMepi = 1,3-bis(6'-methyl-2'-pyridylimino)isoindoline) provides critical details needed for developing new synthetic strategies based on nitrogen-containing substrates by capturing snapshots of amine, imine, and nitrile intermediates during hydrogen transfer. Primary amines undergo dehydrogenation catalyzed by **1** to selectively form nitriles with the release of 2 equivalents of H_2. Computational, kinetic, and spectroscopic experiments elucidate an inner-sphere dehydrogenation mechanism with a high kinetic barrier to form a Ru–(η^2-H_2) intermediate *via* H^+ transfer between a Ru–NH_2 to Ru–H unit ($\Delta G^{\ddagger}$ = 35(2) kcal/mol for octylamine). The unusual selectivity for nitrile products, rather than secondary amines or imines, depends on a fast second dehydrogenation event and a high binding affinity of imino groups to Ru. Additionally, bulky *ortho*-pyridyl substituents on the pincer ligand are required to stabilize high energy 5-coordinate Ru-amido intermediates. This mechanism is

compared to analogous hydrogen transfer reactions of alcohols, revealing the fundamental differences between substrate classes despite similar elementary steps.

The new chemical knowledge gained from our mechanistic analysis was further applied to develop new hydrogen transfer methodologies for amines and nitriles. The reversibility of hydrogen transfer and high binding affinity of nitrogen was exploited in a new protocol for the stereoretentive H/D exchange of primary amines using D_2O. While **1** promotes the H/D exchange of (*S*)-1-phenylethylamine with 90% ee, the cationic derivative, [Ru(bMepi^{Me})(PPh_3)OTf]OTf, facilitates H/D exchange with complete stereoretention. The binding affinity of a prochiral imino intermediate increases with the increased positive charge on Ru. In addition to the high binding affinity of a Ru-imino intermediate, stereospecific coordination of the chiral amine to Ru and a fast H/D exchange from Ru–H are hypothesized to promote stereoretentive H/D exchange. These studies led to the successful labeling of primary amines with high deuterium content (70-99% D) and complete stereoretention (99% ee) at the α-CH position.

Finally, α,β-unsaturated nitriles are intercepted through hydride insertion to produce novel Ru-ketenimine intermediates. X-ray crystallography of a Ru-ketenimine derived from α-phenylcinnamonitrile reveals a highly unusual bent geometry with Ru–N–C of 141°. Spectroscopic and computational analysis suggest that subsequent reactivity is dictated by the electronic environment of the α,β-unsaturated nitrile, which influence the nucleophilic and electrophilic character of the –C2=C1=N heterocumulene group. To regenerate the Ru–H intermediate and enable catalytic reactivity, electrophilic and nucleophilic additions were performed under an H_2 atmosphere. Under these conditions, the hydrogenation, hydroboration, hydroacylation, and hydrosilylation of α,β-unsaturated nitriles *via* ketenimine intermediates are explored.

Chapter 1: The Role of Hydrogen Transfer in Catalysis

1.1 Introduction and Scope of Thesis

The interconversion between single and multiple covalent bonds through the addition or removal of hydrogen is an elegant strategy to develop atom-economical reactions. Hydrogen is both a fundamental building block and a valuable byproduct widely used in industrial, environmental, and academic applications.[1,2] As a reagent, H_2 (or an H_2 surrogate) is necessary for the manufacture of ammonia, methanol, polymers, and pharmaceuticals, and is common in academic laboratories for fundamental research.

Although highly versatile, H_2 is a stable molecule that requires activation in order to access its utility. Chemists recognized early on that transition metal elements are uniquely suited to cleave the strong covalent bond of H_2. As a result, hydrogen transfer (HT) chemistry has played a pivotal role in our understanding of catalytic processes.[3-5] Homogeneous catalysts are well-defined soluble metal-complexes that allow chemists to obtain detailed mechanistic information during a catalytic reaction. Many early developments in catalysis were based on homogeneous HT studies describing metal-mediated H_2 activation to form dihydride, monodydride, and dihydrogen complexes ($M-(H)_2$, M–H, and $M-(\eta^2\text{-}H_2)$, Figure 1-1).[5-8] These complexes are classically composed of late transition metals with partially filled *d*-orbitals and offer incredible versatility due to countless permutations of ligands (L), metals (M), oxidation states (n), and coordination number. To date, these species are often identified as crucial intermediates for new synthetic methodologies

involving catalytic hydrogen transfer. More broadly, the synthesis and characterization of complexes such as those illustrated in Figure 1-1 advanced the field of organometallic chemistry by introducing rational catalyst design as a general approach for developing new transformations.

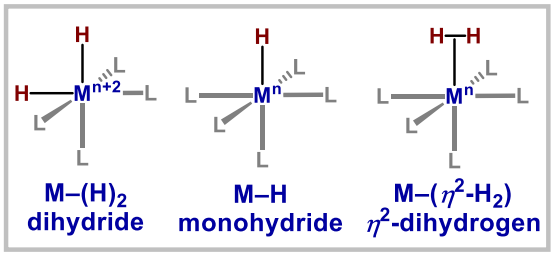

Figure 1-1. Transition-metal dihydride, monohydride, and dihydrogen complexes

Transition-metals prime H_2 toward homolytic or heterolytic cleavage through two key orbital interactions. The first occurs when the σ-bond of H_2 donates electron density into an empty metal-based *d* orbital (i.e. the d_z^2 or $d_{x^2-y^2}$ orbital, Figure 1-2, right). The second interaction, π-backbonding, involves an occupied non-bonding orbital residing on the metal (i.e. the d_{xy}, d_{zy}, or d_{zx} orbital) that contributes electron density into the anti-bonding (σ^*) orbital of H_2 (Figure 1-2, left). These two orbital interactions are synergistic and promote facile heterolytic or homolytic cleavage by decreasing the pK_a and bond dissociation energy (BDE) of H_2.[8]

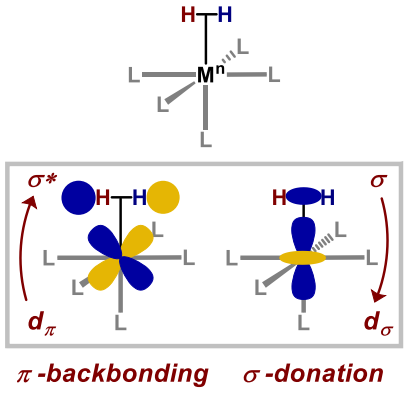

Figure 1-2. The bonding interactions for an octahedral M−(η^2-H_2) complex

The first practical homogeneous hydrogenation catalyst, $RhCl(PPh_3)_3$, was discovered in the 1960's and found to operate at 25 °C under atmospheric pressure of H_2. The complex known as Wilkinson's catalyst is a classic example of H_2 cleavage *via* oxidative addition. Following coordination to the Rh(I) complex, π-back donation from the metal sufficiently activates H_2 and results in the concerted *cis*-addition to form a Rh(III)−$(H)_2$ species (Figure 1-3, top right). The tendency for a complex to promote oxidative addition of H_2 depends on the accessibility of M^n and M^{n+2} oxidation states, the strength of the resulting metal-hydride bonds, and the π-basicity of the ligand *trans* to H_2.[10] The second mode of H_2 activation is the deprotonation of an acidic M−(η^2-H_2) complex. Intermolecular deprotonation of M−(η^2-H_2) may occur with an exogenous base to form a M–H species and the conjugate acid of the added base (Figure 1-3, bottom right). Alternatively, intramolecular deprotonation can occur by a basic ligand site adjacent to the coordinated H_2 ligand (Figure 1-3, left). This latter motif forms the basis for cooperative hydrogen transfer catalysts (discussed in detail in Chapter 2). Noyori-type complexes are highly successful examples of hydrogenation catalysts that operate *via* intramolecular M−(η^2-H_2) heterolysis.[11-12]

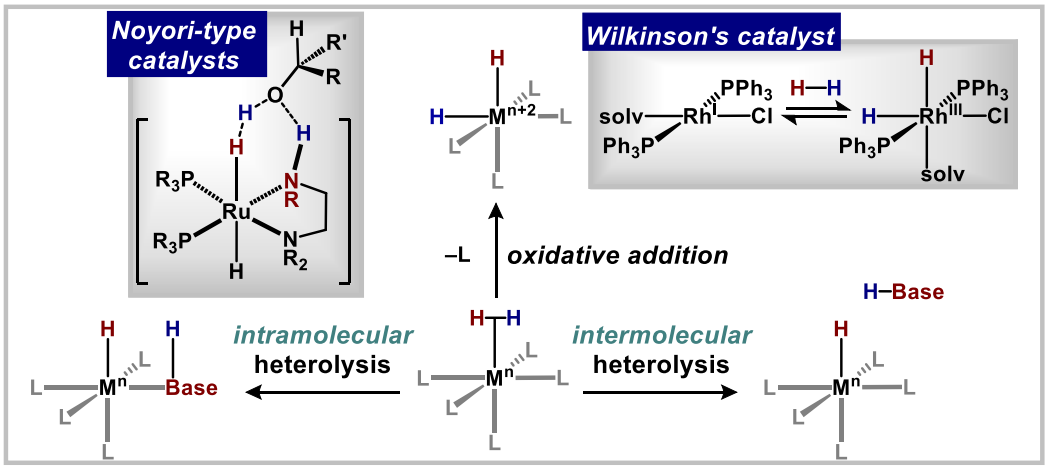

Figure 1-3. Modes of H_2 cleavage *via* a M−(η^2-H_2) complex

Despite significant contributions to our fundamental understanding of catalysis, industrial applications of homogeneous HT catalysis remain limited. The hydrogenation of olefins and carbonyl compounds, including the asymmetric variants pioneered by Nobel laureates, Knowles and Noyori, are the most common HT reactions used in commercial processes.[1-2] Selective catalysts that meet standards for industrial applications are lacking for more challenging substrates, such as nitriles, amides, and heterocycles. Although the long history of homogenous HT catalysis has resulted in a vast library of discrete catalysts with distinct reactivities, these have yet to be broadly applied beyond fundamental studies that only showcase reactivity using simple substrates. At present, our ability to catalyze site-selective transformations starting from highly functionalized compounds is rudimentary. Accurate methods that predict the structure and function relationships of a catalyst *a priori* are necessary to accelerate the growth of the field; however, catalyst development is still largely based on empirical trial and error. A broad goal of the work presented here is to refine our understanding of structure-function relationships – and how this relationship changes between classes of substrates. Chapter 2 provides an overview of the recent advances in HT from a catalyst design standpoint.

The research presented in Chapters 3-5 focus on nitrogen containing substrates that undergo HT reactions catalyzed by ruthenium-bpi pincer complexes (bpi = 1,3-bis(2′-pyridylimino)isoindolate). Compared to HT reactions of alcohols and carbonyl groups, analogous transformations for nitrogenous functional groups are underdeveloped.[5,13] Amines, imines, and nitriles are challenging substrates partly because they can behave as excellent ligands for transition-metals, thus substrate coordination may easily lead to catalyst poisoning. Additionally, ionic (de)hydrogenation reactions, which involve H_2 transfer via H^+ and H^-, typically require harsh

conditions to initiate reactions at the basic nitrogen group. The work presented in Chapters 3-5 elucidate key features of Ru-bpi-type catalysts that enable efficient HT transformations with amines and nitriles. Additionally, because Ru-bpi complexes promote analogous HT transformations with alcohols, ketones, and aldehydes, comparisons between nitrogen and oxygen containing substrates are highlighted throughout.

Chapter 3 reveals the mechanism of primary amine dehydrogenation catalyzed by the ruthenium hydride complex, HRubMepi(PPh_3)$_2$ (bMepi = 1,3-bis(6'-methyl-2'-pyridylimino)isoindolate). The selective formation of nitrile products, rather than secondary imines or amines, is related back to catalyst structure. Kinetic studies, isolation of intermediates, and computational analysis builds the foundation needed for the methodologies described in Chapters 4 and 5. In Chapter 4, a protocol for stereoretentive H/D exchange of α-chiral primary amines using D_2O is presented. Chapter 5 introduces a new method for the interception of ketenimines using hydride transfer to *α,β*-unsaturated nitriles. Finally, Chapter 6 is a guide for future catalyst development based on Ru-bpi complexes.

1.2 Notes and References

(1) Mortreux, A.; Petit, F.; In *Industrial Applications of Homogeneous Catalysis*; Dordrecht: Springer Netherlands, 1988.

(2) Johnson, N. B.; Lennon, I. C.; Moran, P. H.; Ramsden, J. A. *Acc. Chem. Res.* **2007**, *40*, 1291-1299.

(3) McQuillin, F. J.; In *Homogeneous Hydrogenation in Organic Chemistry*; Dordrecht: Springer Netherlands, 1976.

(4) Chaloner, P. A.; Esteruelas, M. A.; Joó, F.; Oro, L. A.; In *Homogeneous Hydrogenation*; Springer Netherlands, 1994.

(5) de Vries, J. G.; Elsevier, C. J. In *The Handbook of Homogeneous Hydrogenation*; Wiley-VCH: John Wiley & Sons, Incorporated, **2008**.

(6) Esteruelas, M. A.; Oro, L. A. Dihydrogen Complexes as Homogeneous Reduction Catalysts *Chem. Rev.* **1998**, *98*, 577-588.

(7) Kubas, G. J., Metal Dihydrogen and Sigma-Bond Complexes. Kluwer Academic/Plenum, New York, 2001.

(8) Jessop, P. G.; Morris, R. H. Reactions of Transition Metal Dihydrogen Complexes Coord. *Chem. Rev.* **1992**, *121*, 155-284.

(9) Dobereiner, G. E.; Crabtree, R. H. *Chem. Rev.* **2010**, *110*, 681-703.

(10) Crabtree, R. H. Oxidative Addition and Reductive Elimination. In *The Organometallic Chemistry of the Transition Metals*; John Wiley & Sons, Inc.: 2014, p 163-184.

(11) Noyori, R.; Yamakawa, M.; Hashiguchi, S. Metal-Ligand Bifunctional Catalysis: A Nonclassical Mechanism for Asymmetric Hydrogen Transfer between Alcohols and Carbonyl Compounds. *J. Org. Chem.* **2001**, 66, 7931−7944.

(12) Yamakawa, M.; Ito, H.; Noyori, R. The Metal−Ligand Bifunctional Catalysis: A Theoretical Study on the Ruthenium(II)- Catalyzed Hydrogen Transfer between Alcohols and Carbonyl Compounds. *J. Am. Chem. Soc.* **2000**, 122, 1466−1478.

(13) Wang, D.; Astruc, D. The Golden Age of Transfer Hydrogenation. *Chem. Rev.* **2015**, *115*, 6621-6686.

Chapter 2: Hydrogen Transfer Catalysis beyond the Primary Coordination Sphere

Portions of this chapter have been published:

Hale, L. V. A.; Szymczak, N. K.; Hydrogen Transfer Catalysis beyond the Primary Coordination Sphere. *ACS Catal.* **2018**, *8*, 6446-6461.

2.1 Introduction

This Chapter outlines recent examples of homogeneous transition-metal hydrogen transfer catalysts for which functionality within the complex's outer coordination sphere influences the outcome of a reaction. Secondary-sphere groups are often applied to hydrogen transfer reactions, but their specific role during catalysis is not always well-understood. New experimental and theoretical work details the complexity associated with predicting secondary-sphere interactions and therefore designing improved catalysts. The following sections highlight examples of catalysts containing secondary-sphere groups that (1) accelerate a key turnover-limiting step such as H_2 heterolysis or hydride transfer, (2) limit competing catalytic cycles, (3) prevent catalyst decomposition, and/or (4) provide access to new catalysts through post-metalation modifications. The examples described herein emphasize numerous roles of the secondary sphere in hydrogen transfer catalysis and illustrate how the optimal use of these interactions is predicated on the analyses of key reaction intermediates in a catalytic reaction.

Advances in transition-metal catalysis stem from the systematic variation of electronic and geometric properties of the catalyst. Ligand design has therefore become a vital aspect of homogeneous catalysis, where a carefully chosen ligand can stabilize uncommon oxidation states of a metal, improve the turnover number (TON) of a reaction, and/or hinder decomposition pathways. The interplay between the primary and secondary spheres of a transition-metal complex significantly impacts the outcome of many catalytic transformations.[1–7] Primary-sphere effects are derived from the electronic and geometric arrangement of the atoms directly coordinated to the metal (i.e., the acidity/basicity of ligands, the *trans* effect/influence, and hydricity of metal hydrides) (Figure 2-1, left). The secondary sphere is more broadly defined in the literature.[6] In this work, atoms in the ligand framework that are not directly coordinated to the metal center are defined as secondary-sphere groups. Secondary-sphere interactions are established when atoms within the ligand framework interact with an exogenous atom or molecule (e.g., an organic nucleophile/electrophile[8] or Lewis acid/base[9–15]) (Figure 2-1, right).

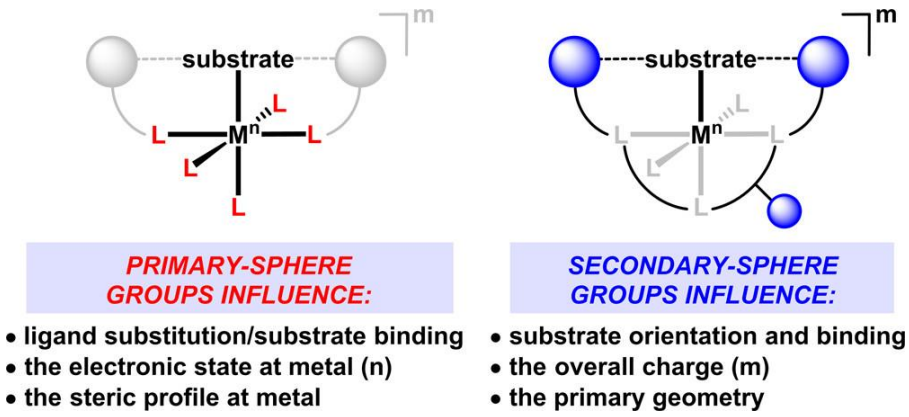

Figure 2-1. Influence of primary-sphere and secondary-sphere groups in a metal−ligand complex

While primary-sphere trends in catalysis are well-established, such as those involving Tolman electronic and cone angle parameters, secondary-sphere interactions that promote

enhanced catalytic behavior are still difficult to predict *a priori*. Precisely defining these interactions and understanding how they affect the primary sphere and ultimately the outcome of a catalytic reaction are of high importance for the field of transition-metal catalysis.

Secondary-sphere groups can impart a broad range of ligand-based reactivity during catalysis. Interactions with a molecule's secondary sphere encompass non-covalent (e.g., electrostatic, hydrogen-bonding, charge-transfer, and van der Waals forces)[16] and covalent (e.g., protonation or alkylation)[15,17,18] interactions. The focus of this Chapter is to delineate ligand design principles that dictate chemical reactivity for transition metal-based (de)hydrogenation and hydrofunctionalization catalysis. Numerous features imparted by the ligand must be considered, including the spatial proximity of appended groups to metal-coordinated substrates, matching of acid/base properties to promote substrate activation, and the pK_a and hydricity characteristics of M−(η^2-H_2) and M−H complexes. Two ligand design strategies in this field are to incorporate ligand-based functional groups that are either (1) proximal to the metal center, which can directly participate in substrate activation, or (2) remote from the metal center, which can be used as a handle for late-stage or in situ catalyst modification. Because hydrogen transfer is largely determined by the characteristics of M−H and/or M−(η^2-H_2) intermediates, both strategies generally influence the catalyst through acidity/hydricity tuning, and thus, this Chapter includes a brief overview of hydricity and pK_a considerations for hydrogen transfer reactions. Because of the proximity of appended groups to the metal center, the first strategy may enable a cooperative mechanism in which a substrate is activated toward bond cleavage through the synergistic action of the ligand and metal. In contrast, a remote site can be modified (reversibly or irreversibly) and thus influence a change in catalytic activity without perturbing the geometry of the primary

coordination sphere. The goal of this Chapter is to outline recent studies from our group and others that identify the role of secondary sphere groups, including how they influence the primary coordination sphere and facilitate productive catalytic reactivity.

2.2 Hydricity and pK_a Considerations for Hydrogen Transfer Catalysts

The high bond dissociation energy (102 kcal/mol)[19] and pK_a (~50 in THF)[20,21] of H_2 preclude homolytic or heterolytic splitting without activation. For transition-metal-mediated ionic hydrogenations, H_2 is activated toward heterolytic cleavage through the formation of a M−(η^2-H_2) complex. Sufficient electrophilic activation of the coordinated H_2 ligand facilitates heterolysis and transfer of H^+ and H^- to a polar double bond (e.g., R_2C=O, R_2C=NR), which may occur in a stepwise or concerted fashion.[19,22–24] Importantly, the hydridic and protic character of the catalyst and reaction components must be well matched near equilibrium values for efficient catalytic turnover (Figure 2-2, left).[21,25] Knowledge of pK_a and hydricity (ΔG_{H^-}) values for reactants and intermediates can be used to guide reaction design. The mechanisms by which H_2 heterolysis and transfer occur depend in part on the relative thermodynamic *para* meters of each reaction component. For example, proton transfer from an acidic M−(η^2-H_2) intermediate can be facilitated by an exogenous Brønsted base, a basic site on the ligand, or an organic substrate (R_2C=O, R_2C=NR) (Figure 2-2, right).[19,21] Ultimately, the differences in acidity and hydricity between the reaction components will determine which substrates and solvents are compatible with the catalyst, whether additives are required for a given reaction, and whether a cooperative metal− ligand interaction is possible. The thermodynamic properties of the metal component are highly tunable. Experimental pK_a values of M−(η^2-H_2) complexes as low as −6 ($[Os(H_2)(CO)(dppp)_2]^{2+}$ (dppp = 1,3-bis(diphenylphosphino)propane)) in CD_2Cl_2 have been reported,[21] and hydricity values (ΔG_H

◦–) for transition-metal hydrides span a range of at least 50 kcal/mol.[26] The ligand environment, overall charge, geometry, and identity of the metal contribute to the pK_a and hydricity of catalytic intermediates.[21,27] A significant body of work has been established for estimating the pK_a values of M−H and M−(η^2-H_2) complexes on the basis of ligands in the primary coordination sphere.[21] The ligand acidity constant (LAC) method developed by Morris[21] provides estimated acidity values for diamagnetic metal hydrides and dihydrogen complexes (groups 6−10). This approach considers the identity of the ligand at each coordination site, the charge of the conjugate base, the row of the transition metal, and the geometry of the conjugate base. Many ligand substituent and solvation effects are not considered in this model; however, estimates match many known pK_a^{THF} or pK_a^{DCM} values for transition-metal complexes within 3 pK_a units. Since M−H and M−(η^2-H_2) are common intermediates for (de)hydrogenation and hydrofunctionalization catalysis, the LAC model provides a useful starting point for predicting the thermodynamic profile of a catalyst.

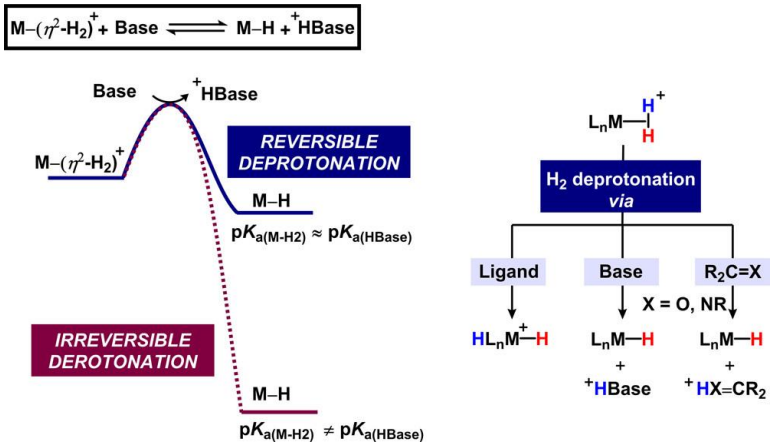

Figure 2-2. (left) pK_a considerations for the reversible protonation of a hydrogen transfer catalyst and (right) three possible routes for H_2 deprotonation.

2.3 Intramolecular M−(η^2-H_2) Deprotonation and M−H Protonation

Intramolecular heterolytic H_2 activation of a M−(η^2-H_2) species via protonation of a basic site in the secondary sphere is a fundamental step in many synthetic and biological hydrogen transfer catalysts.[8,28−55] Notably, additives (e.g., an exogenous base) may be omitted when a catalyst can facilitate intramolecular proton exchange, making this an attractive catalyst design strategy for atom-economical transformations.[56,57] However, the relationship between the protonation state of the ligand and the electronic state of the metal can complicate *a priori* predictions.[58,59] Protonation of a ligand based site will change the overall charge of the complex, which affects the reduction potential, hydride donor ability, and pK_a values of M−(η^2-H_2) intermediates. Moreover, protonation of a ligand-based site may even introduce unforeseen deactivation pathways.

The development of electrocatalysts for H_2 production exemplifies the complex relationship between secondary- and primary-sphere interactions required to promote rapid proton transfer during catalysis. The nickel complex containing two pendent amine groups, $[Ni(PPh_2NPh)_2](BF_4)_2$ (Figure 2-3, right), catalyzes the production of H_2 with a turnover frequency (TOF) of 106,000 s^{-1}.[60] Analogous $Ni(P_2N_2)^{2+}$ catalysts with four pendent amines facilitate H_2 production with TOF values at least 2 orders of magnitude lower than that of $[Ni(PPh_2NPh)_2](BF_4)_2$. A proposed transition state for H_2 formation with $Ni(P_2N_2)^{2+}$ catalysts involves protonation of a Ni−H intermediate with one pendent amine group (Figure 2-3, middle).[61]

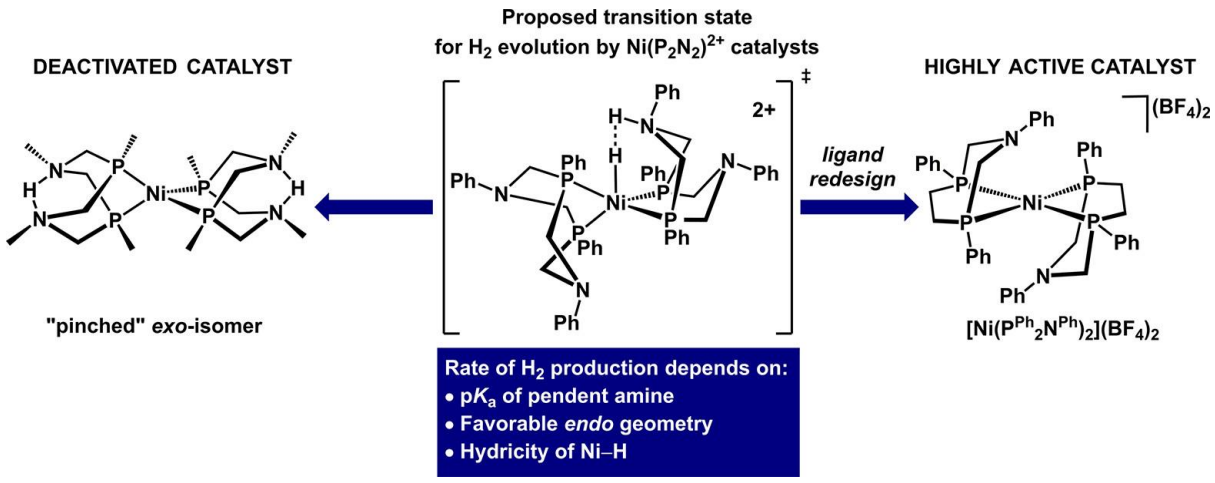

Figure 2-3. Development of Ni catalysts with pendent amines for H_2 production.

Three factors contribute to the remarkable rate enhancement of $[Ni(PPh_2NPh)_2](BF_4)_2$ over $[Ni(PPh_2NPh_2)_2]^{2+}$ analogues. The first is the pK_a of the pendent base, which facilitates intramolecular proton transfer to the Ni−H. For $[Ni(PPh_2NPh_2)_2](BF_4)_2$, modification of the N−Ph aromatic groups to include electron-withdrawing *p*-Br substituents promotes hydride protonation and the release of H_2. The second factor is the presence of only two pendent amines in $[Ni(PPh_2NPh)_2](BF_4)_2$, in contrast to $[Ni(PPh_2NPh_2)_2](BF_4)_2$. The PPh_2NPh_2 ligand forms catalytically inactive "pinched" complexes (Figure 2-3, left) which are avoided by limiting the number of pendent amines. Finally, the square-planar geometry of $[Ni(PPh_2NPh)_2](BF_4)_2$, enabled by minimal steric crowding from the PPh_2NPh ligand, results in a more hydridic Ni−H compared with the distorted $[Ni(PPh_2NPh_2)_2](BF_4)_2$ catalysts. The more reactive Ni−H bond facilitates faster H_2 bond formation and elimination from Ni; elementary steps that are turnover-limiting during proton reduction.[60–63] The success of $Ni(P_2N_2)^{2+}$ complexes is largely due to the identification of productive secondary-sphere interactions, which epitomizes the profound impact of rational catalyst design.

Matching the pK_a values between the pendent amine and the M−H/M−(η^2-H_2) intermediates is the first step needed for rapid catalysis involving H_2 cleavage/formation. The rate of H_2 heterolysis can be controlled through systematic ligand modifications, and a series of [CpMo(H)(CO)(P_2N_2H)]$^+$ complexes reveals a linear dependence of the H^+ /H^- exchange rate on the acidity (Figure 2-4). Modifying the basicity properties of the P_2N_2 ligand permits hydride−proton exchange rates that span 4 orders of magnitude, with the highest rate (4.0 × 107 s $^{-1}$ in CD_2Cl_2) corresponding to the most acidic complex (pK_a CD_3CN = 9.3).[64]

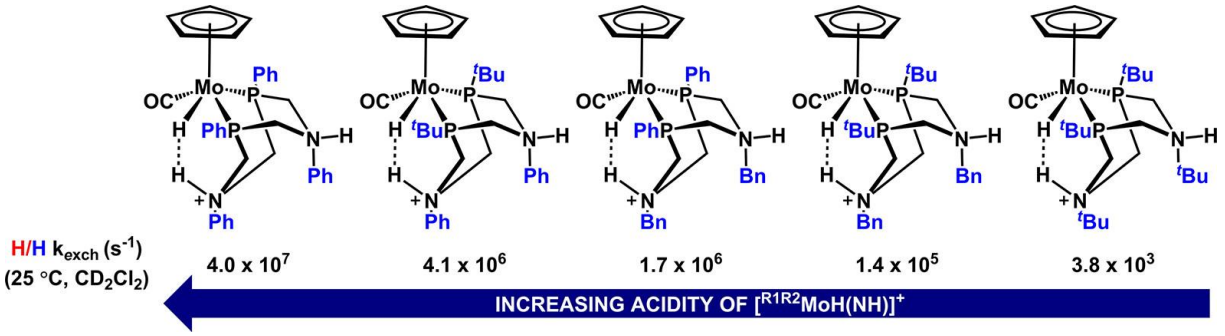

Figure 2-4. Tunable proton–hydride exchange rate with [R^1R^2MoH(NH)]$^+$.

Although intramolecular deprotonation of a M−(η^2-H_2) complex has been reported in many systems,[21] this will not necessarily be the dominant pathway for proton transfer in ligand scaffolds that contain basic sites. Kinetic factors, in addition to the thermodynamic properties of intermediates, heavily influence the outcome of a catalytic reaction. Proton transfer may be further complicated by competitive protonation of a basic metal center or the presence of multiple basic sites on the ligand.[65–67] Differences in protonation selectivity can be illustrated using Ru-based (de)hydrogenation catalysts containing 1,3-bis(2′-pyridylimino)isoindolate (bpi) ligands. These ruthenium complexes have two accessible basic sites, one in the secondary sphere and the other in the primary sphere (Figure 2-5): an imine unit (A), and a Ru−hydride (B). A depiction of selected

filled molecular orbitals of $HRu(bpi)(PPh_3)_2$ shows that the HOMO (−4.43 eV) is mainly composed of the conjugated bpi π-orbitals, with the electrons of the central amido nitrogen delocalized across the adjacent imine nitrogen atoms. The σM−H orbital is the low-lying HOMO−7 (−6.30 eV) and includes a σ-donor contribution from the *trans*-amido nitrogen.

The preferred site of protonation is challenging to predict on the basis of the thermodynamic properties of each basic site. The difference in free energy of protonation between the Ru−H (site B) to form a Ru−(η^2-H_2) intermediate versus protonation of the imine nitrogen (site A) is only 0.4 kcal/ mol.[70] Although protonation or alkylation at the imine nitrogen occurs in the absence of the hydride ligand, the Ru−H is the kinetic site of protonation during catalytic (de)-hydrogenation.[68,69] Complexes such as $HRu(bpi)(PPh_3)_2$ (Figure 2-5, bottom left) and $HRu(bMepi)(PPh_3)_2$ (bMepi = 1,3-bis(6′-methyl-2′-pyridylimino)isoindolate) are catalysts for the acceptorless dehydrogenation of alcohols and amines and operate through a hydride protonation mechanism upon coordination of the substrate (e.g., Figure 2-5, bottom right).[68,70] Hydride protonation is likely facilitated by dihydrogen bonding in the transition state between the coordinated substrate, a second proton donor, and the basic Ru−H.

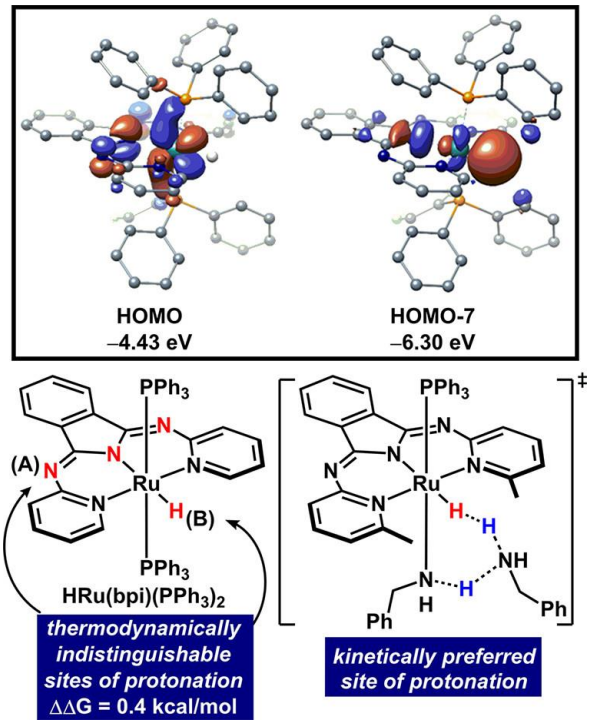

Figure 2-5. Two potential sites of protonation for HRu(bpi)(PPh$_3$)$_2$ and the molecular orbitals HOMO and HOMO–7.

2.4 Electronic Changes in the Primary Sphere Based on Secondary Sphere Proton Transfer

The identity and protonation state of the base in the second coordination sphere affects the hydricity and acidity of M−H/ M−(η^2-H$_2$) intermediates (*vide supra*) and the redox potential of the metal.[62] Thus, a critical aspect to consider for predicting and understanding the reactivity of hydrogen transfer catalysts is the electronic change at the metal center upon protonation/ deprotonation in the secondary sphere.

Our group and others have systematically probed the interdependent nature of the primary and secondary spheres during proton transfer using 2-hydroxypyridine-type ligands.[15,18,37,71−85] This ligand framework is modeled after the [Fe]-HMD hydrogenase enzyme, where the deprotonated pyridinol group is proposed to act as a base during H$_2$ heterolysis.29,86

Deprotonation of 2-hydroxypyridine-type ligands affords distinct ligand binding modes. The tridentate pincer ligand 6,6′-dihydroxyterpyridine (dhtp) is an L_3-type ligand when fully protonated, as in the case of the cationic complex $[Ru(CO)(dhtp)(Cl)(PPh_3)]PF_6$ (Figure 2-6, left). Upon deprotonation, $Ru(CO)(dhtp')(L)(PPh_3)$ (Figure 2-6, right; L is thought to be coordinated solvent) is formed with dhtp as an LX_2-type ligand. The increase in electron density at ruthenium can be observed by IR spectroscopy, where the deprotonated tautomer has a lower CO stretching frequency ($\nu CO = 1969\ cm^{-1}$) compared with the protonated complex ($\nu CO = 2046\ cm^{-1}$).

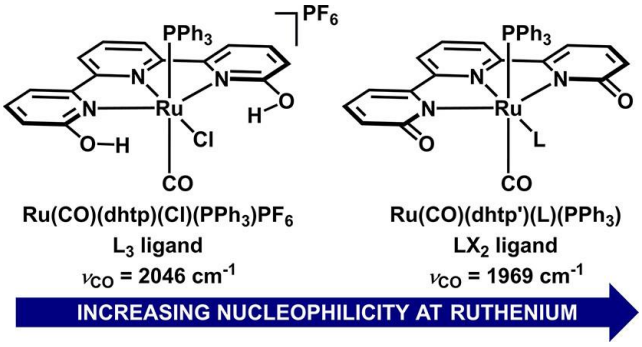

Figure 2-6. Electronic dependence between the two protonation states of the 6,6′-dihydroxyterpyridine (dhtp) ligand.

In contrast to the two tautomeric states observed with the dhtp ligand platform, the ruthenium−BH_3PI (BH_3PI = bis(2′- hydroxy-6′-iminopyridyl)isoindoline) system provides access to four distinct and isolable protonation states (Figure 2-7). In addition to the appended −OH groups from the 2- hydroxypyridine moiety, the basic imine in the ligand backbone of BH_3PI can also undergo protonation. Successive protonation of complex 1 affords a more electron-deficient metal center, and the ruthenium redox event undergoes an anodic shift with increasing protonation state (E_{ox} = −660, −460, and 195 mV vs Fc/Fc+ for complexes 1−3.

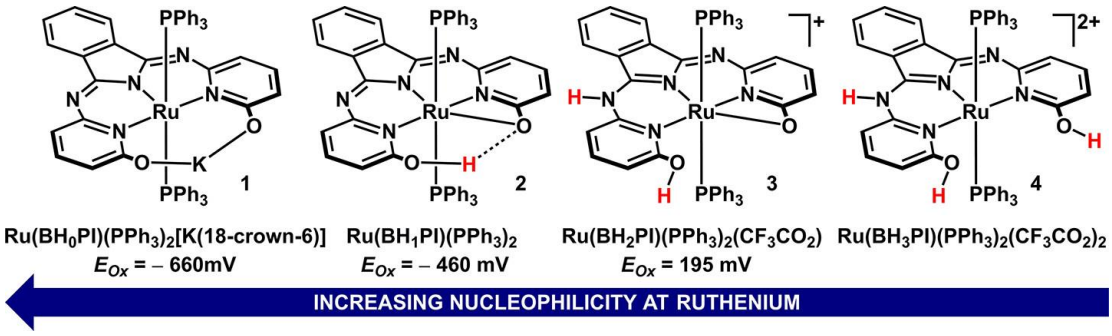

Figure 2-7. Electronic dependence between the four protonation states of the ruthenium–BH_3PI system.

2.5 Substrate Activation in the Secondary Coordination Sphere

Complexes with functional groups positioned adjacent to the metal center can serve a dual purpose of engaging a substrate in cooperative interactions while also electronically tuning the metal center. Cooperative and bifunctional ligands have played an important role in developing atom-economical hydrogen transfer and hydrofunctionalization reactions,[53,87–89] and the definition of cooperativity and bifunctionality continues to change over time.[8,90,91] Bifunctional ligands were originally defined as those that undergo a reversible bond cleavage event during a bond activation reaction,[92,93] such as the reversible proton transfer facilitated by Ni(P_2N_2) catalysts. Another classic example of a metal−ligand bifunctional catalyst is Shvo's ruthenium hydride complex, which facilitates (de)hydrogenation reactions of polar substrates. (Figure 2-8).[40,94,95] The ketone group on the cyclopentadienone ligand is proposed to participate in the solvent-assisted heterolytic activation of H_2 and also direct the hydrogenation of ketones through an outersphere transfer of a hydride (H^-) from the metal center and a proton (H^+) from the hydroxyl group on the cyclopentadienyl ligand (TS-1; Figure 2-8).[96,97] Following the success of this and related

bifunctional catalysts,[98,99] numerous metal−ligand complexes that contain Brønsted base/acid groups have been developed for hydrogen transfer reactions.[72,89,100]

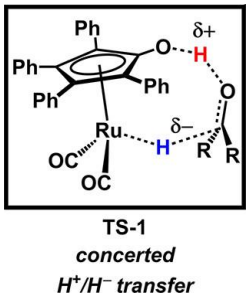

Figure 2-8. Outer-sphere transfer of H^+ and H^- to a carbonyl substrate by Shvo's catalyst.

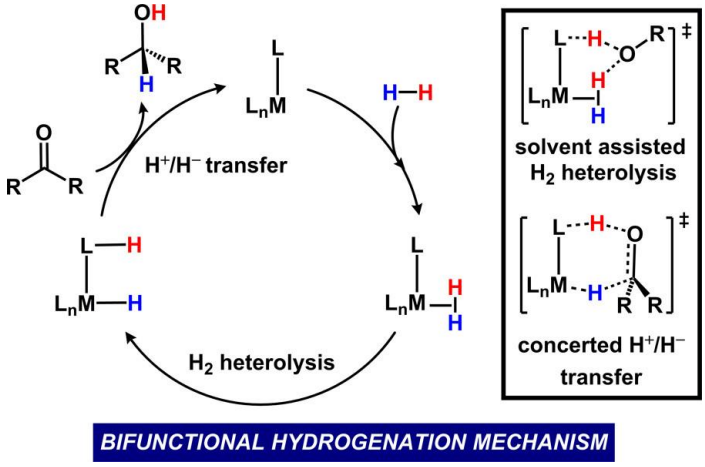

Figure 2-9. Noyori's mechanism for the hydrogenation of C=O bonds. Reversible ligand protonation occurs via secondary-sphere interactions with the solvent and/or substrate.

A recent description of cooperativity encompasses the concept of bifunctionality: a cooperative ligand interacts with a substrate through non-covalent interactions that stabilize and orient the substrate toward bond breaking but does not require a bond cleavage event on the ligand.[90,101] For example, Noyori type bifunctional catalysts hydrogenate polar C–O and C=N bonds through non-covalent bonding interactions of the chelating diamine ligand and Ru−H/Ru−(η^2-H_2) intermediates.[8,90,91,102] Although early mechanistic studies proposed reversible H^+ transfer to the substrate with the −NH group of the ligand following H_2 heterolysis (Figure

2-9).[92,103–108] recent computational studies show that the secondary-sphere group does not formally undergo bond cleavage.[8,91] Rather than reversible proton transfer, the role of the –NH unit is to stabilize the transition states via hydrogen-bonding interactions. In TS-2 (Figure 2-10), ion-pairing interactions between the substrate and ligand orient the C=O bond and lower the kinetic barrier for hydride transfer.[8,109] Under basic conditions with alkali metal alkoxides, such as KO^{t}Bu, the amino group is associated with a Lewis acid instead of H^+ , which also stabilizes the transition states via non-covalent interactions.

These mechanistic differences refocus the design approach needed to facilitate hydrogen transfer reactions. For cooperative catalysts containing acidic XH (X = O, N, C) groups, distinct mechanistic regimes have been established.[8] For example, while some *N*-alkylated Noyori-type catalysts are less active because of the absence of non-covalent bonding interactions, other examples show beneficial activity from alkylation.[91] These developing new paradigms serve to illustrate the complexity associated with predicting the role of appended groups in bifunctional catalysis.

Cooperative substrate–Lewis acid interactions facilitated by Ru–dhtp and Ru–BH_3PI catalysts work in concert with the electronic regulation at the metal during hydrogen transfer catalysis.[15,18,73] Under basic conditions, the transfer hydrogenation of ketones with Ru–dhtp and hydroboration of nitriles with Ru–BH_3PI both involve a high-energy transition state for H^- transfer to a polar unsaturated substrate. The deprotonated 2-hydroxypyridine group results in a more nucleophilic ruthenium center (vide supra), which in turn translates into a more hydridic Ru–H during catalysis. In addition to modulating the hydricity at Ru, the deprotonated ligands engage in cooperative substrate activation using an exogenous Lewis acid. The substrate is positioned for

hydride insertion via a secondary-sphere interaction with an alkali metal ion (for Ru−dhtp-catalyzed transfer hydrogenation) or borane (for Ru−BH_3PI-catalyzed hydroboration) (TS-3 and TS-4, respectively; Figure 2-11).

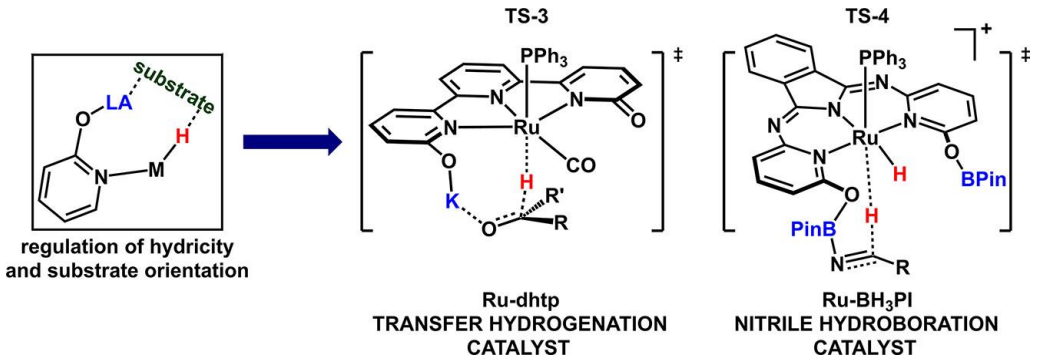

Figure 2-10. Dual role of proton-responsive groups in the 2-hydroxypyridine motif.

Similar to the Noyori system, the presence of an alkali metal is crucial for efficient catalysis by Ru−dhtp complexes during the transfer hydrogenation of ketones. The appended −OH groups in dhtp direct the ketone for hydride transfer through alkali metal ion coordination (TS-3; Figure 2-11).[73] Under basic conditions, the cooperative −OH group facilitates hydrogen transfer as O−M+ (M = Li, Na, K, Cs) through ion-pairing with the polar substrate and the alkali metal ion. This interaction has three important features that contribute to efficient and selective transfer hydrogenation. First, the identity of the alkali metal cation further influences the electronic character (hydricity) of catalytically active Ru−hydride intermediates, where the initial rate for acetophenone reduction increases with a decrease in the Lewis acidity of the alkali metal. Thus, cesium was identified as the optimal cation for the transfer hydrogenation to acetophenone using [Ru(CO)(dhtp)(Cl)(PPh_3)]PF_6.

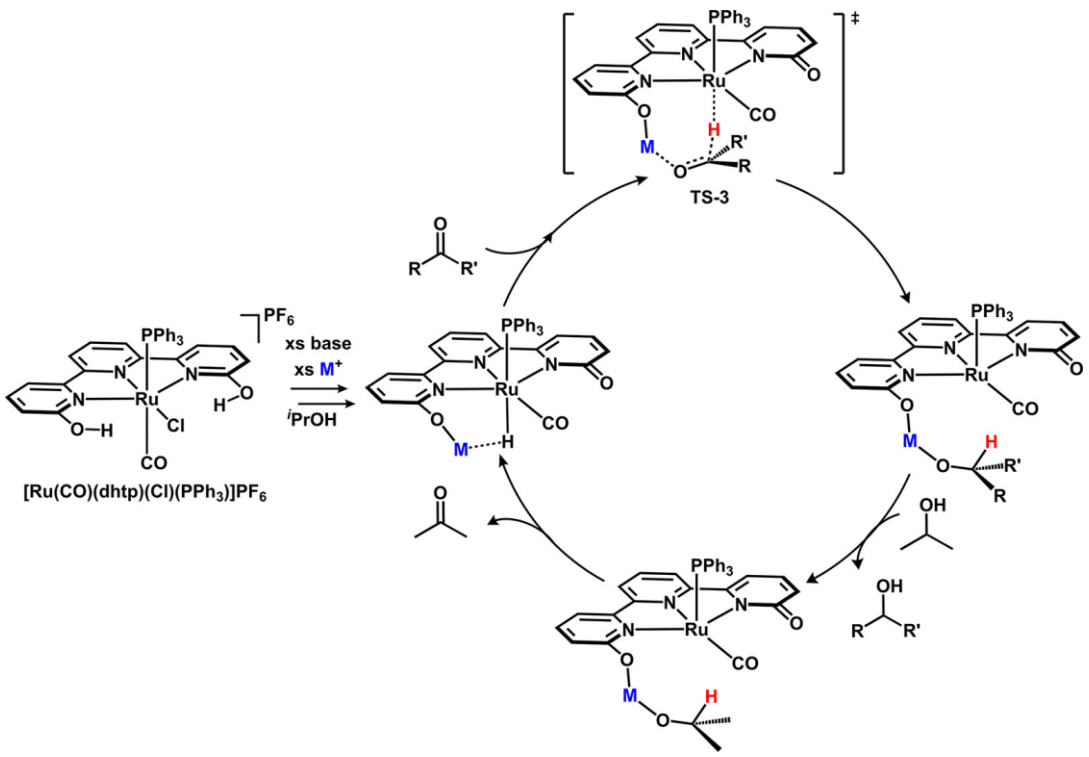

Figure 2-11. Proposed catalytic cycle for transfer hydrogenation of ketones catalyzed by [Ru(CO)(dhtp)(Cl)(PPh$_3$)]PF$_6$

Second, the alkali metal ion−substrate interaction, which is enabled by the positions of the protic groups, orients the ketone substrate for outer-sphere hydride transfer. When the protic groups are positioned away from the metal center in [Ru(CO)(4-dhtp)(Cl)(PPh$_3$)]PF$_6$, the transfer hydrogenation of acetophenone is half as fast compared with that using the 2-hydroxypyridine variant despite almost identical electronic environments at ruthenium. Third, a direct consequence of the substrate−alkali metal ion interaction is complete chemoselectivity for polar bonds over nonpolar bonds, a feature illustrated by the polarized transition state of TS-3 during hydride transfer (Figure 2-11). Overall, the pyridinol groups impart both electronic regulation of the Ru−H nucleophilicity and a cooperative substrate interaction to drive selective product formation. We anticipate that these design principles will extend beyond simple hydrogen transfer reactions.

Boron Lewis acids in the secondary sphere may also behave as directing groups in hydrogen transfer and hydrofunctionalization reactions.[110,111] This substrate-directing effect is highlighted by the selective semi-hydrogenation of alkynes using appended borane Lewis acids in the Ru−bMepi system.[112] The Ru−bMepi catalyst without appended boron Lewis acids, $HRu(bMepi)(PPh_3)_2$, exhibits poor activity and selectivity for the hydrogenation of alkynes (5; Figure 2-12). In contrast, the catalyst with an appended 9-BBN group (6; Figure 2-12) is an active catalyst for the semi-hydrogenation of alkynes, providing quantitative conversion to (Z)-alkenes. The chemoselectivity for alkyne over alkene substrates is likely due to a stronger interaction of the alkyne π system with the boron atom.

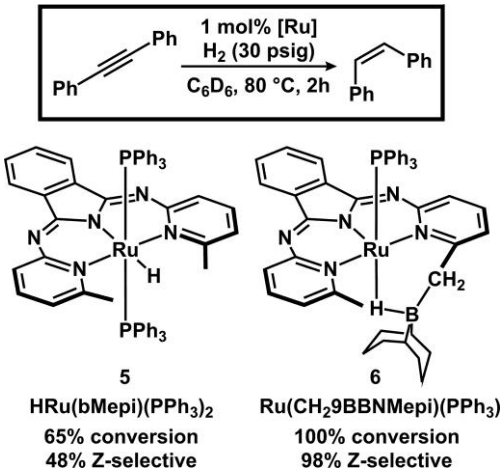

Figure 2-12. Selective alkyne semi-hydrogenation catalyzed by Ru–bMepi derivatives with appended boron Lewis acids.

The role of appended boron Lewis acids during hydrofunctionalization catalysis is fundamentally similar to what has been discussed for hydrogen transfer reactivity, where a "tethered" Lewis acid behaves as a directing group, assists in H_2 heterolysis, and/or stabilizes a reactive intermediate through non-covalent interactions.[15] The ruthenium−BH_3PI system facilitates the hydroboration of ketones and nitriles with the aid of a pendent boron Lewis acid.

The activity is highly dependent on the ligand's protonation state (vide supra); the protonated complex, 3, facilitates the hydroboration of acetophenone in only trace amounts, whereas the fully deprotonated complex, 1, has one of the highest reported activities at room temperature (Figure 2-13).[15] The hydroboration of more challenging substrates, such as nitriles, cannot be achieved using 3, but catalysis is enabled using the monoprotonated complex 2 and is further accelerated by 2 orders of magnitude upon full deprotonation of BH_3PI (1). As in the case of the dhtp ligand, the proton-responsive groups of BH_3PI serve the dual purpose of modifying the electronics at Ru and tethering a Lewis acidic group to direct substrate coordination.

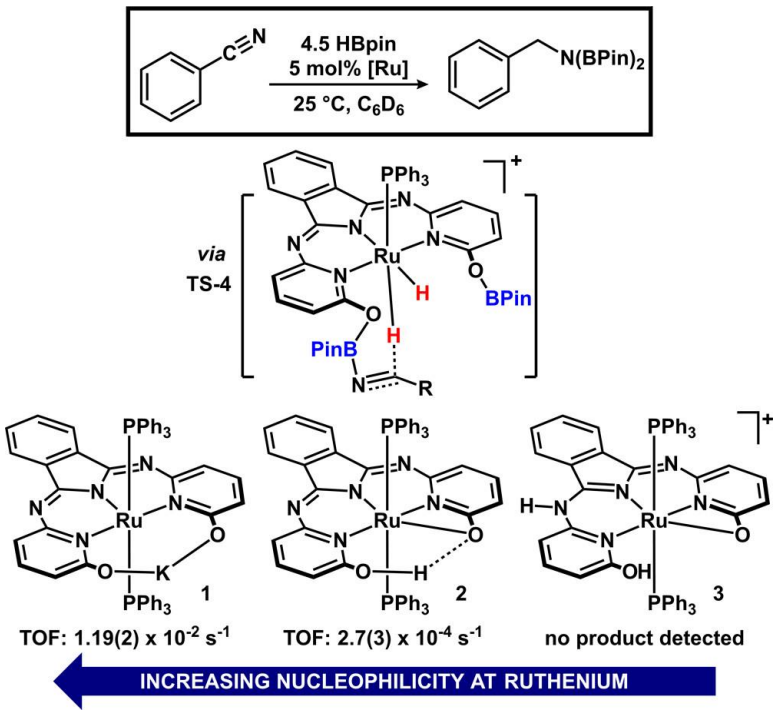

Figure 2-13. Increase in the initial TOF of benzonitrile hydroboration with increasing hydricity at ruthenium.

When pursuing catalyst redesign studies, efforts should be made to first identify whether secondary-sphere groups truly serve a cooperative role during a given catalytic reaction. The results of these studies will inform on whether redesign should be focused on the secondary-sphere

groups or alternatively on the steric/electronic properties of the complex. For example, complexes that contain methylpyridine-based pincer ligands (i.e., 2,6-bis(di-*tert*-butylphosphinomethyl)pyridine (PNP^{t}Bu) or 2-(di-tert-butylphosphinomethyl)-6-diethylaminomethyl)- pyridine (PNN^{t}Bu)) exhibit metal−ligand cooperative processes based on aromatization/dearomatization via deprotonation of a methylene unit (Figure 2-14).[57] These catalysts and analogous pincer-type complexes[113−115] have been applied to a vast number of hydrogen transfer and hydrofunctionalization reactions. Because of their broad applicability in hydrogen transfer reactions, cooperative pincer complexes have been the subject of many experimental and theoretical mechanistic studies.[57,87,116−129] For (de)hydrogenation and dehydrogenative coupling reactions by PNP and PNN catalysts, the dearomatized intermediate is commonly proposed to facilitate X−H activation (X = H, C, O, N).

Figure 2-14. Metal–ligand cooperativity based on the aromatization/dearomatization process.

Although ligand (de)aromatization is one potential pathway that may enable catalytic turnover, it is not always apparent whether this is the dominant pathway for X−H activation.[120,122−124,130−134] Mechanistic studies of the hydrogenation of C=O bonds by Ru−PNP and Fe−PNP complexes have shown that the protonated (L_3-type) state of the ligand is required for turnover, while the deprotonated (L_2X-type) state is not involved in the catalytic cycle.[122,123,132] Theoretical studies have compared a metal−ligand cooperative pathway (mechanism A, Figure 2-15) and a direct reduction mechanism (mechanism B, Figure 2-15) for ketone hydrogenation

using the model system (PNP^{Me})FeH(CO)Br.[122,123] Each mechanism begins with a dearomatized species (7a), which is experimentally observed in the presence of KO^tBu.[135] Mechanism A involves coordination of the carbonyl substrate to 7a to form the coordinatively saturated species 7b. Hydride insertion from 7b provides the five-coordinate Fe−alkoxide intermediate 7c. Following association of H_2 to 7c, H_2 is heterolytically cleaved through a cooperative step involving the PNP ligand, resulting in aromatization of the central pyridine ring and the formation of 7d. Finally, the dearomatized intermediate (7a) is regenerated after deprotonation of the ligand by the coordinated alkoxide. The computed high energy barrier of 40.8 kcal/mol is associated with hydride insertion to acetophenone, and is inconsistent with the room-temperature conditions reported for ketone hydrogenation by Fe(PNP) catalysts.[135]

Mechanism B shows the direct reduction of C=O bonds by an Fe−dihydride catalyst (7e) without bond cleavage events in the secondary sphere. The dearomatized intermediate 7a serves as a precatalyst for the formation of 7e in the presence of EtOH and H_2. Importantly, (^{i}PrPNP)Fe(CO)(H)2 is experimentally observed,[135] and the modeled MePNP analogue 7e is 21.1 kcal/ mol more stable than 7a.[123] Facile hydride transfer from the Fe−H bond to the C=O bond occurs without coordination of the substrate in 7f. Ligand substitution with H_2 releases the alkoxide to afford cationic Fe−(H_2) species 7g, which then undergoes H_2 heterolysis. In contrast to a metal−ligand cooperative pathway for H_2 heterolysis (mechanism A), the free alkoxide is responsible for H_2 deprotonation in intermediate 7h. A calculated total free energy barrier of 19.8 kcal/mol corresponds to the association of H_2 to form 7g from 7f using acetophenone as the model substrate. A total free energy barrier of 19.8 kcal/mol was found to result from ligand exchange of $PhMeCHO^-$ for H_2 (involving transformations between 7f and 7g).

The thermodynamic favorability of the Fe−$(H)_2$ intermediate 7e over 7a, and a significantly lower kinetic barrier of mechanism B compared to mechanism A (19.8 vs 40.8 kcal/ mol) support an Fe−dihydride pathway over metal−ligand cooperativity for acetophenone reduction by Fe(PNP) catalysts. Similar comparisons were made in the case of CO_2 hydrogenation, where reaction pathways without cleavage of the PNP ligand are found to be ∼20 kcal/mol more favorable than metal−ligand bifunctional mechanisms.[122]

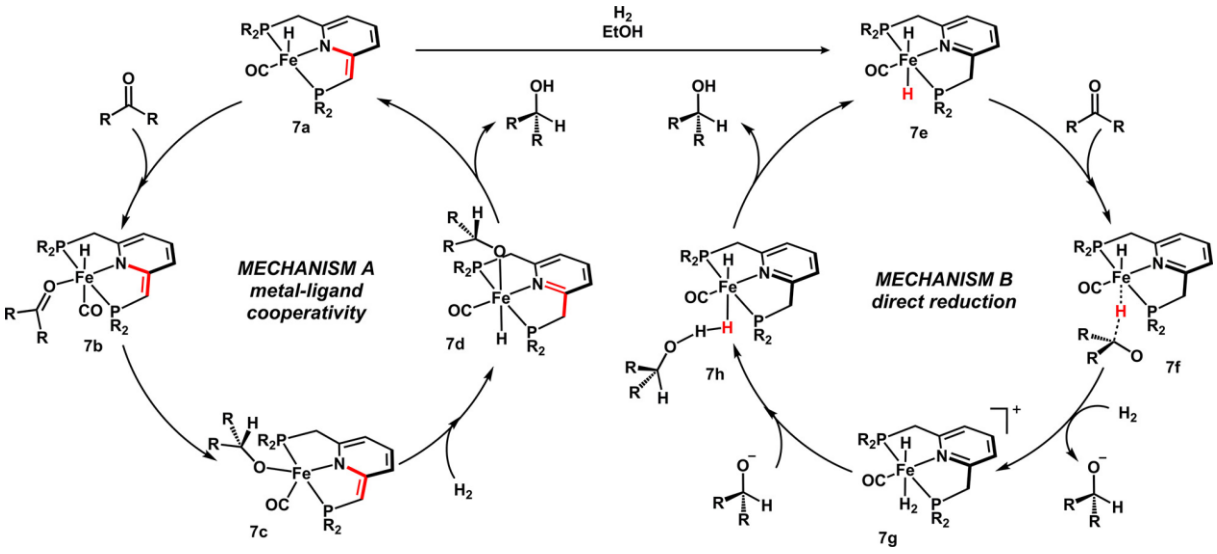

Figure 2-15. Proposed Mechanisms for C═O Reduction by (PNP^R)FeH(CO)[122,123]

Although a bifunctional mechanism is unlikely during the hydrogenation of ketones with Fe(PNP) catalysts, the proton responsive site on the ligand may still serve an important role during hydrogenation. Weak non-covalent interactions between the acidic −CH_2 groups, polar substrates, and/or protic solvents may help stabilize high-energy intermediates and transition states in both Fe− and Ru−PNP systems.[8,120,125] Non-covalent interactions are already well-recognized in enzymatic catalysis,[136] organocatalysis,[137] and asymmetric transition-metal catalysis[138] and should be considered as a central design element for developing new transformations based on transition-

metal catalysts.[139–142] To summarize, the secondary-sphere $-CH_2$ groups of PNP-type ligands can serve at least two important functions during hydrogen transfer reactions: (1) acting as an intramolecular H^+ shuttle and (2) providing contact points to enable stabilizing non-covalent interactions. Whether either of these functions are operative and/or beneficial during a given catalytic process is reaction specific and requires in-depth mechanistic studies to elucidate.

2.6 Deactivation Pathways in the Secondary Sphere

A significant challenge in the field of ligand design is predicting and navigating an array of deleterious interactions that secondary-sphere groups can introduce. Understanding how the secondary-sphere facilitates productive pathways in addition to deactivation pathways is critical to redesign more effective catalysts.[143] For example, H_2 production is hindered with Ni(P_2N_2) catalysts containing four pendent amines because of the formation of an inactive "pinched" isomer (Figure 2-3). Identification of the inactive isomers led to modified catalysts with enhanced rates.[60] Dearomatized PNP complexes readily react with electrophiles to form new C−X (X = H, C, B, O) bonds in the secondary sphere.[87] For example, Ru(PNP^{t}Bu)(CO)(H) and Ru(PNN^{t}Bu)(CO)(H) react with CO_2 to form a new a C−C bond in the secondary sphere (Figure 2-15, left).[124,132,144,145] This interaction is reversible at low pressures of CO_2 (1 atm); however, the equilibrium becomes slow at high pressures of CO_2 or with more reactive bifunctional ligands.[124,132,144] Shvo's catalyst is deactivated during the dehydrogenation of ammonia borane (Figure 2-16, right). A bridged Cp−O−B species is formed via hydroboration of an unsaturated Ru intermediate, inhibiting productive dehydrogenation.[146,147] The identification of these detrimental interactions provides an entry point for targeted redesign strategies that lead to improved catalysts.[124,147]

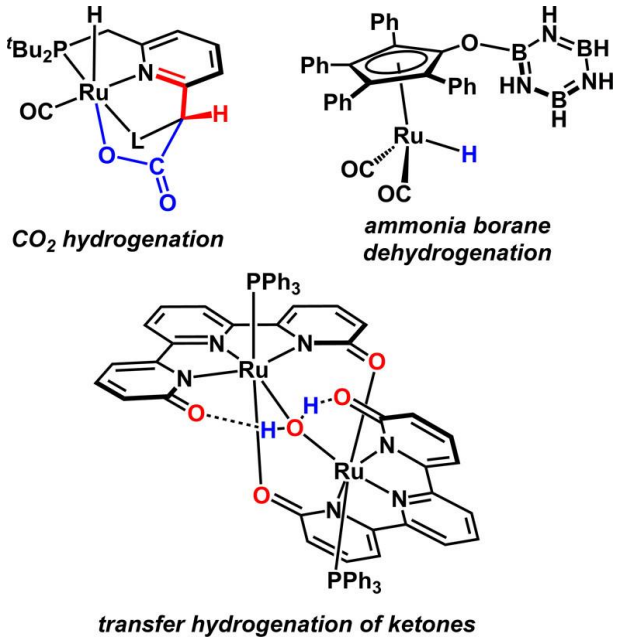

Figure 2-16. Selected examples of catalyst deactivation by secondary sphere groups.

Complexes containing the deprotonated dhtp ligand react with adventitious water in solution to form catalytically inactive aquo-bridged dimers (e.g., $[Ru(PPh_3)(dhtp)]_2(\mu\text{-}OH_2)$ (Figure 2-16). This pathway can be overcome by changing the secondary sphere groups from −OH to sterically bulky −NHR (R = mesityl) groups. Modification of the secondary-sphere groups furnishes highly active Ru catalysts for reactions in the presence of water and hydroxide.[14] The Ru catalyst $[Ru(H_2TpyNMes)(PPh_3)_2Cl]PF_6$ ($H_2TpyNMes$ = 6,6″-bis(mesitylamino)terpyridine) (Figure 2-16) avoids the decomposition pathway observed for Ru−dhtp complexes and facilitates a hydrogen transfer reaction that requires H_2O: the oxidant-free dehydrogenative oxidation of primary alcohols to carboxylates.[14]

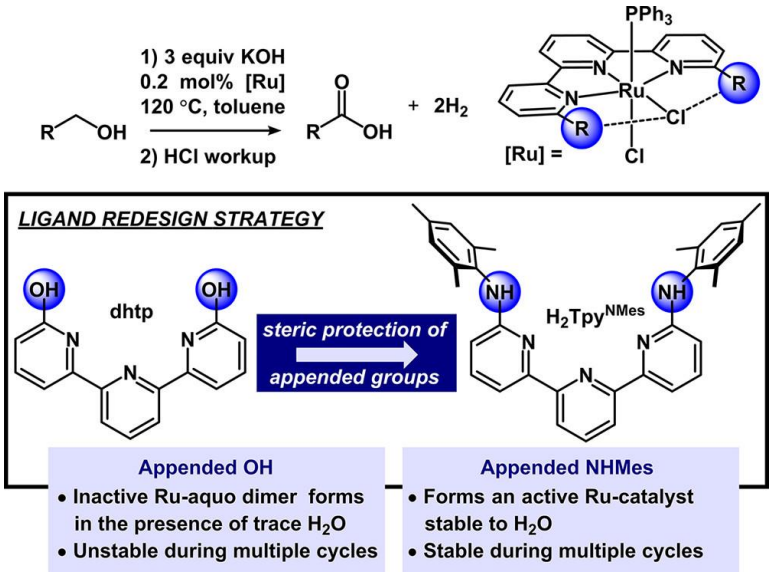

Figure 2-17. Ligand design strategy to overcome the deactivation pathway of Ru–dhtp catalysts in the presence of H_2O.

2.7 Protic Groups Remote from the Reactive Site

In contrast to cooperative groups proximal to the metal center, remote groups are less likely to interact with a substrate and therefore impart largely an electronic effect on the catalytic system without perturbing the primary coordination environment. This feature can be used to decouple a cooperative interaction from an electronic effect of a group in the secondary sphere.[15,37,73] Additionally, electronic perturbation in the secondary sphere can directly impact an elementary step within a catalytic cycle, such as hydride insertion, oxidative addition, reductive elimination, or ligand exchange. This design strategy has been employed for a wide range of complexes, where protonation/deprotonation, interactions with a Lewis acid, or addition of an electrophile in the secondary sphere has led to significant rate enhancements in stoichiometric and catalytic processes (Figure 2-18).[73,148−165]

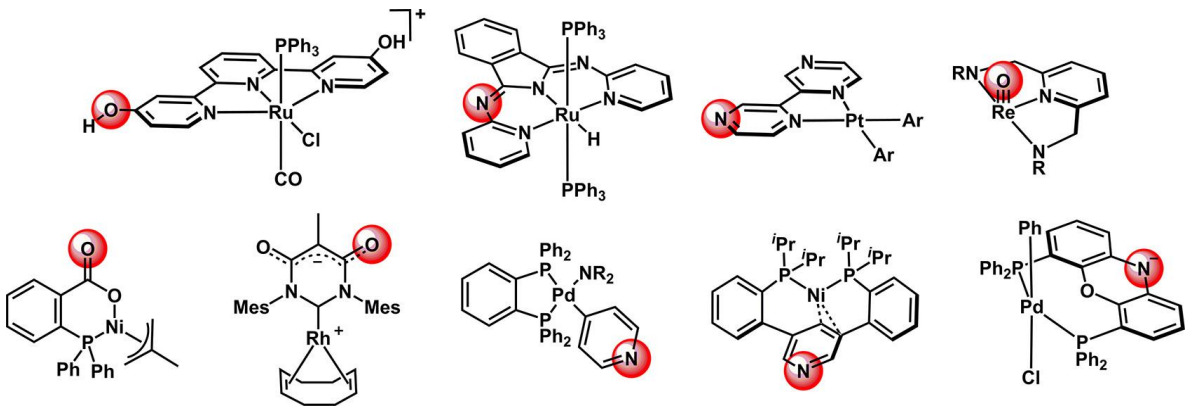

Figure 2-18. Selected complexes with ligands that enable late-stage electronic perturbations.

Electronic modifications of a catalyst have been classically achieved through ligand exchange, such as replacing X-type donors with neutral L-type donors. During the development of alkene hydrogenation catalysts, cationic Rh complexes were found to have distinct reactivity profiles compared with their neutral counterparts. For example, compared with the neutral complex $RhCl(PPh_3)_3$,[166,167] cationic species such as $[Rh(NBD)(diphos)]^+$ promote faster alkene binding, higher turnover frequencies for hydrogenation, and enabled the hydrogenation of more challenging substrates such as tetra-substituted olefins.[168–173] Other synthetic strategies for modifying the electronics at a metal site have included using modified phosphine ligands,[176,177] or alternatively, zwitterionic complexes.[174,175]

As an alternative to these rather time-intensive strategies, post-metalation modifications of a ligand scaffold can provide a simple route to perturb the electronic structure of a catalyst. Late-stage electronic changes can be achieved by reversible binding of H^+ or a Lewis acid to a basic site within the secondary sphere of a catalyst.[9,178,179] This creates a more electrophilic metal center, which can impact many metal-mediated reactions. For example, coordination of $B(C_6F_5)_3$ to a remote site on a platinum−bipyrazine (bpyz) complex accelerates biaryl reductive elimination by

a factor of 64,000 relative to the borane-free system (Figure 2-19).[150,151] In the absence of ligand-based binding sites, temporary electron perturbations can also be achieved with Z-type metal−metal interactions.[178,180] The addition of $Zn(C_6F_5)_2$ to a platinum(II) diaryl complex without remote binding sites on the bidentate ligand (1,10-phenanthroline or 2,2′-bipyridine) also results in an accelerated rate of reductive elimination.[180] These examples allude to the potential role of Lewis acid additives during a catalytic process. In line with the role of a Lewis acidic alkali metal ion during transfer hydrogenation processes (vide supra), transient electronic modifications at a remote site in the secondary sphere or through direct metal−metal interactions may play a fundamental role in a broad scope of catalytic reactions.

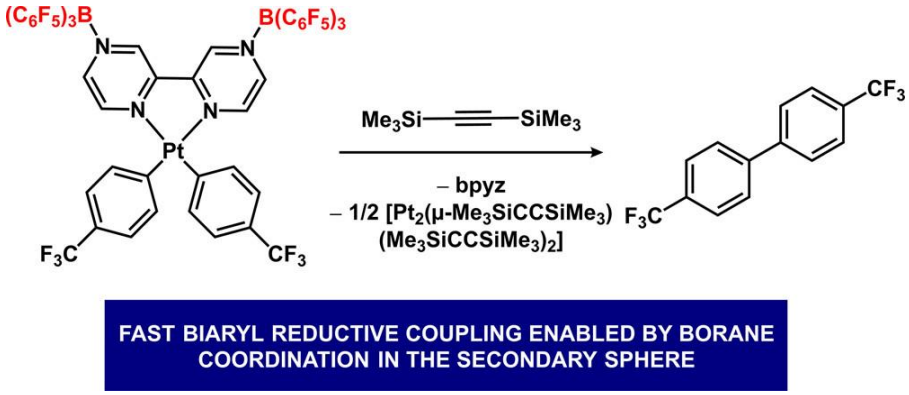

Figure 2-19. Acceleration of biaryl reductive elimination by binding of a boron Lewis acid to a bipyrazine–diarylplatinum(II) complex.

In addition to reversible protonation/deprotonation or Lewis acid/base interactions, irreversible modification of a remote basic site can be achieved by alkylation. Irreversible late-stage modification can provide new ligands that are not accessible using metal-free synthetic routes.[17] Metal−bpi complexes undergo selective methylation at the imine nitrogen using MeOTf, and the resulting $M(bpi^{Me})(OTf)_2$ (M = Ru, Fe) species can be evaluated further as catalysts with a more electrophilic metal center compared to their non-alkylated counterparts.

Alkylation of amine or imine nitrogen groups in the secondary sphere of Ru and Fe complexes increases the overall charge of the complex and thus the electrophilicity of the metal.[148,149,164,181] For example, the reaction of Fe− and Ru− bMepi complexes with MeOTf converts the X-type amido ligand into a neutral L-type imino ligand (e.g., Figure 2-20).[68,148,149] The enhanced electrophilicity can be characterized by voltammetry experiments, and the alkylated complex Fe(bMepi^{Me})(OTf)$_2$ exhibits an anodic shift of 390 mV relative to Fe(bMepi)(THF)(OTf). Thus, a simple late-stage modification that transforms an anionic ligand into a neutral ligand provides access to metal complexes that are more easily reduced. When the alkylated Ru− and Fe−bMepi^{Me} complexes are used in place of the analogous bMepi complexes, improved reactivity and/or selectivity is observed for Fe-catalyzed hydroboration of alkenes[148] and Ru-catalyzed H/D exchange reactions.[149]

The application of electrophilic bMepi^{Me} catalysts is highlighted with a unique hydrogen transfer method for stereoretentive H/D exchange.[149] Racemization of a chiral center typically occurs during the H/D exchange of alcohols and amines with a metal−hydride catalyst: following dehydrogenation, the prochiral ketone or imine intermediate can undergo reversible *β*-hydride elimination and ligand dissociation.[97] Rotation of the prochiral intermediate and reinsertion of deuterium can occur on either face of the sp^2 carbon−oxygen or carbon−nitrogen bond. A more electrophilic metal center may reduce the rate of substrate dissociation and mitigate erosion of stereochemistry (Figure 2-20). While the amine dehydrogenation catalyst HRu(bMepi)(PPh$_3$)$_2$ has a high binding affinity for nitrogen-containing substrates,[70] the chiral primary amine (*S*)-(−)-1-phenethylamine undergoes H/D exchange at the *α*-C−H bond with 90% ee (Figure 2-20, left).[182] The cationic complex [Ru(bMepi^{Me})(PPh$_3$)(OTf)]OTf (Figure 2-20, right) further mitigates

racemization.[183] H/D exchange of (*S*)-(−)-1-phenethylamine and other chiral amines using [Ru(bMepi^{Me})(PPh$_3$)(OTf)]OTf occurs with complete stereoretention (99% ee). In addition to the increased binding affinity for Ru−bMepi^{Me} compared with Ru−bMepi catalysts, enantiospecific coordination of the *α*-chiral amine substrate to the asymmetric bMepi^{Me} ligand may bias the deuteride insertion toward one face of the imine intermediate. This example highlights the practical application of remote modifications in the secondary sphere, where a facile late-stage alkylation enhances activity and selectivity through electronic and geometric perturbations of the primary sphere.

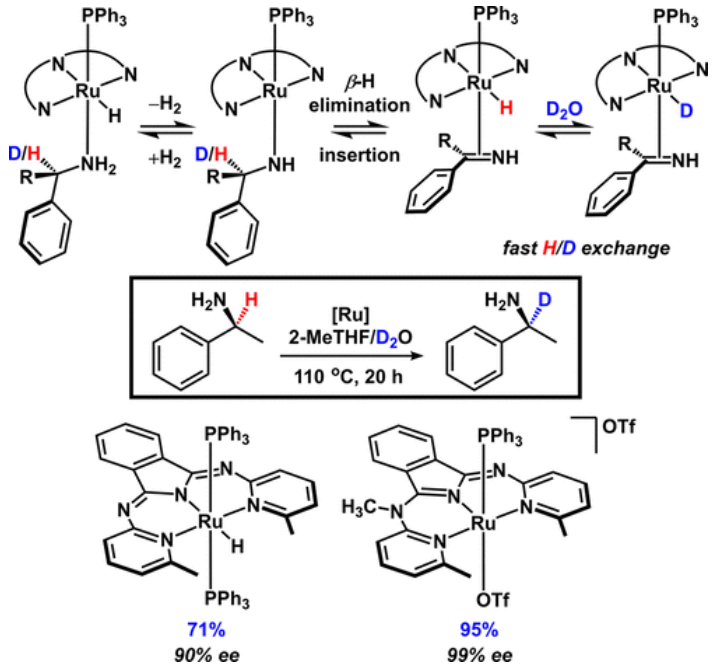

Figure 2-20. Requirements for stereoretentive H/D exchange of *α*-chiral amines by HRu(bMepi)(PPh$_3$)$_2$ and [Ru(bMepi^{Me})(PPh$_3$)(OTf)]OTf.

2.8 Summary and Outlook

Decades of research on discrete catalysts has focused on the primary coordination sphere, providing chemists with an expansive ligand library and powerful predictive tools for optimizing

a catalyst system. A similar systematic understanding of secondary-sphere effects is now being developed, leading to improved catalytic systems and the discovery of new approaches and catalytic transformations. Utilizing an extended ligand scaffold provides more variability in catalyst design. However, this is both advantageous and challenging from a synthetic perspective. Catalyst design strategies are still limited by our inability to accurately predict all possible metal, ligand, substrate, and solvent interactions during catalysis. Thus, the importance of understanding the properties of a discrete complex, such as acidity, hydricity, binding affinity, and decomposition pathways, cannot be understated.

In this Chapter, we have emphasized the synergistic role of outer-sphere and inner-sphere effects with a focus on hydrogen transfer and hydrofunctionalization reactions. In addition to mechanistic analyses, the consideration of pK_a and hydricity parameters for these metal−ligand systems is crucial. These parameters dictate the mechanism of H_2 and X−H activation and hydride transfer. The thermodynamic parameters of a metal−ligand complex also affect the extent of cooperative interactions in the secondary sphere. Protic groups in the secondary sphere can act as a proton reservoir or serve to orient and direct substrate coordination through non-covalent interactions.[8] This mechanistic distinction has broad implications for design strategies and will likely drive the advancement new cooperative catalysts.

The position of a protic group in the secondary sphere has a large impact on a catalytic system. Secondary sphere groups proximal to the metal center often exhibit dual substrate directing and electronic effects, while groups remote from the metal center can be utilized solely for electronic modifications. The function of both proximal and remote secondary-sphere groups relies on reversible non-covalent Lewis acid/base interactions, such as with alkali metal ions or boron-

based Lewis acids. Given the large scope of Lewis acid catalysis, there is a significant amount of chemical space to explore using acidic groups in the secondary sphere.

Finally, a major challenge for developing new catalyst systems with secondary-sphere interactions is the synthetic effort required for each new ligand design. Because it is difficult to determine the role of a functionalized ligand *a priori*, the large effort required to build each new ligand scaffold may slow the development of this field. However, major advances have been made with simple ligand scaffolds that enable late-stage functionalization, which is still an underutilized strategy in catalyst design. The application of post-metalation modifications to known catalyst systems and systematic comparisons to the unmodified catalysts will provide a strong foundation for developing more complex systems.

Among the various roles of secondary-sphere interactions in a metal−ligand complex, the stabilization of reactive intermediates and transition states is a common theme for productive catalysis. This is a fundamental concept for the rational design of catalysts and can be applied beyond hydrogen transfer and hydrofunctionalization reactions. State-of-the-art catalysts are currently being developed that incorporate Lewis acids into a metal−ligand scaffold to stabilize electron-rich first row metals or initiate halide transfer.[178] We believe that further exploration of through-space non-covalent interactions, such as ion-pair and dispersive or repulsive interactions, represents a highly promising direction for catalyst design.[4,142,184]

2.9 Notes and References

(1) Shook, R. L.; Borovik, A. S. Role of the Secondary Coordination Sphere in Metal-Mediated Dioxygen Activation. *Inorg. Chem.* **2010**, 49, 3646−3660.

(2) Lucas, R. L.; Zart, M. K.; Murkerjee, J.; Sorrell, T. N.; Powell, D. R.; Borovik, A. S. A Modular Approach toward Regulating the Secondary Coordination Sphere of Metal Ions: Differential Dioxygen Activation Assisted by Intramolecular Hydrogen Bonds. *J. Am. Chem. Soc.* **2006**, 128, 15476−15489.

(3) Zhao, M.; Wang, H.-B.; Ji, L.-N.; Mao, Z.-W. Insights into Metalloenzyme Microenvironments: Biomimetic Metal Complexes with a Functional Second Coordination Sphere. *Chem. Soc. Rev.* **2013**, 42, 8360−8375.

(4) Lu, G.; Liu, R. Y.; Yang, Y.; Fang, C.; Lambrecht, D. S.; Buchwald, S. L.; Liu, P. Ligand−Substrate Dispersion Facilitates the Copper-Catalyzed Hydroamination of Unactivated Olefins. *J. Am. Chem. Soc.* **2017**, 139, 16548−16555.

(5) Colquhoun, H. M.; Stoddart, J. F.; Williams, D. J. Second-Sphere Coordination−a Novel Role for Molecular Receptors. *Angew. Chem., Int. Ed. Engl.* **1986**, 25, 487−507. Liu, Z.; Schneebeli, S. T.; Stoddart, J. F. Second-Sphere Coordination Revisited. *Chimia* **2014**, 68, 315−320.

(6) Cook, S. A.; Borovik, A. S. Molecular Designs for Controlling the Local Environments around Metal Ions. *Acc. Chem. Res.* **2015**, 48, 2407−2414.

(7) Dub, P. A.; Gordon, J. C. Metal−Ligand Bifunctional Catalysis: The "Accepted" Mechanism, the Issue of Concertedness, and the Function of the Ligand in Catalytic Cycles Involving Hydrogen Atoms. *ACS Catal*. **2017**, 7, 6635−6655.

(8) Maity, A.; Teets, T. S. Main Group Lewis Acid-Mediated Transformations of Transition-Metal Hydride Complexes. *Chem. Rev.* **2016**, 116, 8873−8911.

(9) Hazari, A.; Labinger, J. A.; Bercaw, J. E. A Versatile Ligand Platform That Supports Lewis Acid Promoted Migratory Insertion. *Angew. Chem., Int. Ed.* **2012**, 51, 8268−8271.

(10) Kita, M. R.; Miller, A. J. M. An Ion-Responsive Pincer-Crown Ether Catalyst System for Rapid and Switchable Olefin Isomerization. *Angew. Chem., Int. Ed.* **2017**, 56, 5498−5502.

(11) Bellini, R.; Reek, J. N. H. Application of Supramolecular Bidentate Hybrid Ligands in Asymmetric Hydroformylation. *Chem. - Eur. J.***2012**, 18, 13510−13519.

(12) Rakowski Dubois, M.; Dubois, D. L. Development of Molecular Electrocatalysts for CO_2 Reduction and H_2 Production/Oxidation. *Acc. Chem. Res.* **2009**, 42, 1974−1982.

(13) Dahl, E. W.; Louis-Goff, T.; Szymczak, N. K. Second Sphere Ligand Modifications Enable a Recyclable Catalyst for Oxidant-Free Alcohol Oxidation to Carboxylates. *Chem. Commun*. **2017**, 53, 2287− 2289.

(14) Geri, J. B.; Szymczak, N. K. A Proton-Switchable Bifunctional Ruthenium Complex That Catalyzes Nitrile Hydroboration. *J. Am. Chem. Soc.* **2015**, 137, 12808−12814.

(15) Mahadevi, A. S.; Sastry, G. N. Cooperativity in Noncovalent Interactions. *Chem. Rev*. **2016**, 116, 2775−2825.

(16) Metal Mediated Template Synthesis of Ligands; Costisor, O., Linert, W.; Eds.; World Scientific: Singapore, **2004**.

(17) Moore, C. M.; Szymczak, N. K. 6,6′-Dihydroxy Terpyridine: A Proton-Responsive Bifunctional Ligand and Its Application in Catalytic Transfer Hydrogenation of Ketones. *Chem. Commun*. **2013**, 49, 400−402.

(18) Berke, H. Conceptual Approach to the Reactivity of Dihydrogen. *ChemPhysChem* **2010**, 11, 1837−1849.

(19) Abdur-Rashid, K.; Fong, T. P.; Greaves, B.; Gusev, D. G.; Hinman, J. G.; Landau, S. E.; Lough, A. J.; Morris, R. H. An Acidity Scale for Phosphorus-Containing Compounds Including Metal Hydrides and Dihydrogen Complexes in THF: Toward the Unification of Acidity Scales. *J. Am. Chem. Soc.* **2000**, 122, 9155−9171.

(20) Morris, R. H. Brønsted−Lowry Acid Strength of Metal Hydride and Dihydrogen Complexes. *Chem. Rev*. **2016**, 116, 8588−8654.

(21) Bullock, R. M. Catalytic Ionic Hydrogenations. *Chem. - Eur. J.***2004**, 10, 2366−2374.

(22) Bullock, R. M. Ionic Hydrogenations. In Handbook of Homogeneous Hydrogenation; Wiley-VCH: Weinheim, Germany, **2008**; pp 153−197.

(23) Papish, E. T.; Magee, M. P.; Norton, J. R. Chapter 2 - Protonation of Transition Metal Hydrides to Give Dihydrogen Complexes: Mechanistic Implications and Catalytic Applications. In Recent Advances in Hydride Chemistry; Peruzzini, M., Poli, R., Eds.; Elsevier: Amsterdam, **2001**; pp 39−74.

(24) Rinne, B. L.; Lathem, A. P.; Heiden, Z. M. Influence of Intramolecular vs. Intermolecular Phosphonium-Borohydrides in Catalytic Hydrogen, Hydride, and Proton Transfer Reactions. *Dalton Trans.* **2017**, 46, 9382−9393.

(25) Jacobsen, H.; Berke, H. Chapter 4 - Hydridicity of Transition Metal Hydrides and Its Implications for Reactivity. In Recent Advances in Hydride Chemistry; Peruzzini, M., Poli, R., Eds.; Elsevier: Amsterdam, **2001**; pp 89−116.

(26) Wiedner, E. S.; Chambers, M. B.; Pitman, C. L.; Bullock, R. M.; Miller, A. J. M.; Appel, A. M. Thermodynamic Hydricity of Transition Metal Hydrides. *Chem. Rev.* **2016**, 116, 8655−8692.

(27) Heinekey, D. M.; Oldham, W. J., Jr. Coordination Chemistry of Dihydrogen. *Chem. Rev.* **1993**, 93, 913−926.

(28) Kubas, G. J. Fundamentals of H_2 Binding and Reactivity on Transition Metals Underlying Hydrogenase Function and H_2 Production and Storage. *Chem. Rev.* **2007**, 107, 4152−4205.

(29) Jessop, P. G.; Morris, R. H. Reactions of Transition Metal Dihydrogen Complexes. Coord. *Chem. Rev.* **1992**, 121, 155−284.

(30) Kubas, G. J. Heterolytic Splitting of H-H, Si-H, and Other σ Bonds on Electrophilic Metal Centers. Adv. *Inorg. Chem.* **2004**, 56, 127−177.

(31) Crabtree, R. H.; Siegbahn, P. E. M.; Eisenstein, O.; Rheingold, A. L.; Koetzle, T. F. A New Intermolecular Interaction: Unconventional Hydrogen Bonds with Element-Hydride Bonds as Proton Acceptor. *Acc. Chem. Res.* **1996**, 29, 348−354.

(32) Belkova, N. V.; Epstein, L. M.; Filippov, O. A.; Shubina, E. S. Hydrogen and Dihydrogen Bonds in the Reactions of Metal Hydrides. *Chem. Rev.* **2016**, 116, 8545−8587.

(33) Seino, H.; Misumi, Y.; Hojo, Y.; Mizobe, Y. Heterolytic H_2 Activation by Rhodium Thiolato Complexes Bearing the Hydrotris- (pyrazolyl)borato Ligand and Application to Catalytic Hydrogenation Under Mild Conditions. *Dalton Trans.* **2010**, 39, 3072−3082.

(34) Jessop, P. G.; Morris, R. H. Hydrogen/Deuterium Exchange Reactions of an Iridium Dithiol Complex. *Inorg. Chem.* **1993**, 32, 2236−2237.

(35) Schlaf, M.; Lough, A. J.; Morris, R. H. Dihydrogen Thiolate vs. Hydride Thiol: Reactivity of the Series of Complexes $MH(CO)(L)(PPh_3)_2$ (M = Ru, Os; L = Pyridine-2-Thiolate,

Quinoline-8-Thiolate) with Acid. X-ray Structure Determination of [Os(CO)(μ2-Spy)-(SpyH)(PPh_3)]2[BF4]2. *Organometallics* **1996**, 15, 4423−4436.

(36) Wang, W.-H.; Muckerman, J. T.; Fujita, E.; Himeda, Y. Mechanistic Insight through Factors Controlling Effective Hydrogenation of CO_2 Catalyzed by Bioinspired Proton-Responsive Iridium(III) Complexes. *ACS Catal*. **2013**, 3, 856−860.

(37) Wesselbaum, S.; Moha, V.; Meuresch, M.; Brosinski, S.; Thenert, K. M.; Kothe, J.; Stein, T. v.; Englert, U.; Hoelscher, M.; Klankermayer, J.; Leitner, W. Hydrogenation of Carbon Dioxide to Methanol Using a Homogeneous Ruthenium-Triphos Catalyst: From Mechanistic Investigations to Multiphase Catalysis. *Chem. Sci.* **2015**, 6, 693−704.

(38) Gellrich, U.; Khusnutdinova, J. R.; Leitus, G. M.; Milstein, D. Mechanistic Investigations of the Catalytic Formation of Lactams from Amines and Water with Liberation of H_2. *J. Am. Chem. Soc.* **2015**, 137, 4851−4859.

(39) Shvo, Y.; Czarkie, D.; Rahamim, Y.; Chodosh, D. F. A New Group of Ruthenium Complexes: Structure and Catalysis. *J. Am. Chem. Soc.* **1986**, 108, 7400−7402.

(40) vom Stein, T.; Meuresch, M.; Limper, D.; Schmitz, M.; Hoelscher, M.; Coetzee, J.; Cole-Hamilton, D. J.; Klankermayer, J.; Leitner, W. Highly Versatile Catalytic Hydrogenation of Carboxylic and Carbonic Acid Derivatives Using a Ru-Triphos Complex: Molecular Control over Selectivity and Substrate Scope. *J. Am. Chem. Soc.* **2014**, 136, 13217−13225.

(41) O, W. W. N.; Lough, A. J.; Morris, R. H. Factors Favoring Efficient Bifunctional Catalysis. Study of a Ruthenium(II) Hydrogenation Catalyst Containing an N-Heterocyclic Carbene with a Primary Amine Donor. *Organometallics* **2012**, 31, 2137−2151.

(42) Samouei, H.; Miloserdov, F. M.; Escudero-Adan, E. C.; Grushin, V. V. Solid-State Structure and Solution Reactivity of [(Ph3P)4Ru- (H)2] and Related Ru(II) Complexes Used in Catalysis: A Reinvestigation. *Organometallics* **2014**, 33, 7279−7283.

(43) Bullock, R. M.; Helm, M. L. Molecular Electrocatalysts for Oxidation of Hydrogen Using Earth-Abundant Metals: Shoving Protons around with Proton Relays. *Acc. Chem. Res.* **2015**, 48, 2017−2026.

(44) Almeida Lenero, K. Q.; Guari, Y.; Kamer, P. C. J.; van Leeuwen, P. W. N. M.; Donnadieu, B.; Sabo-Etienne, S.; Chaudret, B.; Lutz, M.; Spek, A. L. Heterolytic Activation of Dihydrogen by Platinum and Palladium Complexes. *Dalton Trans.* **2013**, 42, 6495−6512.

(45) Curtis, C. J.; Miedaner, A.; Ciancanelli, R.; Ellis, W. W.; Noll, B. C.; Rakowski DuBois, M.; DuBois, D. L. $[Ni(Et_2PCH_2NMeCH_2PEt_2)_2]^{2+}$ as a Functional Model for Hydrogenases. *Inorg. Chem.* **2003**, *42*, 216−227.

(46) Abdur-Rashid, K.; Clapham, S. E.; Hadzovic, A.; Harvey, J. N.; Lough, A. J.; Morris, R. H. Mechanism of the Hydrogenation of Ketones Catalyzed by *trans*-Dihydrido(diamine)ruthenium(II) Complexes. *J. Am. Chem. Soc.* **2002**, 124, 15104−15118.

(47) Liu, T.; Chen, S.; O'Hagan, M. J.; Rakowski DuBois, M.; Bullock, R. M.; DuBois, D. L. Synthesis, Characterization, and Reactivity of Fe Complexes Containing Cyclic Diazadiphosphine Ligands: The Role of the Pendant Base in Heterolytic Cleavage of H_2. *J. Am. Chem. Soc.* **2012**, 134, 6257−6272.

(48) Lough, A. J.; Park, S.; Ramachandran, R.; Morris, R. H. Switching On and Off a New Intramolecular Hydrogen-Hydrogen Interaction and the Heterolytic Splitting of Dihydrogen. Crystal and Molecular Structure of $[Ir\{H(\eta 1\text{-}SC_5H_4NH)\}_2(PCy_3)_2]BF_4$ $2.7CH_2Cl_2$. *J. Am. Chem. Soc.* **1994**, 116, 8356−8357.

(49) Hulley, E. B.; Welch, K. D.; Appel, A. M.; DuBois, D. L.; Bullock, R. M. Rapid, Reversible Heterolytic Cleavage of Bound H_2. *J. Am. Chem. Soc.* **2013**, 135, 11736−11739.

(50) Gruet, K.; Clot, E.; Eisenstein, O.; Lee, D. H.; Patel, B.; Macchioni, A.; Crabtree, R. H. Ion Pairing Effects in Intramolecular Heterolytic H_2 Activation in an Ir(III) Complex: A Combined Theoretical/Experimental Study. *New J. Chem.* **2003**, 27, 80−87.

(51) Chu, H. S.; Lau, C. P.; Wong, K. Y.; Wong, W. T. Intramolecular N-H···H-Ru Proton-Hydride Interaction in Ruthenium Complexes with (2-(Dimethylamino)ethyl)cyclopentadienyl and (3- (Dimethylamino)propyl)cyclopentadienyl Ligands. Hydrogenation of CO_2 to Formic Acid via the N-H···H-Ru Hydrogen-Bonded Complexes. *Organometallics* **1998**, 17, 2768−2777.

(52) Khusnutdinova, J. R.; Milstein, D. Metal−Ligand Cooperation. *Angew. Chem., Int. Ed.* **2015**, 54, 12236−12273.

(53) Tanaka, R.; Yamashita, M.; Nozaki, K. Catalytic Hydrogenation of Carbon Dioxide Using Ir(III)-Pincer Complexes. *J. Am. Chem. Soc.* **2009**, 131, 14168−14169.

(54) Annibale, V. T.; Song, D. Multidentate Actor Ligands as Versatile Platforms for Small Molecule Activation and Catalysis. *RSC Adv.* **2013**, 3, 11432−11449.

(55) Tseng, K.-N. T.; Rizzi, A. M.; Szymczak, N. K. Oxidant-Free Conversion of Primary Amines to Nitriles. *J. Am. Chem. Soc.* **2013**, 135, 16352−16355.

(56) Gunanathan, C.; Milstein, D. Metal-Ligand Cooperation by Aromatization-Dearomatization: A New Paradigm in Bond Activation and "Green" Catalysis. *Acc. Chem. Res.* **2011**, 44, 588−602.

(57) Chen, S.; Ho, M.-H.; Bullock, R. M.; DuBois, D. L.; Dupuis, M.; Rousseau, R.; Raugei, S. Computing Free Energy Landscapes: Application to Ni-Based Electrocatalysts with Pendant Amines for H_2 Production and Oxidation. *ACS Catal*. **2014**, 4, 229−242.

(58) Raugei, S.; DuBois, D. L.; Rousseau, R.; Chen, S.; Ho, M.-H.; Bullock, R. M.; Dupuis, M. Toward Molecular Catalysts by Computer. *Acc. Chem. Res.* **2015**, 48, 248−255.

(59) Helm, M. L.; Stewart, M. P.; Bullock, R. M.; DuBois, M. R.; DuBois, D. L. A Synthetic Nickel Electrocatalyst with a Turnover Frequency above 100,000 s−1 for H_2 Production. *Science* **2011**, 333, 863−866.

(60) Dupuis, M.; Chen, S.; Raugei, S.; DuBois, D. L.; Bullock, R. M. Comment on "New Insights in the Electrocatalytic Proton Reduction and Hydrogen Oxidation by Bioinspired Catalysts: A DFT Investigation. *J. Phys. Chem. A* **2011**, 115, 4861−4865.

(61) DuBois, D. L.; Bullock, R. M. Molecular Electrocatalysts for the Oxidation of Hydrogen and the Production of Hydrogen − the Role of Pendant Amines as Proton Relays. *Eur. J. Inorg. Chem.* **2011**, **2011**, 1017−1027.

(62) Kilgore, U. J.; Roberts, J. A. S.; Pool, D. H.; Appel, A. M.; Stewart, M. P.; DuBois, M. R.; Dougherty, W. G.; Kassel, W. S.; Bullock, R. M.; DuBois, D. L. [Ni(PPh2NC6H4X 2)2]2+ Complexes as Electrocatalysts for H_2 Production: Effect of Substituents, Acids, and Water on Catalytic Rates. *J. Am. Chem. Soc.* **2011**, 133, 5861−5872.

(63) Zhang, S.; Appel, A. M.; Bullock, R. M. Reversible Heterolytic Cleavage of the H⁻H Bond by Molybdenum Complexes: Controlling the Dynamics of Exchange between Proton and Hydride. *J. Am. Chem. Soc.* **2017**, 139, 7376−7387.

(64) Besora, M.; Lledos, A.; Maseras, F. Protonation of Transition Metal Hydrides: A Not So Simple Process. *Chem. Soc. Rev.* **2009**, 38, 957−966.

(65) Basallote, M. G.; Duran, J.; Fernandez-Trujillo, M. J.; Mańez, M. A.; Rodríguez de la Torre, J. Kinetics of Formation of Dihydrogen Complexes: Protonation of cis-$[FeH_2\{P(CH_2CH_2PPh_2)_3\}$ with Acids in Tetrahydrofuran. J. Chem. Soc., *Dalton Trans.* **1998**, 745−750.

(66) Osipova, E. S.; Belkova, N. V.; Epstein, L. M.; Filippov, O. A.; Kirkina, V. A.; Titova, E. M.; Rossin, A.; Peruzzini, M.; Shubina, E. S. Dihydrogen Bonding and Proton Transfer from MH and OH Acids to Group 10 Metal Hydrides [(^{t}BuPCP)MH] [^{t}BuPCP = κ3 -2,6-(^{t}Bu$_2$PCH$_2$)$_2$C$_6$H$_3$; M = Ni, Pd]. *Eur. J. Inorg. Chem.* **2016**, **2016**, 1415−1424.

(67) Tseng, K.-N. T.; Kampf, J. W.; Szymczak, N. K. Mechanism of N,N,N-Amide Ruthenium(II) Hydride Mediated Acceptorless Alcohol Dehydrogenation: Inner-Sphere B−H Elimination versus Outer Sphere Bifunctional Metal−Ligand Cooperativity. *ACS Catal*. **2015**, 5, 5468−5485.

(68) Csonka, R.; Speier, G.; Kaizer, J. Isoindoline-Derived Ligands and Applications. *RSC Adv.* **2015**, 5, 18401−18419.

(69) Hale, L. V. A.; Malakar, T.; Tseng, K.-N. T.; Zimmerman, P. M.; Paul, A.; Szymczak, N. K. The Mechanism of Acceptorless Amine Double Dehydrogenation by N,N,N-Amide Ruthenium(II) Hydrides: A Combined Experimental and Computational Study. *ACS Catal*. **2016**, 6, 4799−4813.

(70) de Boer, S. Y.; Korstanje, T. J.; La Rooij, S. R.; Kox, R.; Reek, J. N. H.; van der Vlugt, J. I. Ruthenium PNN(O) Complexes: Cooperative Reactivity and Application as Catalysts for Acceptorless Dehydrogenative Coupling Reactions. *Organometallics* **2017**, 36, 1541−1549.

(71) Moore, C. M.; Szymczak, N. K. Appended Functionality in Pincer Ligands. In Pincer and Pincer-Type Complexes; Szabo, K. J.,́ Wendt, O. F., Eds.; Wiley-VCH: Weinheim, Germany, **2014**; pp 71− 94.

(72) Moore, C. M.; Bark, B.; Szymczak, N. K. Simple Ligand Modifications with Pendent Oh Groups Dramatically Impact the Activity and Selectivity of Ruthenium Catalysts for Transfer Hydrogenation: The Importance of Alkali Metals. *ACS Catal*. **2016**, 6, 1981−1990.

(73) Shi, J.; Shang, S.; Hu, B.; Chen, D. Ruthenium NNN Complexes with a 2-Hydroxypyridylmethylene Fragment for Transfer Hydrogenation of Ketones. *Appl. Organomet. Chem.* **2018**, 32, e4100.

(74) Nieto, I.; Livings, M. S.; Sacci, J. B.; Reuther, L. E.; Zeller, M.; Papish, E. T. Transfer Hydrogenation in Water via a Ruthenium Catalyst with OH Groups near the Metal Center on a bipy Scaffold. *Organometallics* **2011**, 30, 6339−6342.

(75) Royer, A. M.; Rauchfuss, T. B.; Gray, D. L. Organoiridium Pyridonates and Their Role in the Dehydrogenation of Alcohols. *Organometallics* **2010**, 29, 6763−6768.

(76) Fujita, K.-I.; Tanaka, Y.; Kobayashi, M.; Yamaguchi, R. Homogeneous Perdehydrogenation and Perhydrogenation of Fused Bicyclic N-Heterocycles Catalyzed by Iridium Complexes Bearing a Functional Bipyridonate Ligand. *J. Am. Chem. Soc.* **2014**, 136, 4829− 4832.

(77) Hull, J. F.; Himeda, Y.; Wang, W.-H.; Hashiguchi, B.; Periana, R.; Szalda, D. J.; Muckerman, J. T.; Fujita, E. Reversible Hydrogen Storage Using CO_2 and a Proton-Switchable Iridium Catalyst in Aqueous Media under Mild Temperatures and Pressures. Nat. Chem. **2012**, 4, 383−388.

(78) Fujita, K.-i.; Kawahara, R.; Aikawa, T.; Yamaguchi, R. Hydrogen Production from a Methanol−Water Solution Catalyzed by an Anionic Iridium Complex Bearing a Functional Bipyridonate Ligand under Weakly Basic Conditions. *Angew. Chem., Int. Ed.* **2015**, 54, 9057−9060.

(79) Zeng, G.; Sakaki, S.; Fujita, K.-i.; Sano, H.; Yamaguchi, R. Efficient Catalyst for Acceptorless Alcohol Dehydrogenation: Interplay of Theoretical and Experimental Studies. *ACS Catal*. **2014**, 4, 1010− 1020.

(80) Wang, W.-H.; Hull, J. F.; Muckerman, J. T.; Fujita, E.; Himeda, Y. Second-Coordination-Sphere and Electronic Effects Enhance Iridium(III)-Catalyzed Homogeneous

Hydrogenation of Carbon Dioxide in Water near Ambient Temperature and Pressure. Energy Environ. Sci. **2012**, 5, 7923−7926.

(81) Onishi, N.; Xu, S.; Manaka, Y.; Suna, Y.; Wang, W.-H.; Muckerman, J. T.; Fujita, E.; Himeda, Y. CO_2 Hydrogenation Catalyzed by Iridium Complexes with a Proton-Responsive Ligand. *Inorg. Chem.* **2015**, 54, 5114−5123.

(82) Chakraborty, S.; Piszel, P. E.; Hayes, C. E.; Baker, R. T.; Jones, W. D. Highly Selective Formation of n-Butanol from Ethanol through the Guerbet Process: A Tandem Catalytic Approach. *J. Am. Chem. Soc.* **2015**, 137, 14264−14267.

(83) Chakraborty, S.; Piszel, P. E.; Brennessel, W. W.; Jones, W. D. A Single Nickel Catalyst for the Acceptorless Dehydrogenation of Alcohols and Hydrogenation of Carbonyl Compounds. *Organometallics* **2015**, 34, 5203−5206.

(84) Moore, C. M.; Dahl, E. W.; Szymczak, N. K. Beyond H_2: Exploiting 2-Hydroxypyridine as a Design Element from [Fe]- Hydrogenase for Energy-Relevant Catalysis. *Curr. Opin. Chem. Biol.* **2015**, 25, 9−17.

(85) Finkelmann, A. R.; Senn, H. M.; Reiher, M. Hydrogen Activation Mechanism of [Fe] Hydrogenase Revealed by Multi-Scale Modeling. *Chem. Sci.* **2014**, 5, 4474−4482.

(86) Gunanathan, C.; Milstein, D. Bond Activation and Catalysis by Ruthenium Pincer Complexes. *Chem. Rev.* **2014**, 114, 12024−12087.

(87) Kuwata, S.; Ikariya, T. Metal-Ligand Bifunctional Reactivity and Catalysis of Protic N-Heterocyclic Carbene and Pyrazole Complexes Featuring *β*-NH Units. *Chem. Commun.* **2014**, 50, 14290−14300.

(88) Bifunctional Molecular Catalysis; Ikariya, T., Shibasaki, M., Eds.; Topics in Organometallic Chemistry, Vol. 37; Springer: Berlin, **2011**.

(89) Dub, P. A.; Gordon, J. C. The Mechanism of Enantioselective Ketone Reduction with Noyori and Noyori-Ikariya Bifunctional Catalysts. *Dalton Trans.* **2016**, 45, 6756−6781.

(90) Dub, P. A.; Scott, B. L.; Gordon, J. C. Why Does Alkylation of the N−H Functionality within M/NH Bifunctional Noyori-Type Catalysts Lead to Turnover? *J. Am. Chem. Soc.* **2017**, 139, 1245−1260.

(91) Noyori, R.; Yamakawa, M.; Hashiguchi, S. Metal-Ligand Bifunctional Catalysis: A Nonclassical Mechanism for Asymmetric Hydrogen Transfer between Alcohols and Carbonyl Compounds. *J. Org. Chem.* **2001**, 66, 7931−7944.

(92) Yamakawa, M.; Ito, H.; Noyori, R. The Metal−Ligand Bifunctional Catalysis: A Theoretical Study on the Ruthenium(II)- Catalyzed Hydrogen Transfer between Alcohols and Carbonyl Compounds. *J. Am. Chem. Soc.* **2000**, 122, 1466−1478.

(93) Blum, Y.; Czarkie, D.; Rahamim, Y.; Shvo, Y. (Cyclopentadienone)Ruthenium Carbonyl Complexes - a New Class of Homogeneous Hydrogenation Catalysts. *Organometallics* 1985, 4, 1459−1461.

(94) Warner, M. C.; Casey, C. P.; Backvall, J.-E. Shvo¨ 's Catalyst in Hydrogen Transfer Reactions. *Top. Organomet. Chem.* **2011**, 37, 85− 125.

(95) Johnson, J. B.; Baeckvall, J.-E. Mechanism of Ruthenium Catalyzed Hydrogen Transfer Reactions. Concerted Transfer of OH and CH Hydrogens from an Alcohol to a (Cyclopentadienone) Ruthenium Complex. *J. Org. Chem.* **2003**, 68, 7681−7684.

(96) Conley, B. L.; Pennington-Boggio, M. K.; Boz, E.; Williams, T. J. Discovery, Applications, and Catalytic Mechanisms of Shvo's Catalyst. *Chem. Rev.* **2010**, 110, 2294−2312.

(97) Casey, C. P.; Guan, H. An Efficient and Chemoselective Iron Catalyst for the Hydrogenation of Ketones. *J. Am. Chem. Soc.* **2007**, 129, 5816−5817.

(98) Casey, C. P.; Guan, H. Cyclopentadienone Iron Alcohol Complexes: Synthesis, Reactivity, and Implications for the Mechanism of Iron-Catalyzed Hydrogenation of Aldehydes. *J. Am. Chem. Soc.* **2009**, 131, 2499−2507.

(99) Gelman, D.; Musa, S. Coordination Versatility of sp3 - Hybridized Pincer Ligands toward Ligand−Metal Cooperative Catalysis. *ACS Catal*. **2012**, 2, 2456−2466.

(100) Trincado, M.; Grützmacher, H. Cooperating Ligands in Catalysis. In Cooperative Catalysis; Wiley-VCH: Weinheim, Germany, **2015**; p 67−110.

(101) Dub, P. A.; Henson, N. J.; Martin, R. L.; Gordon, J. C. Unravelling the Mechanism of the Asymmetric Hydrogenation of Acetophenone by [RuX_2(Diphosphine)(1,2-Diamine)] Catalysts. *J. Am. Chem. Soc.* **2014**, 136, 3505−3521.

(102) Noyori, R.; Sandoval, C. A.; Muniz, K.; Ohkuma, T. Metal Ligand Bifunctional Catalysis for Asymmetric Hydrogenation. *Philos. Trans. R. Soc., A* **2005**, 363, 901−912.

(103) Noyori, R.; Kitamura, M.; Ohkuma, T. Toward Efficient Asymmetric Hydrogenation: Architectural and Functional Engineering of Chiral Molecular Catalysts. *Proc. Natl. Acad. Sci. U. S. A.* **2004**, 101, 5356−5362.

(104) Fryzuk, M. D.; MacNeil, P. A.; Rettig, S. J. Stereoselective Formation of Rhodium and Iridium Hydrides via Intramolecular Hydrogen Bonding. *J. Am. Chem. Soc.* 1987, 109, 2803−2812.

(105) Noyori, R.; Koizumi, M.; Ishii, D.; Ohkuma, T. Asymmetric Hydrogenation via Architectural and Functional Molecular Engineering. *Pure Appl. Chem.* **2001**, 73, 227−232.

(106) Abdur-Rashid, K.; Lough, A. J.; Morris, R. H. Ruthenium Dihydride $RuH_2(PPh_3)_2$((R,R)-Cyclohexyldiamine) and Ruthenium Monohydride $RuHCl(PPh_3)_2$((R,R)-Cyclohexyldiamine): Active Catalyst and Catalyst Precursor for the Hydrogenation of Ketones and Imines. *Organometallics* **2000**, 19, 2655−2657.

(107) Abdur-Rashid, K.; Faatz, M.; Lough, A. J.; Morris, R. H. Catalytic Cycle for the Asymmetric Hydrogenation of Prochiral Ketones to Chiral Alcohols: Direct Hydride and Proton Transfer from Chiral Catalysts Trans-Ru(H)2(Diphosphine)(Diamine) to Ketones and Direct Addition of Dihydrogen to the Resulting Hydridoamido Complexes. *J. Am. Chem. Soc.* **2001**, 123, 7473−7474.

(108) Hartmann, R.; Chen, P. Noyori's Hydrogenation Catalyst Needs a Lewis Acid Cocatalyst for High Activity. *Angew. Chem., Int. Ed.* **2001**, 40, 3581−3585.

(109) Miller, A. J. M.; Labinger, J. A.; Bercaw, J. E. Homogeneous Co Hydrogenation: Dihydrogen Activation Involves a Frustrated Lewis Pair Instead of a Platinum Complex. *J. Am. Chem. Soc.* **2010**, 132, 3301−3303.

(110) Miller, A. J. M.; Labinger, J. A.; Bercaw, J. E. Reductive Coupling of Carbon Monoxide in a Rhenium Carbonyl Complex with Pendant Lewis Acids. *J. Am. Chem. Soc.* **2008**, 130, 11874−11875.

(111) Tseng, K.-N. T.; Kampf, J. W.; Szymczak, N. K. Modular Attachment of Appended Boron Lewis Acids to a Ruthenium Pincer Catalyst: Metal−Ligand Cooperativity Enables Selective Alkyne Hydrogenation. *J. Am. Chem. Soc.* **2016**, 138, 10378−10381.

(112) Chakraborty, S.; Brennessel, W. W.; Jones, W. D. A Molecular Iron Catalyst for the Acceptorless Dehydrogenation and Hydrogenation of N-Heterocycles. *J. Am. Chem. Soc.* **2014**, 136, 8564−8567.

(113) Gusev, D. G. Dehydrogenative Coupling of Ethanol and Ester Hydrogenation Catalyzed by Pincer-Type YNP Complexes. *ACS Catal*. **2016**, 6, 6967−6981.

(114) Filonenko, G. A.; van Putten, R.; Hensen, E. J. M.; Pidko, E. A. Catalytic (De)Hydrogenation Promoted by Non-Precious Metals - Co, Fe and Mn: Recent Advances in an Emerging Field. *Chem. Soc. Rev.* **2018**, 47, 1459−1483.

(115) Qu, S.; Dai, H.; Dang, Y.; Song, C.; Wang, Z.-X.; Guan, H. Computational Mechanistic Study of Fe-Catalyzed Hydrogenation of Esters to Alcohols: Improving Catalysis by Accelerating Precatalyst Activation with a Lewis Base. *ACS Catal*. **2014**, 4, 4377−4388.

(116) Sawatlon, B.; Surawatanawong, P. Mechanisms for Dehydrogenation and Hydrogenation of N-Heterocycles Using PNP-Pincer Supported Iron Catalysts: A Density Functional Study. *Dalton Trans.* **2016**, 45, 14965−14978.

(117) Mukherjee, A.; Nerush, A.; Leitus, G.; Shimon, L. J. W.; Ben David, Y.; Espinosa Jalapa, N. A.; Milstein, D. Manganese-Catalyzed Environmentally Benign Dehydrogenative Coupling of Alcohols and Amines to Form Aldimines and H_2: A Catalytic and Mechanistic Study. *J. Am. Chem. Soc.* **2016**, 138, 4298−4301.

(118) Butschke, B.; Feller, M.; Diskin-Posner, Y.; Milstein, D. Ketone Hydrogenation Catalyzed by a New Iron(II)-PNN Complex. *Catal. Sci. Technol.* **2016**, 6, 4428−4437.

(119) Gorgas, N.; Stöger, B.; Veiros, L. F.; Pittenauer, E.; Allmaier, G.; Kirchner, K. Efficient Hydrogenation of Ketones and Aldehydes Catalyzed by Well-Defined Iron(II) PNP Pincer Complexes: Evidence for an Insertion Mechanism. *Organometallics* **2014**, 33, 6905−6914.

(120) Langer, R.; Iron, M. A.; Konstantinovski, L.; Diskin-Posner, Y.; Leitus, G.; Ben-David, Y.; Milstein, D. Iron Borohydride Pincer Complexes for the Efficient Hydrogenation of Ketones

under Mild, Base-Free Conditions: Synthesis and Mechanistic Insight. *Chem. - Eur. J.***2012**, 18, 7196−7209.

(121) Yang, X. Hydrogenation of Carbon Dioxide Catalyzed by PNP Pincer Iridium, Iron, and Cobalt Complexes: A Computational Design of Base Metal Catalysts. *ACS Catal*. **2011**, 1, 849−854.

(122) Yang, X. Unexpected Direct Reduction Mechanism for Hydrogenation of Ketones Catalyzed by Iron PNP Pincer Complexes. *Inorg. Chem.* **2011**, 50, 12836−12843.

(123) Filonenko, G. A.; Smykowski, D.; Szyja, B. M.; Li, G.; Szczygieł, J.; Hensen, E. J. M.; Pidko, E. A. Catalytic Hydrogenation of CO_2 to Formates by a Lutidine-Derived Ru−CNC Pincer Complex: Theoretical Insight into the Unrealized Potential. *ACS Catal*. **2015**, 5, 1145−1154.

(124) Li, H.; Hall, M. B. Computational Mechanistic Studies on Reactions of Transition Metal Complexes with Noninnocent Pincer Ligands: Aromatization−Dearomatization or Not. *ACS Catal*. **2015**, 5, 1895−1913.

(125) Chen, X.; Yang, X. Mechanistic Insights and Computational Design of Transition-Metal Catalysts for Hydrogenation and Dehydrogenation Reactions. Chem. Rec. **2016**, 16, 2364−2378.

(126) Wei, Z.; Junge, K.; Beller, M.; Jiao, H. Hydrogenation of Phenyl-Substituted C=N, C≡N, C=C, C≡C and C=O Functional Groups by Cr, Mo and W PNP Pincer Complexes - a DFT Study. *Catal. Sci. Technol.* **2017**, 7, 2298−2307.

(127) Lu, Y.; Liu, Z.; Guo, J.; Qu, S.; Zhao, R.; Wang, Z.-X. A DFT Study Unveils the Secret of How H_2 Is Activated in the N-Formylation of Amines with CO_2 and H_2 Catalyzed by Ru(II) Pincer Complexes in the Absence of Exogenous Additives. *Chem. Commun*. **2017**, 53, 12148−12151.

(128) Hou, C.; Zhang, Z.; Zhao, C.; Ke, Z. DFT Study of Acceptorless Alcohol Dehydrogenation Mediated by Ruthenium Pincer Complexes: Ligand Tautomerization Governing Metal Ligand Cooperation. *Inorg. Chem.* **2016**, 55, 6539−6551.

(129) Bertini, F.; Gorgas, N.; Stöger, B.; Peruzzini, M.; Veiros, L. F.; Kirchner, K.; Gonsalvi, L. Efficient and Mild Carbon Dioxide Hydrogenation to Formate Catalyzed by Fe(II) Hydrido

Carbonyl Complexes Bearing 2,6-(Diaminopyridyl)Diphosphine Pincer Ligands. *ACS Catal*. **2016**, 6, 2889−2893.

(130) Bertini, F.; Glatz, M.; Gorgas, N.; Stoger, B.; Peruzzini, M.; Veiros, L. F.; Kirchner, K.; Gonsalvi, L. Carbon Dioxide Hydrogenation Catalysed by Well-Defined Mn(I) PNP Pincer Hydride Complexes. *Chem. Sci.* **2017**, 8, 5024−5029.

(131) Filonenko, G. A.; Conley, M. P.; Coperet, C.; Lutz, M.;́ Hensen, E. J. M.; Pidko, E. A. The Impact of Metal−Ligand Cooperation in Hydrogenation of Carbon Dioxide Catalyzed by Ruthenium PNP Pincer. *ACS Catal*. **2013**, 3, 2522−2526.

(132) Gorgas, N.; Alves, L. G.; Stö ger, B.; Martins, A. M.; Veiros, L. F.; Kirchner, K. Stable, yet Highly Reactive Nonclassical Iron(II) Polyhydride Pincer Complexes: Z-Selective Dimerization and Hydroboration of Terminal Alkynes. *J. Am. Chem. Soc.* **2017**, 139, 8130−8133.

(133) Gorgas, N.; Stö ger, B.; Veiros, L. F.; Kirchner, K. Highly Efficient and Selective Hydrogenation of Aldehydes: A Well-Defined Fe(II) Catalyst Exhibits Noble-Metal Activity. *ACS Catal*. **2016**, 6, 2664−2672.

(134) Langer, R.; Leitus, G.; Ben-David, Y.; Milstein, D. Efficient Hydrogenation of Ketones Catalyzed by an Iron Pincer Complex. *Angew. Chem., Int. Ed.* **2011**, 50, 2120−2124.

(135) Warshel, A.; Sharma, P. K.; Kato, M.; Xiang, Y.; Liu, H.; Olsson, M. H. M. Electrostatic Basis for Enzyme Catalysis. *Chem. Rev.* **2006**, 106, 3210−3235.

(136) Knowles, R. R.; Jacobsen, E. N. Attractive Noncovalent Interactions in Asymmetric Catalysis: Links between Enzymes and Small Molecule Catalysts. *Proc. Natl. Acad. Sci. U. S. A.* **2010**, 107, 20678−20685.

(137) Yamakawa, M.; Yamada, I.; Noyori, R. CH/π Attraction: The Origin of Enantioselectivity in Transfer Hydrogenation of Aromatic Carbonyl Compounds Catalyzed by Chiral η6 -Arene-Ruthenium(II) Complexes. *Angew. Chem., Int. Ed.* **2001**, 40, 2818−2821.

(138) Fang, X.; Sun, M.; Zheng, J.; Li, B.; Ye, L.; Wang, X.; Cao, Z.; Zhu, H.; Yuan, Y. CH2 Linkage Effects on the Reactivity of Bis(Aminophosphine)−Ruthenium Complexes for Selective Hydrogenation of Esters into Alcohols. *Sci. Rep.* **2017**, 7, 3961.

(139) Chattopadhyay, B.; Dannatt, J. E.; Andujar-De Sanctis, I. L.; Gore, K. A.; Maleczka, R. E.; Singleton, D. A.; Smith, M. R. Ir-Catalyzed Ortho-Borylation of Phenols Directed by Substrate−Ligand Electrostatic Interactions: A Combined Experimental/in Silico Strategy for Optimizing Weak Interactions. *J. Am. Chem. Soc.* **2017**, 139, 7864−7871.

(140) Davis, H. J.; Mihai, M. T.; Phipps, R. J. Ion Pair-Directed Regiocontrol in Transition-Metal Catalysis: A Meta-Selective C−H Borylation of Aromatic Quaternary Ammonium Salts. *J. Am. Chem. Soc.* **2016**, 138, 12759−12762.

(141) Kuninobu, Y.; Ida, H.; Nishi, M.; Kanai, M. A Meta-Selective C−H Borylation Directed by a Secondary Interaction between Ligand and Substrate. Nat. Chem. **2015**, 7, 712.

(142) Crabtree, R. H. Deactivation in Homogeneous Transition Metal Catalysis: Causes, Avoidance, and Cure. *Chem. Rev.* **2015**, 115, 127−150.

(143) Huff, C. A.; Kampf, J. W.; Sanford, M. S. Role of a Noninnocent Pincer Ligand in the Activation of CO_2 at (PNN)Ru- (H)(CO). *Organometallics* **2012**, 31, 4643−4645.

(144) Vogt, M.; Gargir, M.; Iron, M. A.; Diskin-Posner, Y.; Ben David, Y.; Milstein, D. A New Mode of Activation of CO_2 by Metal− Ligand Cooperation with Reversible C−C and M−O Bond Formation at Ambient Temperature. *Chem. - Eur. J.***2012**, 18, 9194−9197.

(145) Lu, Z.; Conley, B. L.; Williams, T. J. A Three-Stage Mechanistic Model for Ammonia−Borane Dehydrogenation by Shvo's Catalyst. *Organometallics* **2012**, 31, 6705−6714.

(146) Zhang, X.; Kam, L.; Trerise, R.; Williams, T. J. RutheniumCatalyzed Ammonia Borane Dehydrogenation: Mechanism and Utility. *Acc. Chem. Res.* **2017**, 50, 86−95.

(147) Tseng, K.-N. T.; Kampf, J. W.; Szymczak, N. K. Regulation of Iron-Catalyzed Olefin Hydroboration by Ligand Modifications at a Remote Site. *ACS Catal*. **2015**, 5, 411−415.

(148) Hale, L. V. A.; Szymczak, N. K. Stereoretentive Deuteration of α-Chiral Amines with D_2O. *J. Am. Chem. Soc.* **2016**, 138, 13489− 13492.

(149) Liberman-Martin, A. L.; Levine, D. S.; Liu, W.; Bergman, R. G.; Tilley, T. D. Biaryl Reductive Elimination Is Dramatically Accelerated by Remote Lewis Acid Binding to a 2,2′-Bipyrimidyl−Platinum Complex: Evidence for a Bidentate Ligand Dissociation Mechanism. *Organometallics* **2016**, 35, 1064−1069.

(150) Liberman-Martin, A. L.; Bergman, R. G.; Tilley, T. D. A Remote Lewis Acid Trigger Dramatically Accelerates Biaryl Reductive Elimination from a Platinum Complex. *J. Am. Chem. Soc.* **2013**, 135, 9612−9615.

(151) Huang, J.; Haar, C. M.; Nolan, S. P.; Marcone, J. E.; Moloy, K. G. Lewis Acids Accelerate Reductive Elimination of RCN from P2Pd(R)(CN). *Organometallics* 1999, 18, 297−299.

(152) Shen, Q.; Hartwig, J. F. Lewis Acid Acceleration of C−N Bond-Forming Reductive Elimination from Heteroarylpalladium Complexes and Catalytic Amidation of Heteroaryl Bromides. *J. Am. Chem. Soc.* **2007**, 129, 7734−7735.

(153) Dixon, N. A.; McQuarters, A. B.; Kraus, J. S.; Soffer, J. B.; Lehnert, N.; Schweitzer-Stenner, R.; Papish, E. T. Dramatic Tuning of Ligand Donor Properties in (Ttz)CuCO through Remote Binding of H+ (Ttz = Hydrotris(triazolyl)borate). *Chem. Commun*. **2013**, 49, 5571−5573.

(154) Cesar, V.; Lugan, N.; Lavigne, G. Electronic Tuning of a′ Carbene Center via Remote Chemical Induction, and Relevant Effects in Catalysis. *Chem. - Eur. J.***2010**, 16, 11432−11442.

(155) Horak, K. T.; VanderVelde, D. G.; Agapie, T. Tuning of Metal Complex Electronics and Reactivity by Remote Lewis Acid Binding to π-Coordinated Pyridine Diphosphine Ligands. *Organometallics* **2015**, 34, 4753−4765.

(156) Azoulay, J. D.; Rojas, R. S.; Serrano, A. V.; Ohtaki, H.; Galland, G. B.; Wu, G.; Bazan, G. C. Nickel *α*-Keto-*β*-Diimine Initiators for Olefin Polymerization. *Angew. Chem., Int. Ed.* **2009**, 48, 1089−1092.

(157) Lambic, N. S.; Brown, C. A.; Sommer, R. D.; Ison, E. A. Dramatic Increase in the Rate of Olefin Insertion by Coordination of Lewis Acids to the Oxo Ligand in Oxorhenium(V) Hydrides. *Organometallics* **2017**, 36, 2042−2051.

(158) Xu, T.; Wodrich, M. D.; Scopelliti, R.; Corminboeuf, C.; Hu, X. Nickel Pincer Model of the Active Site of Lactate Racemase Involves Ligand Participation in Hydride Transfer. *Proc. Natl. Acad. Sci. U. S. A.* **2017**, 114, 1242−1245.

(159) Liberman-Martin, A. L.; Ziegler, M. S.; DiPasquale, A. G.; Bergman, R. G.; Tilley, T. D. Functionalization of an Iridium− Diamidocarbene Complex by Ligand-Based Reactions with Titanocene and Zirconocene Sources. *Polyhedron* **2016**, 116, 111−115.

(160) Cisnetti, F.; Gibard, C.; Gautier, A. Post-Functionalization of Metal−NHC Complexes: A Useful Toolbox for Bioorganometallic Chemistry (and Beyond)? J. Organomet. Chem. **2015**, 782, 22−30.

(161) Lee, B. Y.; Bazan, G. C.; Vela, J.; Komon, Z. J. A.; Bu, X. αIminocarboxamidato−Nickel(II) Ethylene Polymerization Catalysts. *J. Am. Chem. Soc.* **2001**, 123, 5352−5353.

(162) Kim, Y. H.; Kim, T. H.; Lee, B. Y.; Woodmansee, D.; Bu, X.; Bazan, G. C. A-Iminoenamido Ligands: A Novel Structure for Transition-Metal Activation. *Organometallics* 2002, 21, 3082−3084.

(163) Brennan, C.; Draksharapu, A.; Browne, W. R.; McGarvey, J. J.; Vos, J. G.; Pryce, M. T. Unexpected Reversible Pyrazine Based Methylation in a Ru(II) Complex Bearing a Pyrazin-2′-yl-1,2,4- triazolato Ligand and Its Effect on Acid/Base and Photophysical Properties. *Dalton Trans.* **2013**, 42, 2546−2555.

(164) Zhang, J.; Bellomo, A.; Trongsiriwat, N.; Jia, T.; Carroll, P. J.; Dreher, S. D.; Tudge, M. T.; Yin, H.; Robinson, J. R.; Schelter, E. J.; Walsh, P. J. Nixantphos: A Deprotonatable Ligand for Room Temperature Palladium-Catalyzed Cross-Couplings of Aryl Chlorides. *J. Am. Chem. Soc.* **2014**, 136, 6276−6287.

(165) Osborn, J. A.; Jardine, F. H.; Young, J. F.; Wilkinson, G. The Preparation and Properties of Tris(Triphenylphosphine)- Halogenorhodium(I) and Some Reactions Thereof Including Catalytic Homogeneous Hydrogenation of Olefins and Acetylenes and Their Derivatives. J. Chem. Soc. *A* **1966**, 1711−1732.

(166) Candlin, J. P.; Oldham, A. R. Selective Hydrogenation of Unsaturated Carbon-Carbon Bonds with Rhodium Complexes. *Discuss. Faraday Soc.* **1968**, 46, 60−71.

(167) Schrock, R. R.; Osborn, J. A. Catalytic Hydrogenation Using Cationic Rhodium Complexes. I. Evolution of the Catalytic System and the Hydrogenation of Olefins. *J. Am. Chem. Soc.* **1976**, 98, 2134− 2143.

(168) Schrock, R. R.; Osborn, J. A. Catalytic Hydrogenation Using Cationic Rhodium Complexes. 3. The Selective Hydrogenation of Dienes to Monoenes. *J. Am. Chem. Soc.* **1976**, 98, 4450−4455.

(169) Schrock, R. R.; Osborn, J. A. Catalytic Hydrogenation Using Cationic Rhodium Complexes. II. The Selective Hydrogenation of Alkynes to Cis Olefins. *J. Am. Chem. Soc.* **1976**, 98, 2143−2147.

(170) Burk, M. J.; Gross, M. F.; Martinez, J. P. Asymmetric Catalytic Synthesis of *β*-Branched Amino Acids via Highly Enantioselective Hydrogenation of *α*-Enamides. *J. Am. Chem. Soc.* **1995**, 117, 9375− 9376.

(171) Kraft, S.; Ryan, K.; Kargbo, R. B. Recent Advances in Asymmetric Hydrogenation of Tetrasubstituted Olefins. *J. Am. Chem. Soc.* **2017**, 139, 11630−11641.

(172) Crabtree, R. Iridium Compounds in Catalysis. *Acc. Chem. Res.* **1979**, 12, 331−337.

(173) Thomas, J. C.; Peters, J. C. Zwitterionic and Cationic Bis(Phosphine) Platinum(II) Complexes: Structural, Electronic, and Mechanistic Comparisons Relevant to Ligand Exchange and Benzene C−H Activation Processes. *J. Am. Chem. Soc.* **2003**, 125, 8870−8888.

(174) Stradiotto, M.; Hesp, K. D.; Lundgren, R. J. Zwitterionic Relatives of Cationic Platinum Group Metal Complexes: Applications in Stoichiometric and Catalytic σ-Bond Activation. *Angew. Chem., Int. Ed.* **2010**, 49, 494−512.

(175) Kendall, A. J.; Zakharov, L. N.; Tyler, D. R. Steric and Electronic Influences of Buchwald-Type Alkyl-Johnphos Ligands. *Inorg. Chem.* **2016**, 55, 3079−3090.

(176) Cooney, K. D.; Cundari, T. R.; Hoffman, N. W.; Pittard, K. A.; Temple, M. D.; Zhao, Y. *a priori* Assessment of the Stereoelectronic Profile of Phosphines and Phosphites. *J. Am. Chem. Soc.* **2003**, 125, 4318−4324.

(177) Guan, W.; Zeng, G.; Kameo, H.; Nakao, Y.; Sakaki, S. Cooperative Catalysis of Combined Systems of Transition-Metal Complexes with Lewis Acids: Theoretical Understanding. *Chem. Rec.* **2016**, 16, 2405−2425.

(178) Gao, Y.; Guan, C.; Zhou, M.; Kumar, A.; Emge, T. J.; Wright, A. M.; Goldberg, K. I.; Krogh-Jespersen, K.; Goldman, A. S. B-Hydride Elimination and C−H Activation by an

Iridium Acetate Complex, Catalyzed by Lewis Acids. Alkane Dehydrogenation Cocatalyzed by Lewis Acids and [2,6-Bis(4,4-dimethyloxazolinyl)-3,5- dimethylphenyl]iridium. *J. Am. Chem. Soc.* **2017**, 139, 6338−6350.

(179) Liberman-Martin, A. L.; Levine, D. S.; Ziegler, M. S.; Bergman, R. G.; Tilley, T. D. Lewis Acid-Base Interactions between Platinum(II) Diaryl Complexes and Bis(Perfluorophenyl)Zinc: Strongly Accelerated Reductive Elimination Induced by a Z-Type Ligand. *Chem. Commun*. **2016**, 52, 7039−7042.

(180) Fanni, S.; Murphy, S.; Killeen, J. S.; Vos, J. G. Site-Specific Methylation of Coordinated 1,2,4-Triazoles: A Novel Route to Sterically Hindered $Ru(bpy)_2$ Complexes. *Inorg. Chem.* **2000**, 39, 1320−1321.

(181) In contrast, the exergonic dissociation of oxygen-containing substrates results in the full racemization of chiral alcohols. See ref 149.

(182) The binding affinity of the prochiral imine intermediate approximately doubles when the Ru−bMepiMe catalyst is used instead of the Ru−bMepi catalyst. Computational analysis of Ru−η1 -imine intermediates revealed binding energies of 4.5 kcal/mol for $LRu(bMepi)(PPh_3)$ and 8.3 kcal/mol for $LRu(bMepiMe)(PPh_3)$ (L = 1-phenylethan-1-imine) calculated at the rB3LYP/6-31g(d,p)(for C, H, N, and P)/SDD(for Ru)//PCM(benzene) level.

(183) Lau, V. M.; Pfalzgraff, W. C.; Markland, T. E.; Kanan, M. W. Electrostatic Control of Regioselectivity in Au(I)-Catalyzed Hydroarylation. *J. Am. Chem. Soc.* **2017**, 139, 4035−4041.

Chapter 3: The Mechanism of Acceptorless Amine Double Dehydrogenation by *N*,*N*,*N*-Amide Ruthenium(II) Hydrides: A Combined Experimental and Computational Study

Portions of this chapter have been published:
Hale, L. V. A.; Malakar, T.; Tseng, K.-T.; Zimmerman, P. M.; Paul, A.; Szymczak, N. K Szymczak, N. K.; The Mechanism of Acceptorless Amine Double Dehydrogenation by *N*,*N*,*N*-Amide Ruthenium(II) Hydrides: A Combined Experimental and Computational Study. *ACS Catal.* **2016**, *6*, 4799-4813

3.1 Introduction

Strategies to prepare nitriles with high atom-economy are broadly needed due to the abundance of this functional group in natural products,[1] industrial applications, [2] and for further synthetic elaboration.[3] One of many strategies to access nitrile-containing compounds is through the oxidation of primary amines using stoichiometric inorganic,[4] iodine-based oxidants,[5] or more recently through transition-metal-catalyzed aerobic oxidation.[6] However, these methods often require (super)stoichiometric quantities of oxidants and/or base, which necessarily produces stoichiometric waste byproducts. Furthermore, the use of an oxidant requires oxidant-compatible functional groups, limiting the synthetic scope of amine oxidation procedures.H_2 activation and hydrogenation by 2-hydroxypyridine ligands.

Transition-metal-catalyzed double dehydrogenation of primary amines represents an alternative atom-economical strategy by avoiding the use of stoichiometric oxidants. Under acceptorless conditions,[7] the reaction is driven by the removal of H_2 gas as the only byproduct

(Figure 3-1, left). Unfortunately, reports of primary amine double dehydrogenation are scarce and most known catalysts are either low yielding[8] or require exogenous base and/or hydrogen acceptors.[9)] For example, the iridium-pincer complex, $[C_6H_3\text{-}2,6\text{-}(OP^tBu_2)_2]IrH_2$, is one of the few well-defined catalysts reported to effect a double dehydrogenation of primary amines; however, a hydrogen acceptor and/or base is required to afford nitrile products.[9]

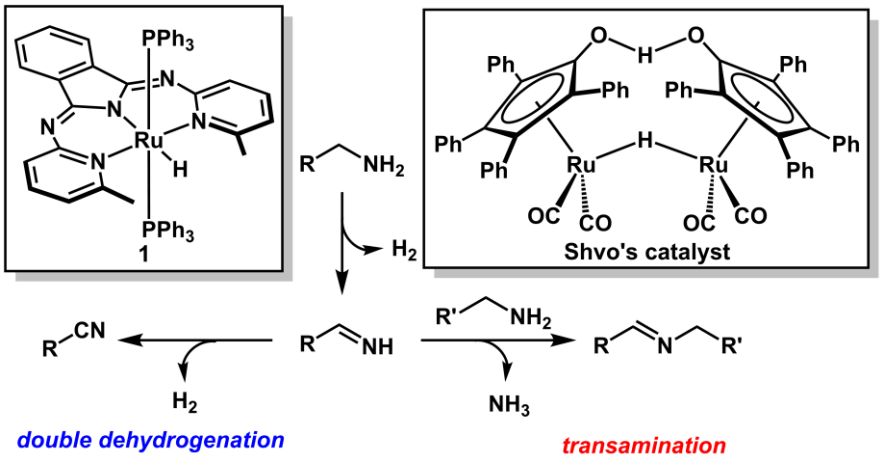

Figure 3-1. Dehydrogenative Oxidation Pathways of Primary Amines

In contrast to the steady development of transition-metal-catalyzed alcohol dehydrogenation,[10] detailed studies of amine dehydrogenation and, in particular, reports of selective nitrile formation are rare.[8, 9, 11] This is likely due to competing dehydrogenation and transamination pathways (Figure 3-1, right). Many known (de)hydrogenation catalysts effect a single dehydrogenation of primary amines, which initially affords an aldimine. This electrophilic product further reacts with another amine substrate and releases ammonia to afford imine or secondary amine products.[10h, 12, 13] Thus, transamination is a reaction pathway that limits the ability of most catalysts to perform the double dehydrogenation of amines. For selective nitrile formation, two key criteria must be met: (1) the aldimine intermediate remains coordinated to the metal center

and (2) the dehydrogenation of the aldimine occurs with a rate constant faster than the nucleophilic attack.

Bifunctional catalysts, which operate via metal–ligand cooperation, are extensively studied in (de)hydrogenation reactions.[10a-10d, 10g, 10j, 10k, 10m, 10n, 14] However, no known bifunctional catalysts facilitate a double dehydrogenation of primary amines. Shvo's catalyst, for example, operates through an outer-sphere proton and hydride transfer from the amine, followed by transamination to form an imine (Figure 3-1, right).[14e] In contrast, the iridium-pincer complex, $[C_6H_3\text{-}2,6\text{-}(OP^tBu_2)_2]IrH_2$, promotes the double dehydrogenation of primary amines through an inner-sphere mechanism involving consecutive N–H oxidative addition and *β*-H elimination to selectively generate nitrile.[9a] While the role of cooperativity in promoterless alcohol dehydrogenation is well-established,[15] the guidelines for rational ligand design in the context of amine dehydrogenation are undefined. Because of the limited reports of amine dehydrogenation, it is unclear whether an inner-sphere, outer-sphere, or cooperative mechanism is advantageous for a double dehydrogenation pathway.

We recently reported a series of *N*,*N*,*N*-bMepi (bMepi = 1,3-(6′-methyl-2′-pyridylimino)isoindolate) Ru^{II} complexes capable of catalyzing acceptorless dehydrogenations of both alcohols and amines.[10i, 11a] Notably, complex 1, $HRu(bMepi)(PPh_3)_2$, facilitates selective amine double dehydrogenation without the addition of any additives (Figure 3-1, left). Complex **1** features an anionic tridentate pincer ligand, with *ortho*-CH_3 substituents on the pyridine rings flanking the Ru–hydride. Compared to other known (de)hydrogenation catalysts, **1** is unique because no oxidants or hydrogen acceptors are required to achieve the high yielding double dehydrogenation of amines. In order to understand the key characteristics of **1** that enable this

transformation, a detailed mechanistic investigation is required. In this combined experimental and computational study, we aim to determine (1) whether an outer-sphere or inner-sphere mechanism is operative and (2) the critical features of the bMepi ligand framework that are required to promote amine double dehydrogenation reactivity. We interrogate three limiting mechanistic scenarios (inner-sphere, outer-sphere, and hemilabile) and show that an inner-sphere mechanism is operative. Importantly, imine intermediates remain coordinated to Ru, precluding the transamination side-reaction. Additionally, we show that the *ortho*-CH_3 substituents on bMepi are necessary in order to stabilize a key Ru–amido intermediate. Without *ortho*-alkyl substituents, such intermediates are highly disfavored. Overall, this manuscript will delineate the fundamental characteristics of Ru–bpi complexes that enable amine double dehydrogenation.

3.2 Limiting Mechanistic Scenarios

Preliminary observations reported by one of our groups(11a) revealed three key findings for acceptorless dehydrogenation of amines by 1: (1) during catalysis, the activity was unaffected by the addition of Hg(0), yet quenched with 1 equiv of 1,10-phenanthroline, consistent with a homogeneous system; (2) the release of PPh_3 from **1** was observed during catalysis, which implicates the presence of an unsaturated 16e^- ruthenium species; and (3) no imine intermediates were observed during catalysis suggesting that any generated imine intermediates are short-lived.[11a]

Ongoing mechanistic studies have revealed the bMepi ligand plays a distinct role in each class of dehydrogenation reactions (alcohols versus amines). In the case of alcohol dehydrogenation, the *ortho*-CH_3 groups impeded catalytic activity, and activity was enhanced

when −H (bpi) replaced −CH_3 (bMepi).[16] In stark contrast, the dehydrogenation of amines requires the *ortho*-CH_3 units (Figure 3-2). No reaction occurred when 3 (*ortho*-H) was used in place of 2 (*ortho*-CH_3) after heating 1-octylamine for 24 h at 130 °C with 5 mol % NaO^{t}Bu, compared to an initial rate of 1.6(4) × 10^{-6} Ms^{-1} under the same conditions with 2. These studies suggest that the *ortho*-CH_3 groups on the bMepi ligand play an essential role in facilitating the amine double dehydrogenation pathway.

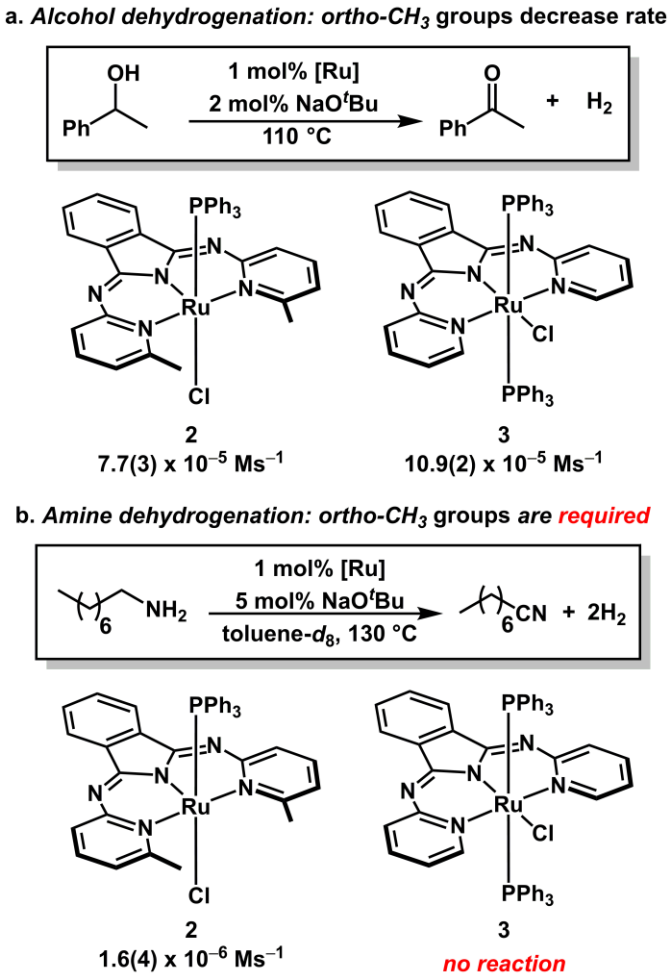

Figure 3-2. (a) 1-phenylethanol dehydrogenation with 2 (*ortho*-CH_3) and 3 (*ortho*-H). (b) 1-octylamine dehydrogenation with 2 (*ortho*-CH_3) and 3 (*ortho*-H).

On the basis of the above observations and a first-order rate dependence on the concentration of **1** (Figure S1), three mechanistic scenarios are proposed for the first dehydrogenation event (Figure 3-3): (A) a common inner-sphere β-H elimination cycle, where proton transfer affords a Ru–amido species that undergoes β-H elimination after release of H_2 to form a Ru–imine species; (B) a ligand-assisted bifunctional pathway, where proton transfer occurs on the imine backbone rather than on the Ru–hydride; and (C) a hemilabile ligand pathway whereby dissociation of a pyridine ligand accommodates the amine substrate and/or modifies the Ru coordination sphere as needed to promote hydrogen transfer. We note that bpi-type ligands have been previously proposed to undergo both protonation of the imine backbone and dissociation of a pyridine arm from the metal center during multistep chemical reactions.[17] Each mechanistic scenario has been evaluated by kinetic studies, catalyst modifications, isolation of proposed intermediates, and computational studies.

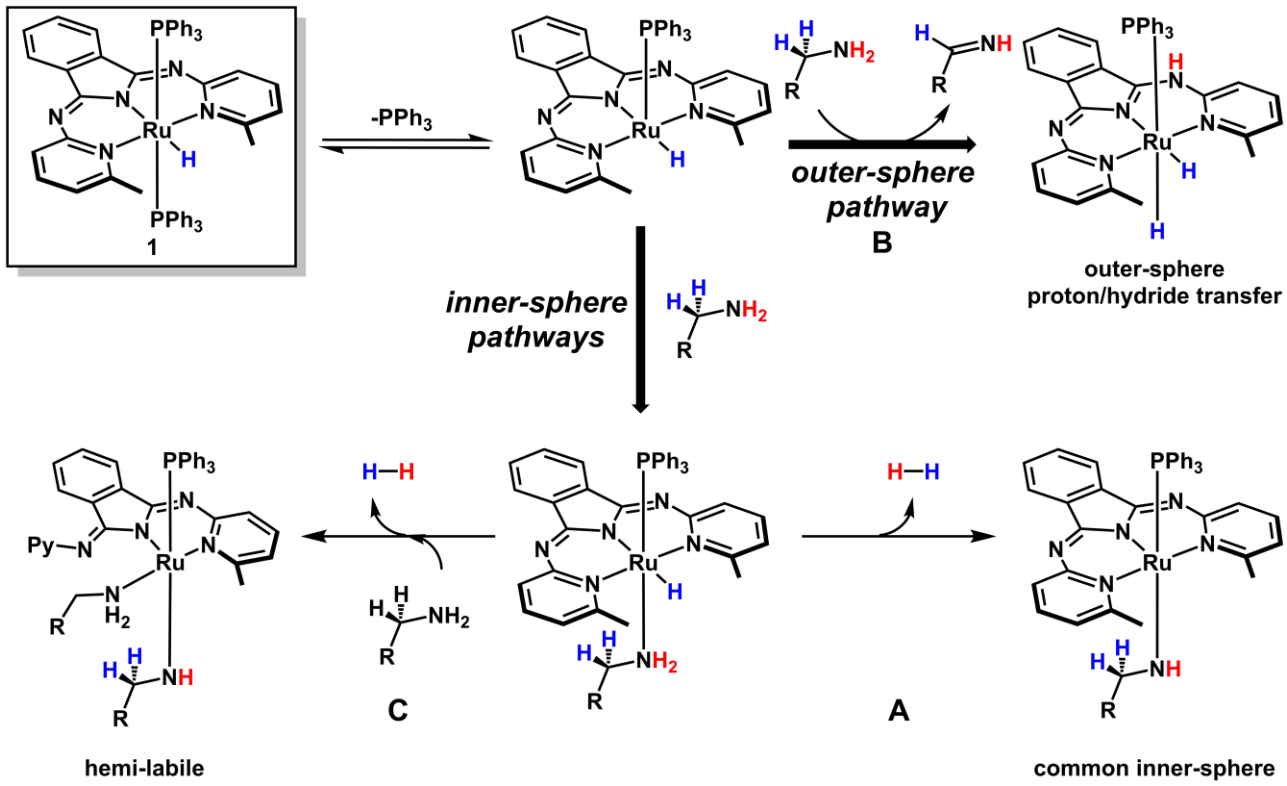

Figure 3-3. Limiting Mechanistic Scenarios for the First Dehydrogenation of Primary Amines: A Common Inner-Sphere Pathway (A), an Outer-Sphere Bifunctional Pathway (B) and an Inner-Sphere Hemilabile Pathway (C)

3.2.1 Inner-Sphere versus Outer-Sphere Mechanisms

3.2.1.1 Amine Ligand Substitution with 1

Two mechanistic regimes, outer-sphere (B) and inner-sphere pathways (A and C), were investigated for this study. Both an inner-sphere pathway and outer-sphere pathway require release of PPh_3. However, an important distinction between an inner-sphere and outer-sphere pathway is that a coordinated amine intermediate is required for the inner-sphere routes (formed via PPh_3 ligand substitution). To distinguish between the two mechanistic regimes, we evaluated the ability

of amine substrates to displace a PPh_3 ligand, as assessed through spectroscopic and computational experiments.

When benzylamine was added to **1** at 25 °C, NMR analysis indicated immediate release of PPh_3 and the formation of a new phosphorus-containing species with a ^{31}P NMR resonance at 74 ppm. The ^{1}H NMR spectrum revealed a new hydride resonance at −9.4 ppm (shifted from −9.6 ppm in 1), a shift in the *ortho*-CH_3 groups from 3.0 ppm for **1** to 3.1 ppm, in addition to symmetric ligand resonances. This species was assigned as the amine substitution adduct of **1** to form $HRu(bMepi)(PPh_3)(NH_2C_7H_7)$ (1b, Figure 3-4). Amine substitution was reversible, with K_{eq} = 0.086(4) M (calculated at 1, 20, and 100 equiv of benzylamine with respect to 1), which corresponds to a slightly endergonic ligand substitution event with ΔG = 1.5(4) kcal/mol. Similar reactions occurred with other substituted benzyl amines or alkylamines. For example, the addition of 100 equiv of 1-octylamine resulted in 93% conversion to $HRu(bMepi)(PPh_3)(NH_2C_8H_{17})$.[18]

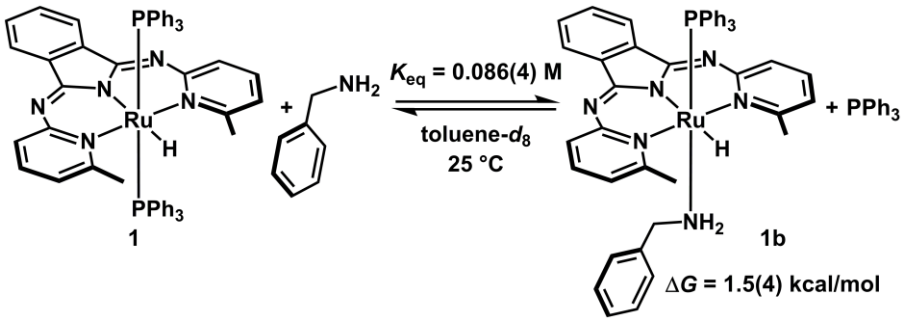

Figure 3-4. Substitution of PPh_3 on 1 for benzylamine.

The experimentally determined equilibrium constant provided an initial benchmark to evaluate the accuracy of theoretical methods employed for investigation of the full catalytic cycle.[19] Commonly used functionals (M06-L, B3LYP, PBE, ωB97XD, M06-L-D3, B3LYP-D3) were screened for amine ligand substitution with 1. Evaluation of ligand exchange between **1** and

benzylamine using the M06-L functional provided $\Delta G = 1.3$ kcal/mol, in excellent agreement with the experimentally derived value ($\Delta G = 1.5(4)$ kcal/mol).[20]

To understand the extent to which the amine binding affinity is influenced by the phosphine electron-donor ability, amine substitution and catalysis was evaluated using the modified complex, $HRu(bMepi)(PMe_3)_2$ (1-PMe_3), containing more electron-donating PMe_3 ligands. In contrast to amine ligand substitution observed with 1, there was no spectroscopic evidence of 1b-PMe_3, although free PMe_3 was observed at 110 °C. Furthermore, no amine dehydrogenation was observed after heating 1-octylamine for 24 h in the presence of 1 mol % 1-PMe_3. Computational assessment of amine ligand substitution with PPh_3 and PMe_3 ligands at 298 K indicates that both phosphine dissociation and benzylamine association are more endergonic for 1-PMe_3 compared to **1** by 8.8 and 8.6 kcal/mol (Figure 3-5). These data indicate that although 1 equiv PMe_3 can be released at elevated temperatures, the subsequent amine binding is less favorable, which is consistent with an inner-sphere pathway.

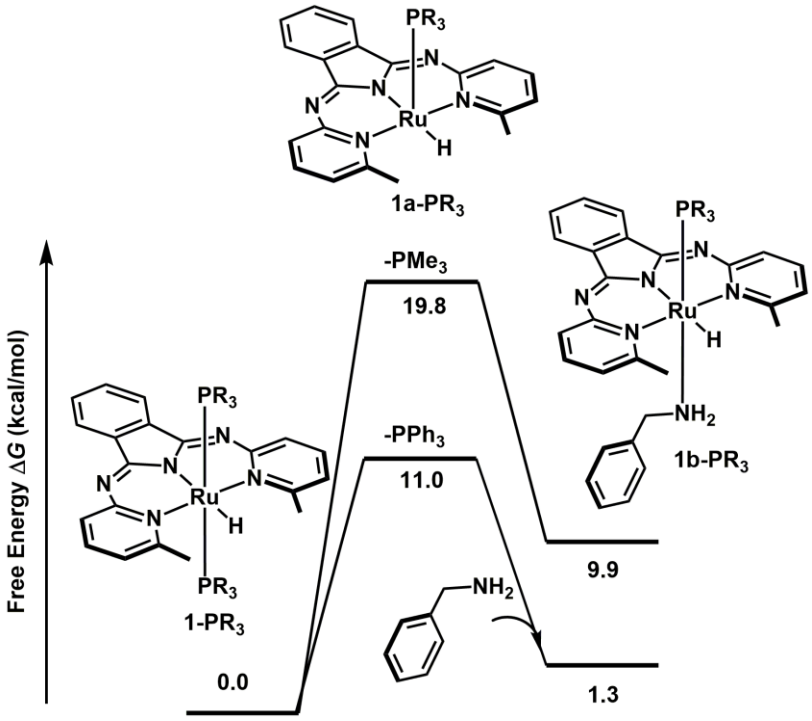

Figure 3-5. Relative Gibbs free energies for benzylamine substitution on 1-PR_3 calculated at M06-L/def2-TZVP//SMD(toluene). All values are at 298 K in kcal/mol.

3.2.1.2 Triphenylphosphine and 1-Octylamine Dependence

To assess the impact of phosphine dissociation or amine ligand substitution on the rate of amine dehydrogenation, the kinetic profile of 1-octylamine dehydrogenation was evaluated, and the order in [PPh_3] and [1-octylamine] was obtained. Reactions were performed in a sealed vessel under static vacuum to remove H_2 from solution. The conversion of 1-octylamine to 1-octanenitrile was monitored by ^{1}H NMR spectroscopy using dioxane as an internal standard. Standard reaction conditions for kinetic studies employed an NMR tube, equipped with a J Young valve, charged with 0.72 M 1-octylamine, 4.4×10^{-2} M dioxane, and 7.3×10^{-3} M (1 mol %) **1** in 0.600 mL of toluene-d_8 (Figure 3-6). The sealed NMR tubes were subjected to successive freeze/evacuation/thaw cycles until a static vacuum of 0.170–0.200 Torr was consistently

maintained. The method of initial rates was used for kinetic experiments and each reaction was performed in triplicate to establish error. Reaction rates were obtained on the basis of the appearance of 1-octanenitrile.[21] After heating to 130 °C for 5 h (4.2% completion), the observed rate constant was $1.4(1) \times 10^{-6}$ Ms^{-1}.[22]

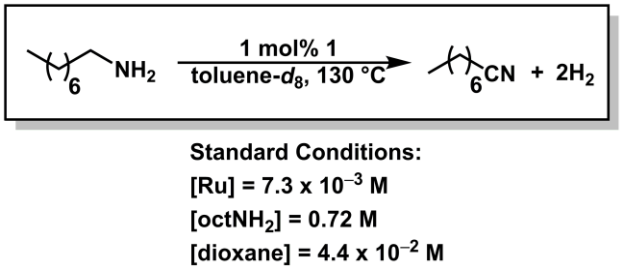

Figure 3-6. Standard reaction conditions of 1-octylamine dehydrogenation catalyzed by 1

The influence of phosphine and/or amine ligand substitution on the rate of amine dehydrogenation by **1** was examined by changing [1-octylamine] or [PPh_3] while holding the initial concentration of **1** constant. The observed rates for 1-octylamine dehydrogenation showed a zero-order dependence on [PPh_3] (Figure 3-7). The zero-order dependence on [PPh_3] suggests that phosphine dissociation is not involved in the rate-determining step, consistent with facile amine ligand substitution with 1. Under standard conditions (100 equiv of 1-octylamine), the equilibrium is shifted to favor formation of amine coordinated intermediate 1b.

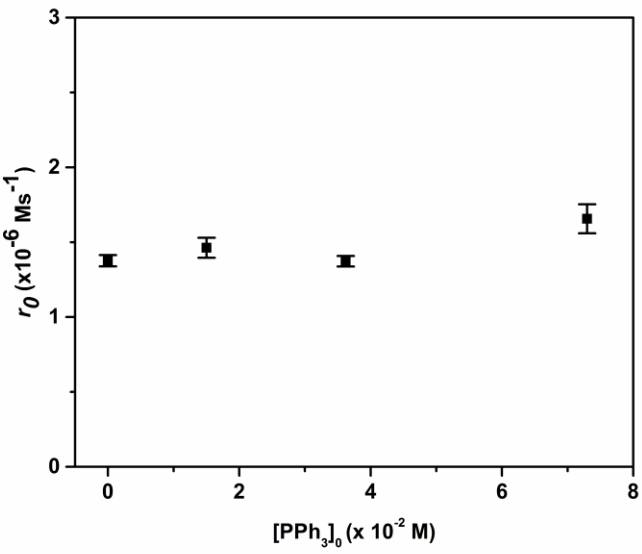

Figure 3-7. Influence of [PPh_3] on the reaction rates for 1-octylamine dehydrogenation catalyzed by 1.

The dehydrogenation of 1-octylamine exhibits saturation kinetics when varying [1-octylamine]. Concentrations of 1-octylamine above 0.54 M resulted in a zero-order dependence, with an average rate of $1.5(3) \times 10^{-6}$ Ms^{-1}. A linear dependence was observed below concentrations of 0.54 M (Figure 3-8). The saturation kinetics observed at high [1-octylamine] suggests a pre-equilibrium step, which is driven to the right with excess amine.

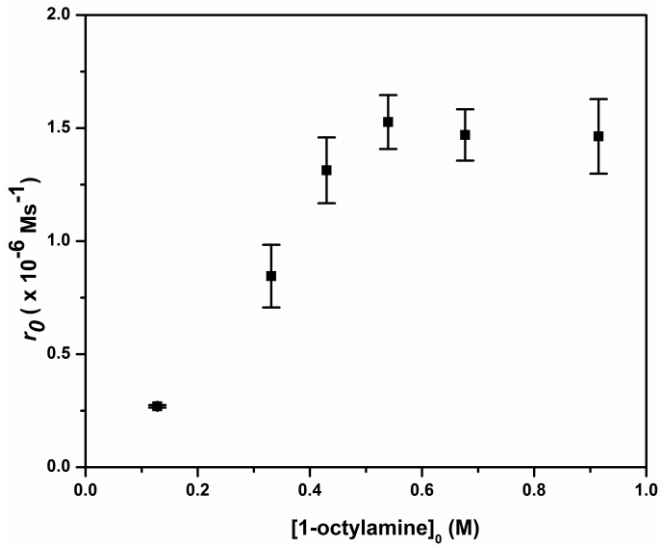

Figure 3-8. Influence of [1-octylamine] on the rate of reaction for 1-octylamine dehydrogenation by 1.

Although in situ observation of amine substitution at room temperature with **1** is consistent with an inner-sphere pathway, the rate studies noted above are also consistent with an outer-sphere mechanism. For example, release of PPh_3 (from 1) or amine substrate (from 1b) at high temperatures would provide an unsaturated 5-coordinate species that could participate in an outer-sphere mechanism, resulting in a zero-order PPh_3 dependence. Likewise, a first-order pathway in [1-octylamine] is expected if the turnover-limiting step at low concentrations involves an outer-sphere proton and/or hydride transfer to ruthenium. To further differentiate between an outer-sphere and inner-sphere pathway, we pursued computational experiments and catalyst modifications that probe proton transfer to the bMepi ligand.

3.2.2 Evaluation of an Outer-Sphere Bifunctional Pathway

An outer-sphere ligand-assisted mechanism with **1** could proceed through a proton and hydride transfer across the metal–ligand framework (Figure 3-9). In this scenario, the formation

of a ruthenium dihydride occurs following the hydrogen transfer from amine substrate. This transfer is necessarily accompanied by loss of the primary aldimine. Because no aldimine or imine-derived products were observed during catalysis, this pathway must be followed by fast release of H_2 and subsequent dehydrogenation of the imine to form the nitrile. Computational experiments indicate that protonation of the imine on bMepi by benzylamine is kinetically and thermodynamically unfavorable. A concerted outer-sphere mechanism, shown in Figure 3-9, results in a prohibitively high activation barrier of 62.5 kcal/mol.[23, 24]

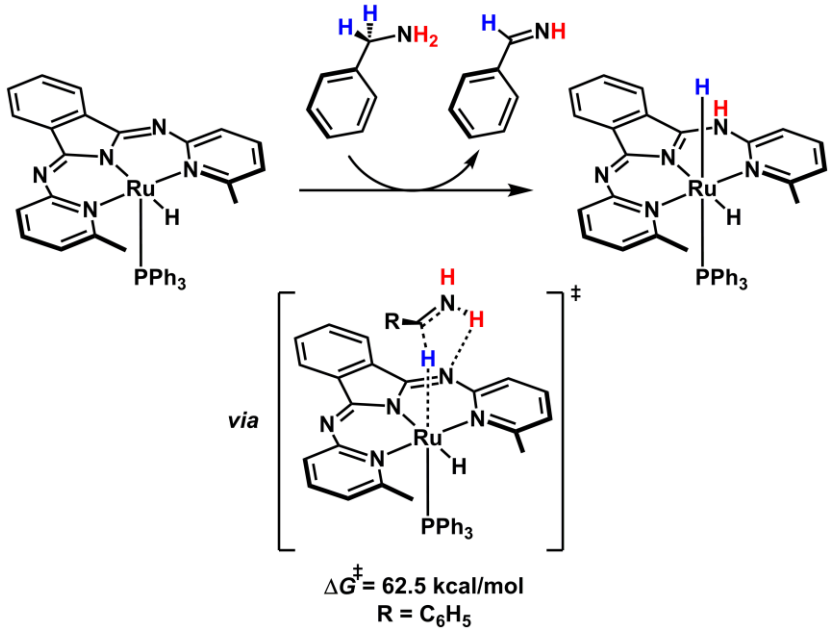

Figure 3-9. Outer-Sphere Hydride and Proton Transfer

We previously established that the modified bMepi complex Ru(bMepi^{Me})(PPh_3)$(OTf)_2$ (4, Figure 6), containing a covalent N–CH_3 bond in the backbone imine on the ligand framework, serves as a convenient mechanistic probe.[16] While protonation events on the imine groups are reversible, alkylation is irreversible, and an additional protonation event on the imine backbone is highly unfavorable.[25] We hypothesized that if an outer-sphere mechanism is operative, amine

dehydrogenation with 4 would proceed with significantly decreased rates. A proton transfer event to the ligand backbone was evaluated by a comparison of the reaction rates of 1-octylamine dehydrogenation catalyzed by 4 and 2 (Figure 3-10). Heating a 0.72 M solution of 1-octylamine containing 1 mol % of 2 and 5 mol % NaO^{t}Bu to 130 °C for 4 h resulted in a rate of 1.6(4) × 10^{-6} Ms^{-1}. Under the same conditions, 4 catalyzed 1-octylamine dehydrogenation at an identical rate, within error, of 1.7(2) × 10^{-6} Ms^{-1}. The identical rates observed with 2 and 4, in conjunction with computational results indicates that a cooperative interaction involving the imine functionality is highly unlikely and not necessary to enable acceptorless amine dehydrogenation by Ru–bMepi complexes.

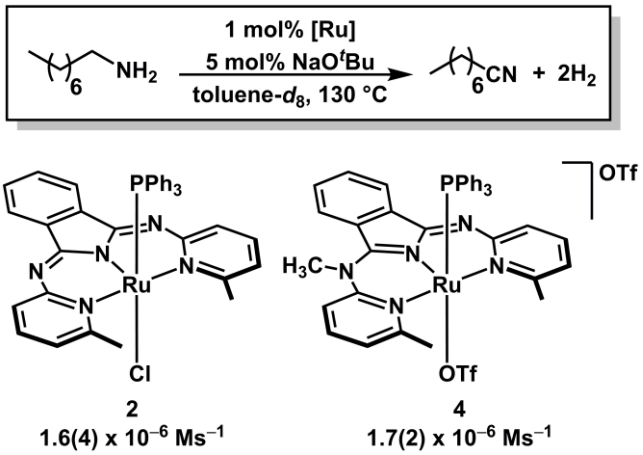

Figure 3-10. Dehydrogenation of 1-octylamine dehydrogenation with 2 and 4.

3.2.3 Common Inner-Sphere versus a Hemilabile Mechanism

Due to the absence of experimental and computational support for an outer-sphere mechanism, we evaluated two alternative pathways: inner-sphere pathway, A, and a hemilabile mechanism, C. As noted previously (Figure 3-2), no amine dehydrogenation occurred when the *ortho*-CH_3 groups were replaced by *ortho*-H (complex 3). The lack of amine dehydrogenation

catalysis by 3 implies that the *ortho*-CH_3 groups play a crucial role to govern reactivity with amines. We note that the steric environment imposed by the *ortho*-CH_3 groups imparts distinct geometric preferences: 2 is a 5-coordinate square pyramidal complex, while 3 is octahedral and thus coordinatively saturated. To account for this difference, we prepared an analogous Ru–hydride complex to 1, HRu(bpi) $(PPh_3)_2$ (1-bpi), which lacks the *ortho*-CH_3 substituents on the bis-pyridyl isoindoline ligand, yet retains an otherwise identical coordination environment.(10i) In contrast to the facile amine substitution reaction observed with the addition of 100 equiv of benzylamine to **1** (82% conversion), benzylamine ligand substitution with 1-bpi proceeded in lower conversion (18%) to HRu(bpi)$(PPh_3)(NH_2C_7H_7)$ (1b-bpi) under identical conditions. The equilibrium constant for benzylamine substitution with 1-bpi (calculated at 1, 10, 20, and 100 equiv benzylamine with respect to 1-bpi) was found to be K_{eq} = 3.4(9) × 10–4 M. This small equilibrium constant corresponds to an experimentally determined ΔG = 5.1(8) kcal/mol. Consistent with these experimental results, computational assessment (Table S2) indicated that the formation of benzylamine-coordinated 1b-bpi is endergonic by 5.0 kcal/mol at 298 K, compared to 1.3 kcal/mol for 1b containing *ortho*-CH_3 groups. In addition to less favorable ligand substitution, no dehydrogenation occurred after 24 h of heating 1-octylamine in the presence of 1-bpi at 110 °C. The lack of catalytic amine dehydrogenation reactivity by 1-bpi further supports our prior assertion that the *ortho* substituents play a crucial role to mediate amine dehydrogenation in the step(s) subsequent to amine ligand substitution (Figure 3-11).

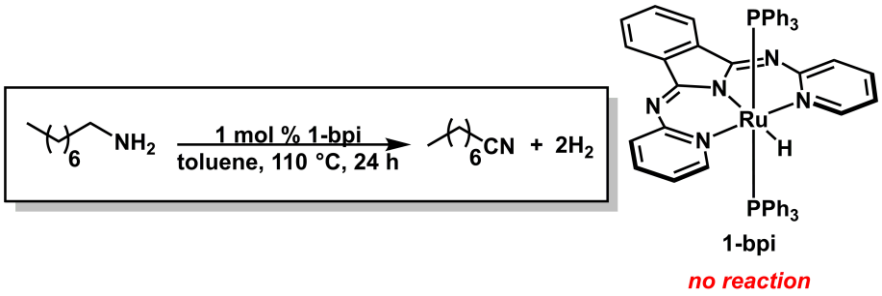

Figure 3-11. Dehydrogenation of 1-octylamine with 1-bpi.

The striking difference between catalysts **1** and 1-bpi for amine dehydrogenation prompted us to explore both the steric and electronic influence of *ortho*-alkyl substituents. We hypothesized that the *ortho* substituents may influence dehydrogenation reactivity due to (1) a steric effect in which sterically bulky substituents enable a hemilabile pathway or (2) an electronic effect in which intermediates are stabilized by the presence of the *ortho*-alkyl substituents. To determine the role of the *ortho* substituents on the first amine dehydrogenation step, both the inner-sphere pathway, A, and hemilabile pathway, C, were computationally and experimentally evaluated with ligands containing varying steric encumbrance at the *ortho* position (*ortho*-H, -CH_3, and -^{i}Pr). For simplicity, only the first dehydrogenation event was examined with each ligand variant. The second dehydrogenation is discussed in further detail with bMepi (vide infra).

3.2.3.1 Inner-Sphere Pathway

Figure 3-12 illustrates the first dehydrogenation for the common inner-sphere pathway, A. Following amine ligand substitution, computational analysis revealed the rate-limiting step is a proton transfer from the coordinated benzylamine to the Ru–hydride (TS-1) with formation of an η^2-Ru–(H_2) complex, 1d. Release of H_2 then affords a Ru–amido intermediate, 1e. Proton transfer was found to occur through a proton shuttle involving another amine substrate in a six-membered

transition state with $\Delta G^{\ddagger}$ = 35.0 kcal/mol.[26] Analysis of the reaction pathway for ligand variants, bpi, bMepi, and b^{i}Prpi, revealed that the activation barrier for proton transfer is minimally affected by modifying the size of the *ortho* substituent. Replacing -CH_3 with -H and -^{i}Pr resulted in slightly larger activation barriers of 37.3 kcal/mol, and 36.5 kcal/mol, respectively.

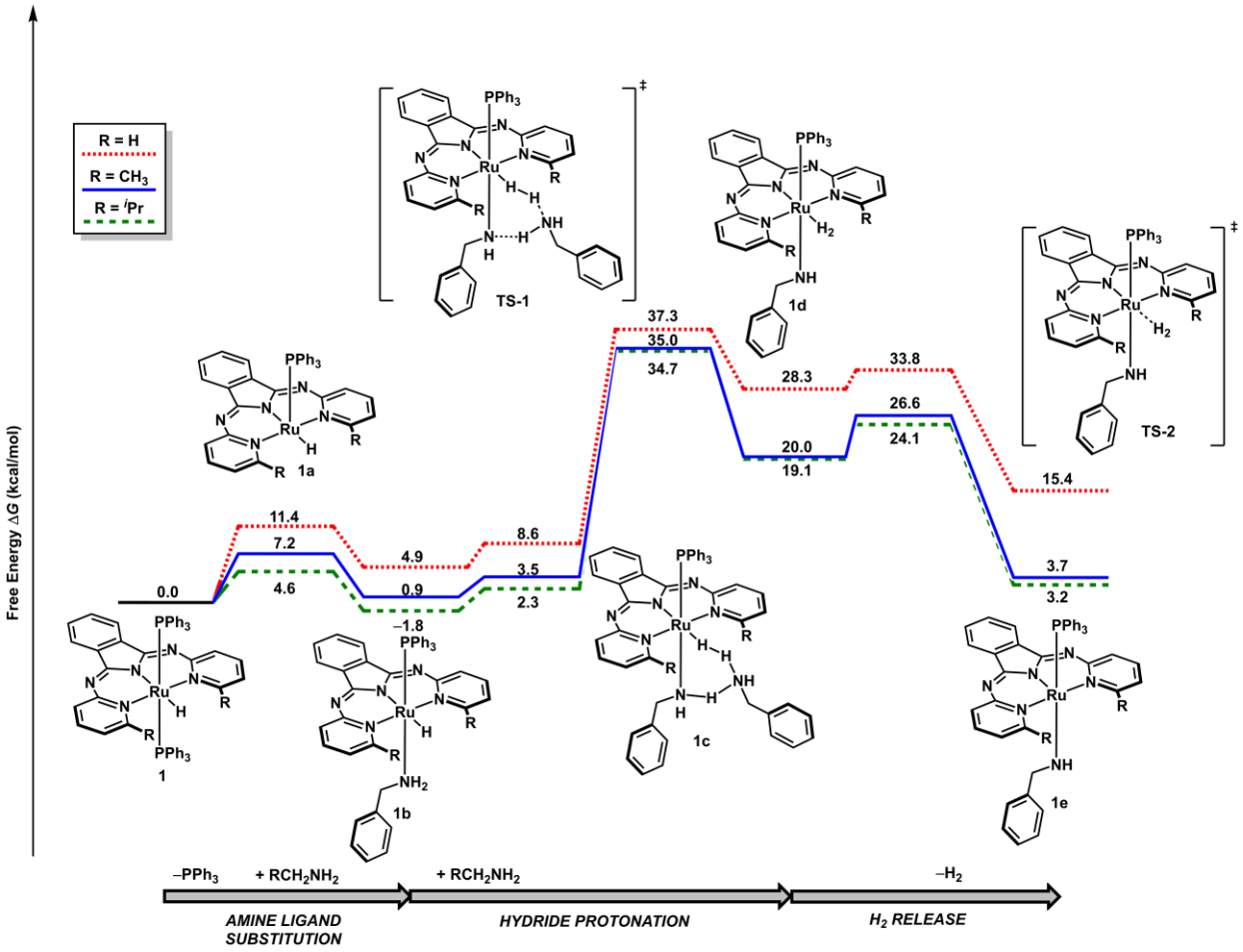

Figure 3-12. Common Inner-Sphere Mechanism (A) Comparing bpi, bMepi, and b^{i}Prpi Ligands

Although the *ortho* substituents have little effect on the kinetic barrier of proton transfer in TS-1, we found a significant difference in the relative stabilities of the intermediates formed along the dehydrogenation routes between the ligands bpi, bMepi, and b^{i}Prpi. Computational results

indicate that formation of the Ru–amido complex, 1e, is significantly higher in energy for *ortho*-H (ΔG = 15.4 kcal/mol) compared to *ortho*-CH_3 (ΔG = 3.2 kcal/mol) and *ortho*-^{i}Pr (ΔG = 3.7 kcal/mol). Thus, computational assessment of the inner-sphere pathway, A, suggests that the presence of *ortho*-alkyl substituents in the ligand framework may stabilize a key Ru–amido intermediate formed from the first deprotonation.

3.2.3.2 Hemilabile Pathway

In the hemilabile pathway, C, dissociation of a pyridine arm occurs prior to proton transfer through an associative mechanism (Figure 3-13). In this scenario, a second benzylamine substrate displaces a pyridine on Ru with $\Delta G^{‡}$ = 30.4 kcal/mol (TS-1′) for *ortho*-CH_3, forming the bis-benzylamine species 1c′.[27] Hydride protonation was found to occur most favorably by the benzylamine coordinated in the axial position, with $\Delta G^{‡}$ = 34.1 kcal/mol (TS-2′) to form an η^2-Ru–(H_2) complex 1d′.[28] In the hemilabile pathway, release of H_2 is the rate-determining step with $\Delta G^{‡}$ = 37.3 kcal/mol for *ortho*-CH_3 (TS-3′).

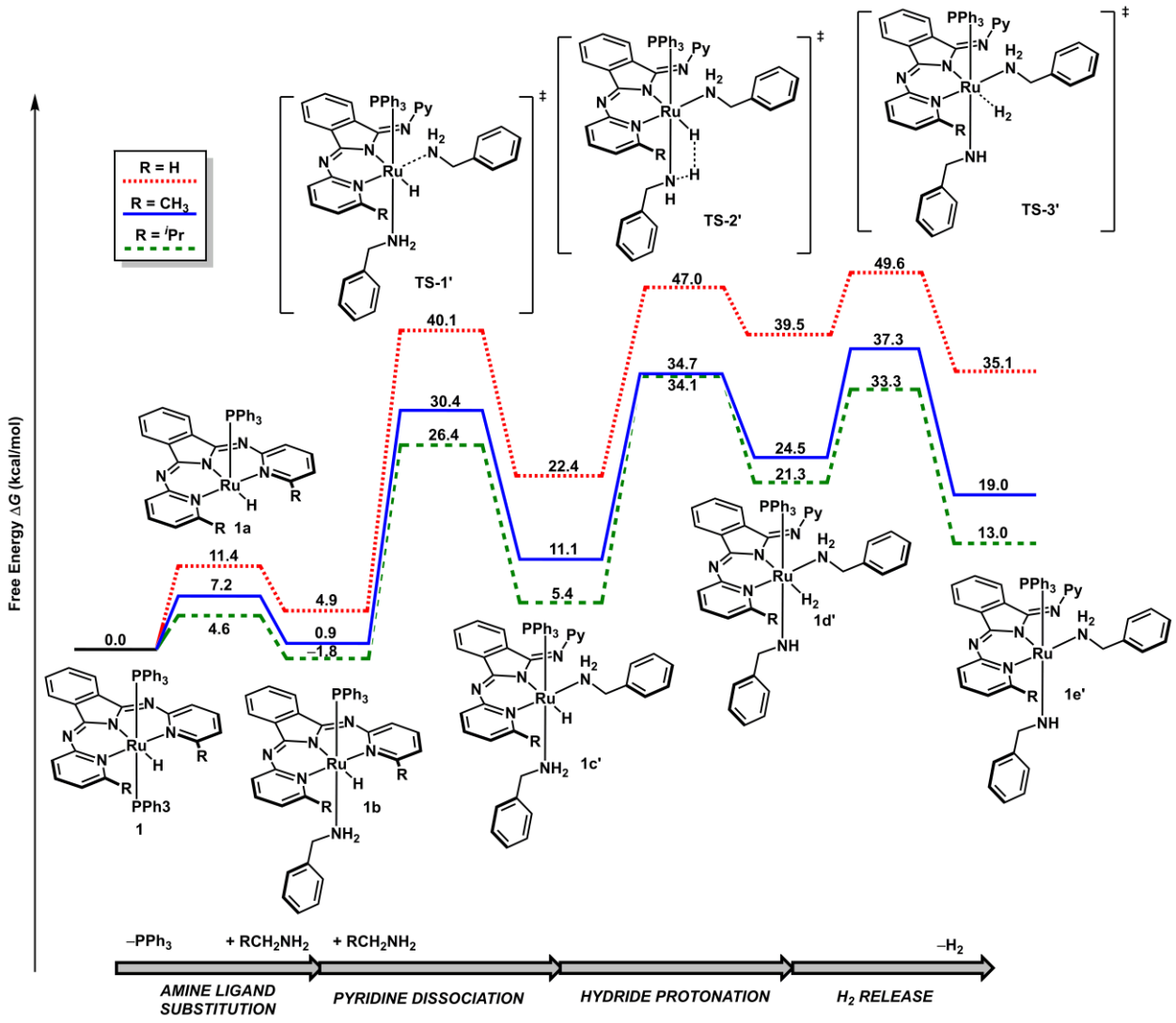

Figure 3-13. Hemilabile Mechanism (C) Comparing bpi, bMepi, and b^{i}Prpi Ligands[a]

Unlike the inner sphere mechanism, we found that the steric environment around the metal center of the catalyst significantly affects three key components of the hemilabile mechanism: (1) pyridine dissociation, (2) release of H_2 from Ru, and (3) the thermodynamic stability of Ru–amido species. For example, in addition to more facile dissociation of a pyridine unit with larger substituents, the release of H_2 has the highest barrier for the *ortho*-H case (TS-3′) with $\Delta G^{‡}$ = 49.6 kcal/mol, while the *ortho*-CH_3 and *ortho*-^{i}Pr transition states resulted in lower activation barriers

for H_2 release ($\Delta G^{‡}$ = 37.3 kcal/mol and $\Delta G^{‡}$ = 35.1 kcal/mol, respectively). Moreover, the difference in the thermodynamic stabilities of the resulting Ru–amido intermediates, 1e′, are even more pronounced in a hemilabile pathway, where ΔG = 35.1 kcal/mol for *ortho*-H, 19.0 kcal/mol for *ortho*-CH_3 and 13.0 kcal/mol for *ortho*-^{i}Pr. Hence, analysis of both pathways A and C indicate that the dehydrogenation of amines by **1** is significantly influenced by the thermodynamic stability of the resulting Ru–amido intermediates, imparted by more sterically bulky bis-pyridyl isoindolate ligands. However, the computationally derived kinetic profiles are distinct depending on the ligand variant. In a hemilabile pathway, the kinetic barrier is significantly reduced with the larger *ortho*-^{i}Pr substituent.

3.3 Influence of *ortho*-alkyl substituents on the rate of amine dehydrogenation

The distinct kinetic profile provided by computations for the hemilabile pathway C eluded to measurable differences in amine dehydrogenation rates between *ortho*-CH_3 and *ortho*-^{i}Pr complexes. In an inner-sphere mechanism, the rate-determining barrier (proton transfer) between bMepi and b^{i}Prpi variants does not differ significantly. Conversely, in a hemilabile mechanism b^{i}Prpi results in a lower energy activation barrier (H_2 release) compared to bMepi. Thus, if a hemilabile pathway is operative, an increase in the reaction rate of amine dehydrogenation is anticipated when using b^{i}Prpi.

In order to experimentally evaluate the effect of increasing the pyridine steric profile on the rate of amine dehydrogenation, we synthesized ClRu(b^{i}Prpi)(PPh_3) (5, Figure 3-14). Similar to the synthesis of 2,(10i) metalation was achieved following the addition of Kb^{i}Prpi to $Ru(PPh_3)_3Cl_2$ over 24 h at 70 °C in THF solvent, which afforded 5 in 52% yield. The ^{31}P NMR

spectrum of 5 exhibits a singlet at 45.8 ppm while the ^{1}H NMR spectrum features symmetric aromatic ligand-based resonances. In the ^{1}H NMR spectrum, the methine isopropyl protons are shifted to a higher field (−0.01 ppm) from the uncoordinated ligand (2.91 ppm), which is consistent with an agostic interaction.(29) Furthermore, analysis of the X-ray structure confirmed agostic Ru–(η^2-C–H) interactions in the solid state with Ru–H methine bond distances (2.229 and 2.467 Å) and angles (122.89° and 131.03°).

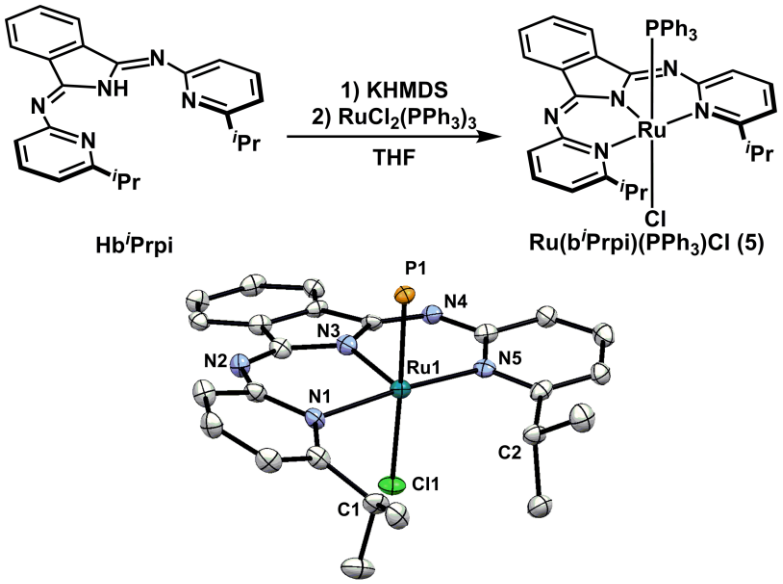

Figure 3-14. Synthesis and crystal structure (thermal ellipsoids of 5 depicted at 50% probability) of Ru(b^{i}Prpi)(PPh$_3$)(Cl) (5). PPh$_3$ phenyl groups and hydrogen atoms are omitted for clarity.

The initial rate observed when 5 was employed as the catalyst, measured under standard conditions, provided a rate of 1.1(1) × 10^{-6} Ms^{-1}. This minor decrease in rate, compared to 1.6(4) × 10^{-6} Ms^{-1} for analogous complex 2 containing *ortho*-CH_3 groups, suggests that an increased steric profile around the Ru center has a minimal effect on catalytic amine dehydrogenation. This

observed rate is inconsistent with a hemilabile pathway, where an increased in rate is anticipated for complex 5 (Figure 3-15).

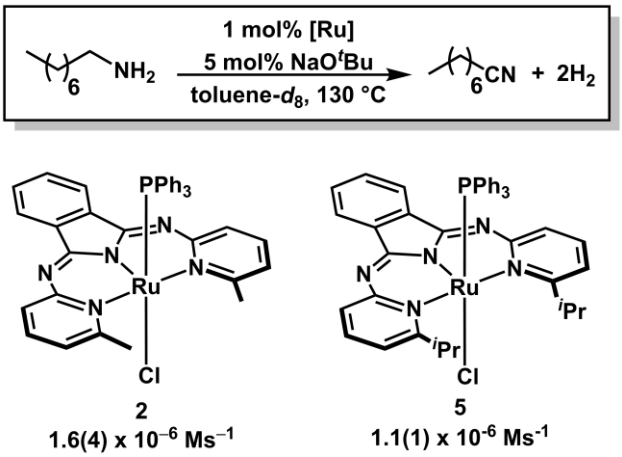

Figure 3-15. Dehydrogenation of 1-octylamine comparing 2 and 5.

3.4 Temperature Dependence

The experimental activation *para* meters for amine dehydrogenation by **1** were obtained through an Eyring analysis and compared to the calculated activation *para* meters for both inner-sphere type pathway, A, and hemilabile pathway, C. Reaction rates were measured over a 40 °C temperature range under standard conditions using **1** and plotted by Eyring analysis to obtain $\Delta G^{\ddagger}$, $\Delta S^{\ddagger}$, and $\Delta H^{\ddagger}$ (Figure 3-16). The experimentally measured $\Delta G^{\ddagger}$ of 35(2) kcal/mol at 130 °C, is consistent with computations for both the inner-sphere mechanism ($\Delta G^{\ddagger}$ = 35.0 kcal/mol) and a hemilabile pathway ($\Delta G^{\ddagger}$ = 37.3 kcal/mol). However, the experimentally determined large negative $\Delta S^{\ddagger}$ of −35(4) eu indicates a highly ordered transition state. The proton transfer step in the inner-sphere pathway requires an ordered six-membered transition state, with a computationally determined entropy for TS-1 with bMepi of $\Delta S^{\ddagger}$ = −28.6 eu.(30) Conversely, the transition state for a hemilabile mechanism, with release of H_2, was computationally determined

to have a more positive $\Delta S^{\ddagger}$ of −21.3 eu. Additionally, computed enthalpy $\Delta H^{\ddagger}$ of 23.2 kcal/mol is in agreement with the experimentally determined $\Delta H^{\ddagger}$ of 20(1) kcal/mol, consistent with bond breaking character in the transition state.[31] Taken together, the theoretical results, experimental rate data with complex 5, and activation *para* meters provide compelling evidence against a hemilabile type pathway, and instead, for an inner-sphere pathway.

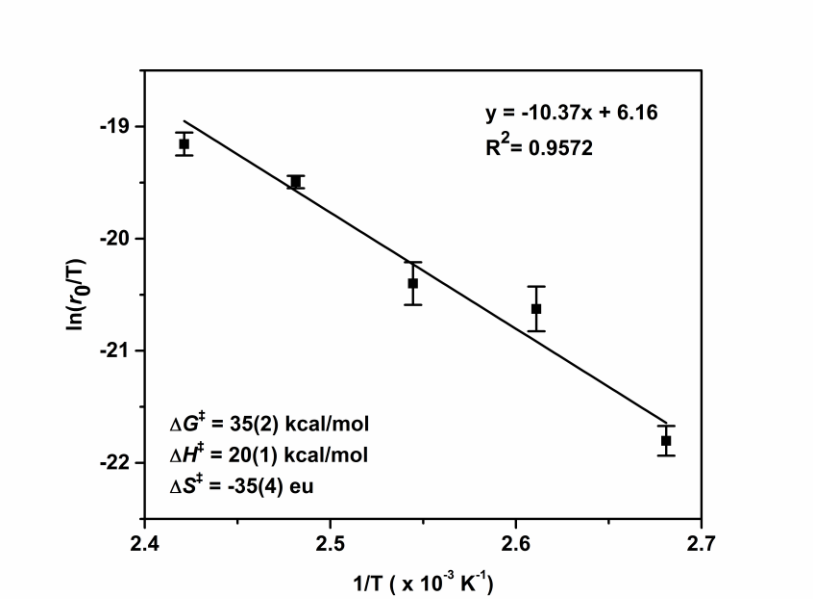

Figure 3-16. Eyring analysis based on the temperature dependence of 1-octylamine dehydrogenation by 1.

3.5 Thermodynamic stability of Ru–amido species: NBO, AIM, and NCI analysis

To provide insight into the differences in the thermodynamic stability between Ru–amido (1e) intermediates (bpi, bMepi and b^{i}Prpi), we conducted Natural Bond Order (NBO), Atoms In Molecules (AIM), and Non-Covalent Interaction (NCI) analyses. NBO analysis can be used to characterize the charge transfer interaction between donor and acceptor orbitals through the application of second-order perturbation theory and in turn provides insight on the origin of

thermodynamic stabilization.[32] The stabilization energy (E^2) due to charge transfer is indicative of the extent of charge delocalization and bonding interaction between the occupied and acceptor orbital. Complementary to NBO analysis, AIM and NCI analyses can be used to identify noncovalent interactions such as hydrogen bonding, dihydrogen bonds, and agostic interactions between neighboring atoms within the molecule.[33] Thus, both the NBO and AIM/NCI methods provide complementary chemical information that can be used to analyze the origins of a given thermodynamic stabilization effect.

When applied to the Ru–amido intermediates (1e), NBO analysis clearly indicated the presence of significant intramolecular charge transfer from the bonding orbital of σRu1–N1 to the antibonding orbital σ*Ru1–P1 for both *ortho*-CH_3 and *ortho*-^{i}Pr complexes, with E^2 = 24.2 and 25.0 kcal/mol, respectively. In contrast, the stabilizing interaction is reduced considerably for the *ortho*-H Ru–amido intermediate (1e-bpi), with E^2 = 10.8 kcal/mol. Close inspection of the respective optimized structures of 1e-bMepi and 1e-bpi revealed that the *ortho*-CH_3 groups enforce a favorable geometrical orientation (∠ N1–Ru1–P1 = 171.0°) of the bonding σRu1–N1 and antibonding σ*Ru1–P1 orbital (Figure 3-17). This in turn facilitates a productive intramolecular charge transfer in complexes containing *ortho*-alkyl substituents (CH_3 and ^{i}Pr). When the *ortho* substitutes are replaced by -H, in the case of 1e-bpi, the bond angle (∠ N1–Ru1–P1 = 131.9°) becomes shortened, and the bonding σRu1–N1 and antibonding σ*Ru1–P1 orbitals no longer remain in the *trans* position and thus deviate from the optimal geometry for intramolecular charge transfer to occur.

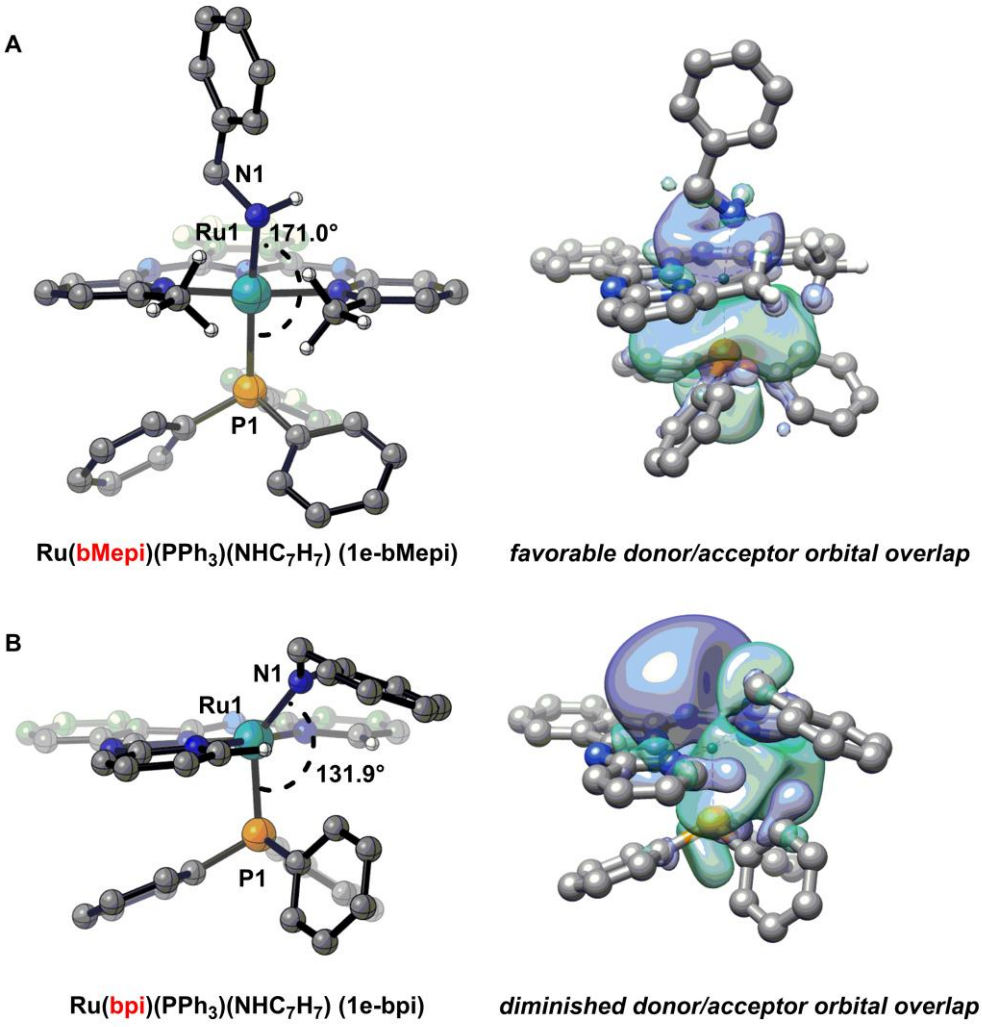

Figure 3-17. (a) M06-L optimized geometry (left) and NBO orbital interaction for 1e-bMepi (*ortho*-CH_3) (right). (b) M06-L optimized geometry (left) and NBO orbital interaction for 1e-bpi (*ortho*-H) (right).

AIM and NCI analyses provided further clarification into features governing the higher stability of Ru–amido intermediates of 1e-bMepi and 1e-b^{i}Prpi compared to 1e-bpi. Similar to the experimentally observed agostic interactions for 5-coordinate pre-catalysts containing *ortho*-CH_3[16] and *ortho*-^{i}Pr substituents, an intramolecular interaction was observed for the Ru–amido

intermediates. AIM analysis revealed Bond Critical Points (BCPs) between the *ortho*- CH_3 units and the coordinated amido ligand. However, given the ambiguity associated with assigning noncovalent interactions by using BCPs,[33b, 34] NCI analysis was also used to complement the AIM data. NCI analysis revealed a weak noncovalent interaction (by analysis of the NCI isosurface) between the basic amido nitrogen and the weakly acidic *ortho*-CH_3 protons of 1e-bMepi and *ortho*-CH protons of 1e-b^{i}Prpi. Two noncovalent interactions were found between the amido nitrogen (N1) and the *ortho*-CH_3 protons attached to 1e-bMepi, with N1–H1 distance of 2.49 Å and N1–H_2 distance of 2.51 Å (Figure 3-18).[35] While the hydrogen-bonding ability of methyl groups has been assessed,[36] to the best of our knowledge, intramolecular noncovalent interactions to metal-amido species have not been observed.[37] Late transition metal-amido species are of significant interest for catalytic transformations of amines,[38] yet there is a paucity of structurally characterized nonchelating amido complexes.[39] Moreover, very few structurally characterized examples contain β-hydrogen atoms.[40, 32] In the present case, the stability of the Ru–amido complex 1e is imparted by steric as well as noncovalent contributions. Both of these effects serve to orient the amido unit in an appropriate geometry to maximize the donor/acceptor orbital interaction as illustrated by NBO. These data reveal that atypical secondary coordination sphere interactions can provide thermodynamic stabilization for bpi Ru–amido variants and otherwise unstable intermediates.

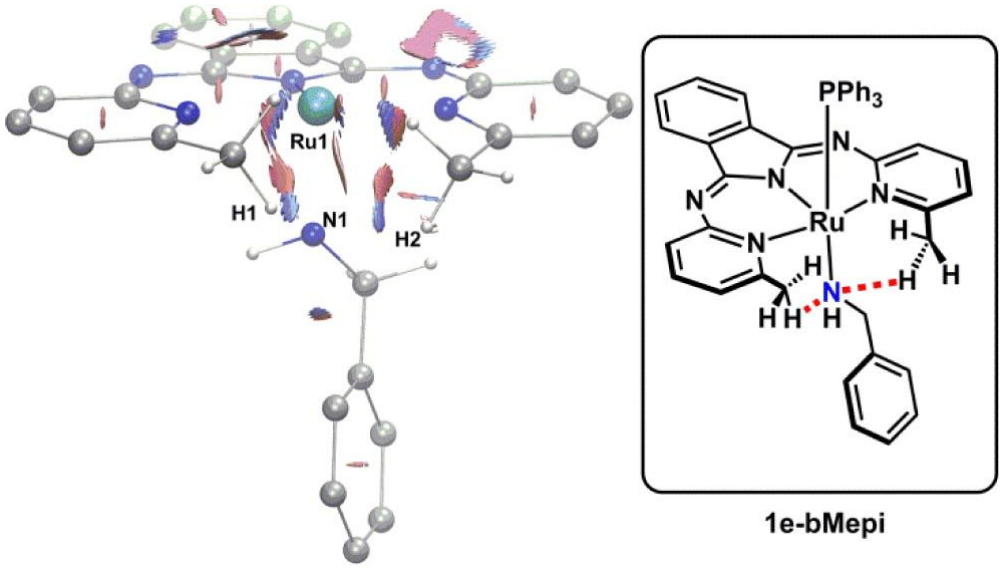

Figure 3-18. Noncovalent interactions observed in 1e-bMepi through NCI analysis. PPh_3 groups and hydrogen atoms are omitted for clarity.

3.6 Characterization of Ru–amido-type intermediates

In order to experimentally interrogate proposed Ru–amido species 1e, we attempted to isolate 1e-bMepi through stoichiometric reactions with 2 and an amine in the presence of a base. The addition of **1** equiv 4-methylbenzylamine and (trimethyl)silylmethyllithium ($(CH_3)3SiCH_2Li$) to 2 at −78 °C in THF quantitatively afforded a new species as assessed by NMR spectroscopy, assigned as Ru(−CH_2CH_3pi)(PPh_3) ($NH_2C_8H_9$) (6, Figure 3-19). ^{1}H NMR analysis revealed asymmetric bMepi ligand resonances and two methyl resonances in the alkyl region integrating to three hydrogens each, consistent with a noncoordinating *ortho*-CH_3 substituent and coordinated 4-methylbenzylamine. The ^{31}P NMR spectrum of 6 exhibits a singlet at 62.5 ppm, which is identical to the resonance observed prior to catalysis under base-catalyzed amine dehydrogenation conditions with 2 (Figure S35 and S36) and to a minor resonance observed under base-free conditions with Ru–hydride catalyst 1. These experimental findings indicate that 6 is a relevant

intermediate formed under base-catalyzed conditions and an off-cycle intermediate under base-free conditions.

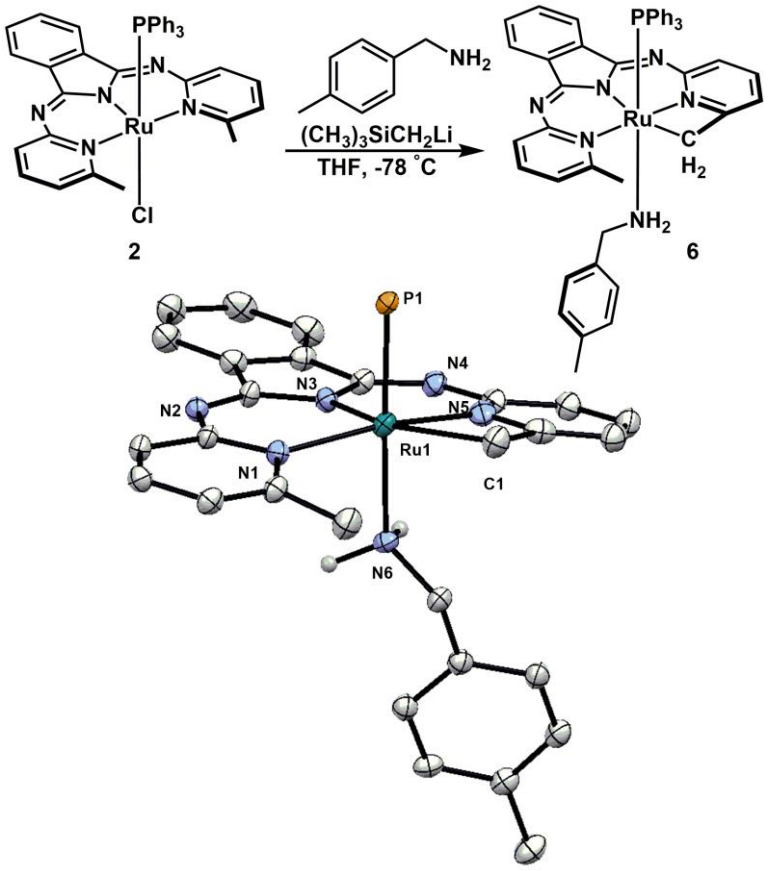

Figure 3-19. Synthesis and crystal structure (thermal ellipsoids of 6 depicted at 50% probability) of Ru(−CH_2CH_3pi) (PPh_3) ($NH_2C_8H_9$) (6). PPh_3 phenyl groups and hydrogen atoms are omitted for clarity.

A diffraction quality single crystal of 6 was obtained by layering a concentrated benzene solution with pentane and cooling to −35 °C. In contrast to the computationally predicted Ru–amido intermediate 1e, the solid-state structure revealed a ruthenium–amine species, with a singly deprotonated *ortho*-CH_3. Under stoichiometric conditions, with 1 equiv of 4-methylbenzylamine, 6 readily decomposes to a Ru–dimer, $[Ru(CH_2Mepi)PPh_3]_2$,[16] and is not isolable. In the presence

of excess amine, however, productive catalysis ensues. In silico experiments predict that the transformation of 6 to Ru–amido 1e intermediate occurs through migration of a proton from the axially coordinated amine to the methylene arm, with a free energy of activation of 15.2 kcal/mol. Additionally, Ru–amido species 1e is thermodynamically favored over 6 by 6.7 kcal/mol. In the presence of base and excess benzylamine, however, we propose 6 as the kinetic product (supported by NMR spectroscopy) which then converts to 1e. Because no 1e is observed during catalysis, we propose a fast *β*-H elimination step. Conversely, species 6 cannot undergo *β*-H elimination and is thus an off-cycle intermediate that must re-enter the cycle through deprotonation of coordinated amine prior to *β*-H elimination.

3.7 Double dehydrogenation versus transamination

In the presence of primary amines, many known dehydrogenation catalysts mediate transamination to form secondary amines or imines.[10h,12,13] To understand the preference for a double dehydrogenation pathway rather than transamination by 1, the steps subsequent to the first dehydrogenation were evaluated. The computed free energy profile for the second dehydrogenation of benzylamine to benzonitrile is illustrated in Figure 3-20 using **1** with bMepi. After formation of the Ru–amido intermediate 1e, *β*-H elimination occurs with a $\Delta G^{\ddagger}$ of 20.2 kcal/mol (TS-3). The resulting Ru–imine species, 1f, initially coordinated through the π-system, affords the more stable σ-bond isomer 1g. The second dehydrogenation event, occurring from the coordinated imine, 1g, proceeds through a six-membered transition state involving another amine molecule (TS-4).

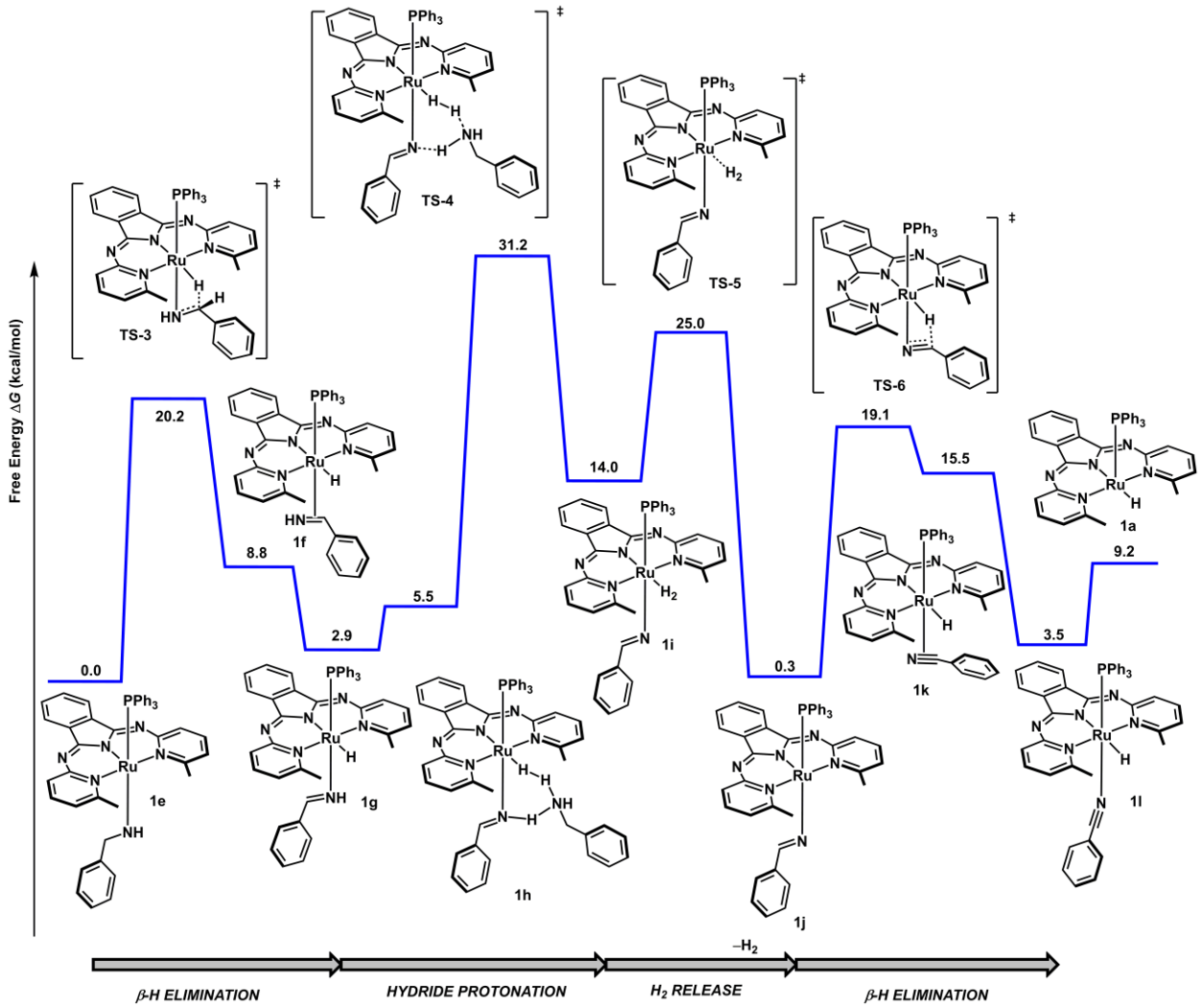

Figure 3-20. Second Dehydrogenation Pathway and Formation of Benzonitrile with 1a

Computations and stoichiometric experiments confirm *β*-H elimination and insertion processes of amido and imido intermediates by **1** are reversible. For example, the conversion of Ru–amido 1e to Ru–imine 1g is almost thermoneutral (2.9 kcal/mol). The entropic gain due to release of the gaseous hydrogen is required to drive the reaction in the forward direction. Facile *β*-H elimination from a ruthenium-coordinated imido is further supported by stoichiometric experiments employing benzonitrile derivatives and 1. Addition of benzonitrile at room

temperature to **1** resulted in a new phosphorus containing species at 26.8 ppm, in addition to free PPh_3 and the disappearance of the hydride resonance. The consumption of the ruthenium hydride is consistent with an insertion reaction into the nitrile triple bond, forming the Ru–imido intermediate 1j, and at 10 equiv of benzonitrile, 43% conversion to species 1j was observed (Figure 3-21). Consistent with an insertion reaction, a higher conversion (93%) was obtained when using 10 equiv of *p*-CF_3-benzonitrile, a substrate that is more susceptible to hydride transfer. The equilibrium constant, K_{eq} = 0.029(7) M (determined at 1, 10, 20, and 100 equiv benzonitrile with respect to 1), corresponds to a ΔG = 2.1(1) kcal/mol. Attempts at isolation of Ru–imido intermediates were unsuccessful; however, in situ $^{1}H/^{13}C$-HSQC experiments revealed imine ^{1}H NMR resonances at 6.7 (R = H) ppm and δ 7.3 (R = CF_3), and ^{13}C NMR resonances at δ 154 (R = H) and 160 (R = CF_3), consistent with metal-coordinated imido complexes.([12a, 41])

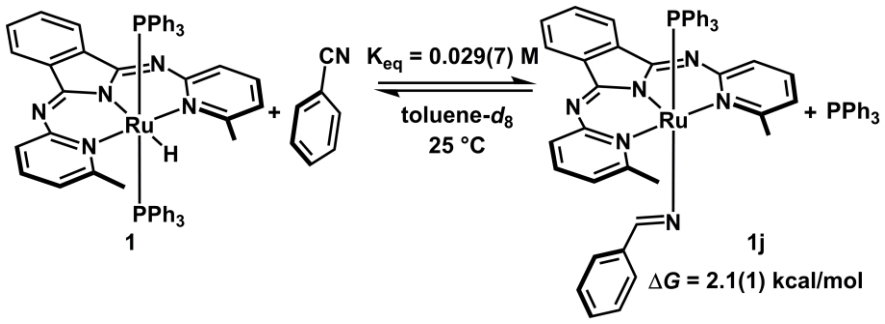

Figure 3-21. Insertion of benzonitrile into the Ru–H bond on 1.

Calculations revealed that the second proton transfer occurs with a $\Delta G^{‡}$ = 31.8 kcal/mol, a lower barrier than the first dehydrogenation ($\Delta G^{‡}$ = 35.0 kcal/mol, TS-1). Therefore, a facile second dehydrogenation may prevent a buildup of imine intermediates. However, we note that the difference between the first dehydrogenation and the second dehydrogenation is only 3.8 kcal/mol. In addition to a more facile second dehydrogenation, we hypothesized that imine intermediates

may also remain coordinated to Ru throughout the catalytic cycle. To assess the extent of imine coordination, comparison of the relative binding energies of PPh_3, benzylamine, benzylimine, and benzonitrile to 1a, revealed that benzylimine exhibits stronger binding to the ruthenium center (8.2 kcal/mol), compared to benzonitrile (5.7 kcal/mol) and benzylamine (6.3 kcal/mol) at 413 K. The higher binding affinity calculated for benzylimine is consistent with the experimental observation that free imine is not detected during amine dehydrogenation.

Primary aldimines are known to undergo transamination in the presence of amines; however, mechanistic details of metal-catalyzed transamination reactions are limited. Several studies indicate nucleophilic attack occurs on a metal-coordinated imine intermediate.[12] Therefore, we investigated a postulated metal-mediated transamination pathway from 1g (Figure 3-22). No transition state was found along the path for nucleophilic attack on the metal-coordinated imine intermediate, consistent with a computed minimum energy path showing this attack is an uphill process by 37.3 kcal/mol (see Supporting Information (SI)).[42] Nonetheless, an intermediate, 1m, generated from nucleophilic attack of the metal-coordinated imine was located. Proton transfer from 1m involved a six-membered transition state and was predicted to occur with a prohibitively high free energy activation barrier of 42.7 kcal/mol at 413 K (see SI for details). These data are consistent with the experimentally observed nitrile selectivity, which is determined by the kinetics of the second dehydrogenation as well as the binding affinity of imine intermediates.

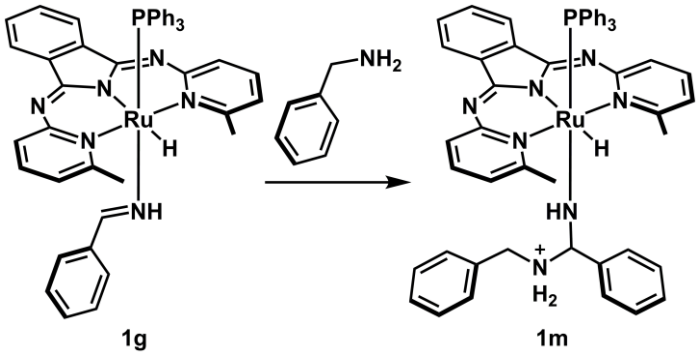

Figure 3-22. Nucleophilic attack on the Ru–imine intermediate 1g.

3.8 Amine versus alcohol dehydrogenation

In principle, amines and alcohols can undergo similar dehydrogenation reactions; however, reports of amine dehydrogenation are less common. The challenges of amine dehydrogenation include the high nucleophilicity of amines, which can lead to either catalyst deactivation or transamination, as well as slower β-H elimination of amido species compared to alkoxide intermediates.(10h) Given the current underdeveloped state of amine dehydrogenation, we sought to delineate the key differences in reactivity for a competent catalyst (1) that facilitates the dehydrogenation reactions of both alcohols and amines.

The dehydrogenation of amines and alcohols by **1** follow similar mechanistic pathways.[16] Coordination of the substrate (alcohol or amine) is followed by Ru–H protonation to form a high-energy η^2-Ru–(H_2) intermediate. H_2 release results in a Ru–alkoxide or amido intermediate, which can then undergo β-H elimination. Although dehydrogenation follows similar pathways, different ligand characteristics are required for amine dehydrogenation compared to alcohol dehydrogenation by Ru–bpi complexes. For amine dehydrogenation, the *ortho*-alkyl substituents on the bis-pyridyl isoindolate ligand are required. Conversely, we observed an increase in the rate

of alcohol dehydrogenation when *ortho*-CH_3 were replaced with *ortho*-H (Figure 3-1).[16] A comparison of the thermodynamic profiles for alcohol and amine dehydrogenation illustrates the role of the *N*,*N*,*N*-ligand for each class of substrate (Figure 3-23), as well as delineates inherent thermodynamic differences that will be useful for future design of (de)hydrogenation catalysts.

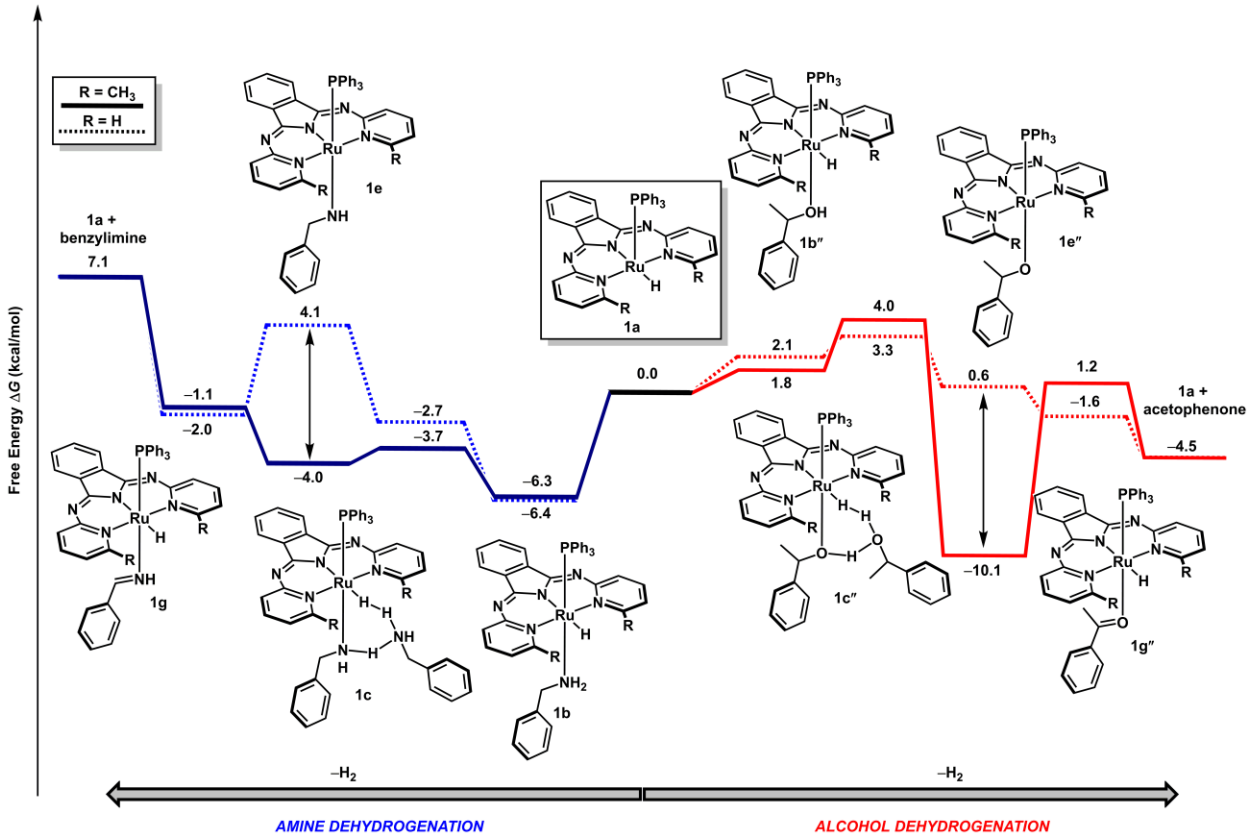

Figure 3-23. Benzylamine versus 1-phenylethanol dehydrogenation

The overall thermodynamic profile for alcohol dehydrogenation is less demanding than the analogous amine dehydrogenation. Figure 3-23 depicts the dehydrogenation of 1-phenylethanol to acetophenone as well as the first dehydrogenation of benzylamine to benzylimine, and it further compares bpi (*ortho*-H) and bMepi (*ortho*-CH_3) ligand variants. Starting from the unsaturated species 1a, acetophenone formation is exergonic by −4.5 kcal/mol, while benzylimine is

endergonic by +7.1 kcal/mol. The less favorable thermodynamic profile for amine dehydrogenation likely impedes the development of amine dehydrogenation catalysts compared to alcohol dehydrogenation catalysts.

Complex **1** overcomes this thermodynamic challenge by providing increased thermodynamic stability of the key Ru–amido intermediate 1e. Ru–amido (1e) and Ru–alkoxide (1e″) intermediates vary significantly in stability, and thus, the lower stability of Ru–amido species without *ortho*-alkyl substituents severely limits amine dehydrogenation. Notably, the stabilization imparted by the -CH_3 groups of bMepi is illustrated in both the case of alcohol and amine dehydrogenation, with the Ru–amido stabilized by −4.0 kcal/mol and the Ru–alkoxide by −10.1 kcal/mol. While this stabilization effect is essential for amines, it is not necessary for alcohol dehydrogenation as evident by the ability of both 1-bMepi and 1-bpi to facilitate alcohol dehydrogenation.

Our detailed experimental and computational analyses of both alcohol[16] and amine dehydrogenation has illustrated fundamentally similar mechanisms by Ru–bpi complexes. However, key thermodynamic differences between the classes of substrates highlight the unique role of the *N*,*N*,*N*-ligand. Due to the overall more demanding thermodynamic profile of amine dehydrogenation, catalysts that can stabilize high-energy intermediates, such as the Ru–amido intermediate, will play an essential role in the development of amine dehydrogenation reactions. The observations described in this manuscript may help to guide the further development of (de)hydrogenation catalysts and broaden the scope of amine dehydrogenation systems.

3.9 Conclusion

Dehydrogenation is a mild and atom-economical strategy for the synthesis of nitriles; however, there are few catalysts that can achieve selective double dehydrogenation of primary amines. In contrast to the in-depth analyses of alcohol dehydrogenation systems, well-defined amine dehydrogenation catalysts are rare. In this manuscript, we have employed experimental and computational analyses to elucidate the key characteristics of **1** that enable the catalytic dehydrogenation of amines.

Experimental and computational results support an inner-sphere catalytic cycle for the double dehydrogenation of primary amines by **1** (Figure 3-24). Reversible amine ligand substitution occurs with 1, to generate an amine coordinated Ru^{II}–hydride species 1b that can undergo irreversible H_2 loss via rate-determining proton transfer, resulting in a thermodynamically stable Ru–amido intermediate. Ru–amido 1e then undergoes β-H elimination to yield a Ru–imine species that remains coordinated to Ru. The second dehydrogenation occurs in a similar fashion with a lower activation barrier, resulting in the formation of nitrile. We have attributed the source of selectivity for nitrile, compared to imine products, to both a high binding affinity of imine intermediates, and a kinetically accessible second dehydrogenation event compared to transamination.

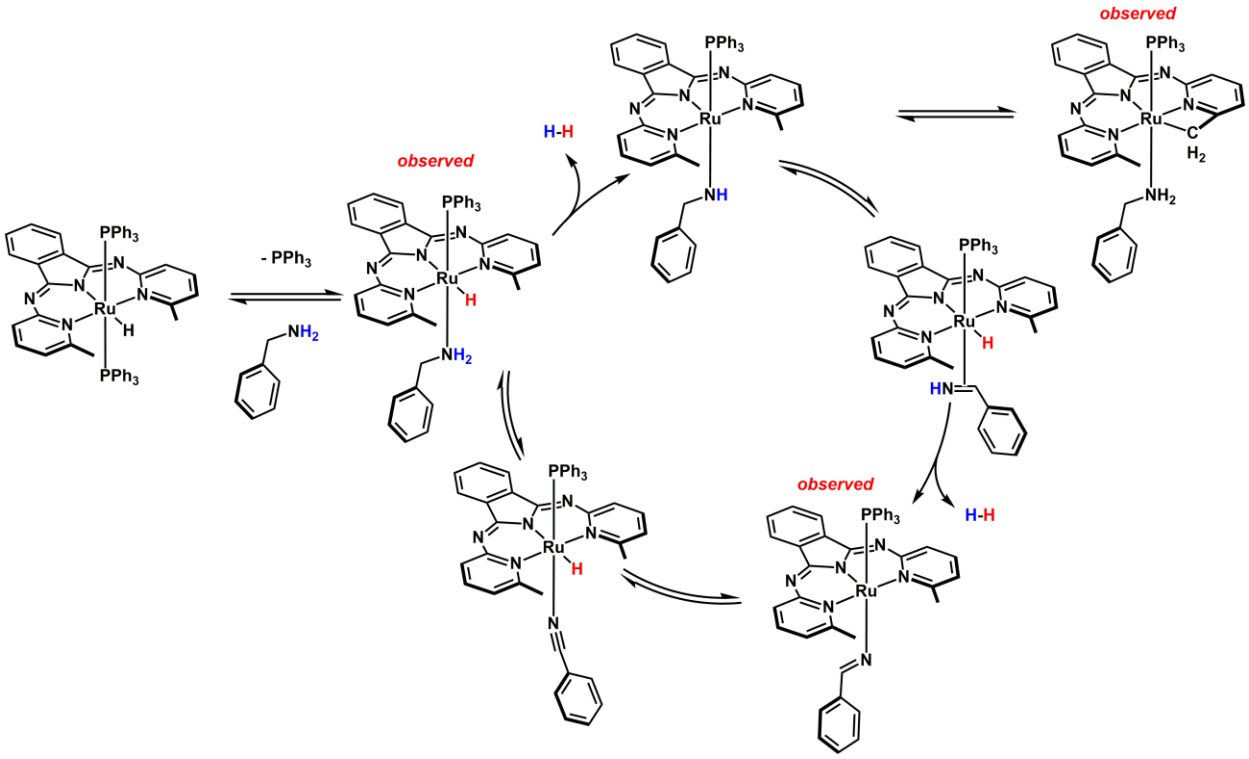

Figure 3-24. Proposed Cycle for Catalytic Amine Dehydrogenation by 1

The role of the *ortho*-CH_3 was found to be crucial for amine double dehydrogenation, as evaluated through catalyst modifications and computational studies. Rate analysis with the more sterically hindered catalyst, 5, suggests that a hemilabile mechanism is unlikely. Instead, computational data revealed large differences in thermodynamic stability of the Ru–amido species 1e between ligand variants bpi, bMepi, and b^{i}Prpi. Without *ortho* substituents, the formation of a Ru–amido species is disfavored, consistent with the observation of ligand exchange but no catalysis with 1-bpi. Importantly, the unique stability of the Ru–amido species is governed by steric, as well as noncovalent interactions of the *ortho*-alkyl substituents, assessed through NBO, AIM, and NCI analyses.

We have developed a series of *N*,*N*,*N*-Ru(II) complexes that are effective at promoting the dehydrogenation of both alcohols and amines. In this manuscript, we presented key differences between alcohol and amine dehydrogenation by 1. Although amine dehydrogenation is thermodynamically more challenging than alcohol dehydrogenation, the ability to stabilize key Ru–amido intermediates facilitates productive catalysis by 1. Ruthenium complexes of bis-pyridyl isoindoline ligands containing *ortho*–alkyl substituents are the only known catalysts to effect an oxidant-free, acceptorless double dehydrogenation of primary amines. Our mechanistic studies have determined the features which make **1** and analogous variants effective at this transformation. Furthermore, we have illustrated the importance of imine coordination in an inner-sphere type pathway for a second dehydrogenation event to occur over known side reactions. Overall, these mechanistic details provide new insight for the field of (de)hydrogenation chemistry as well as for catalyst design in the organic transformations of amines.

3.10 Experimental

General Considerations All reactions were conducted under a dry nitrogen atmosphere using standard Schlenk techniques, or under nitrogen atmosphere in a glovebox, unless otherwise stated. All reagents were purchased from commercial vendors. NaO^tBu (Sigma-Aldrich), $NaHBEt_3$ (Sigma-Aldrich), and (trimethylsilyl)methyllithium (Sigma-Aldrich) was used without further purification. 1-octylamine, benzylamine, 4- methylbenzylamine, and benzonitrile were distilled form CaH_2 under a nitrogen atmosphere and then stored over 3 Å molecular sieves for at least 24 h. Toluene-d8 and C_6D_6 were degassed using evacuation/refill cycles and then stored over 3 Å molecular sieves for at least 24 h. The following compounds were synthesized according to

literature methods: $HRu(bMepi)(PPh_3)_2$ (1), $Ru(bMepi)(PPh_3)Cl$ (2), $Ru(bpi)(PPh_3)Cl$, 2 6-(1-methylethyl)-2-pyridinamine, and $Hb^{i}Prpi$. The 3 Å molecular sieves were dried at 250 °C under dynamic vacuum for 24 h. Tetrahydrofuran (THF), dichloromethane (DCM), diethyl ether (Et_2O), pentane, and benzene (C_6H_6) were purified using a Glass Contour solvent purification system consisting of a copper catalyst, neutral alumina, and activated molecular sieves then passed through an in-line, 2 µm filter immediately before being dispensed. NMR spectra were recorded on Varian Inova 500, Varian MR400, Varian vnmrs 500 and Varian vnmrs 700 spectrometers at ambient temperature, unless otherwise stated. ^{1}H and ^{13}C shifts are reported in parts per million (ppm) relative to TMS with the residual solvent peak used as an internal reference. ^{31}P spectra were referenced on a unified scale to their respective ^{1}H NMR spectra. The following abbreviations are reported as follows: singlet (s), doublet (d), doublet of doublets (dd), triplet (t), quartet (q), multiplet (m), and triphenyl phosphine (PPh_3). ^{13}C NMR resonances were observed as singlets unless otherwise stated. Solid state IR spectra were collected using a Nicolet iS10 spectrometer equipped with a diamond attenuated total reflectance (ATR) accessory. Elemental analyses were performed by Midwest Microlab, LLC and Atlantic Microlab, Inc.

3.10.1 General procedure for rate studies 1-octylamine dehydrogenation catalyzed by 1

1-octylamine (82 µL, 0.5 mmol) was added to a 20 mL vial charged with 1 (4.7 mg, 0.005 mmol), dioxane (2.5 µL, 0.03 mmol), and toluene-d8 (0.600 µL). The liquid was then transferred to a NMR tube equipped with a J Young valve. The sealed NMR tube was frozen and evacuated until reaching 0.200 Torr, then thawed. This process was repeated until a consistent atmosphere of 0.200 Torr was maintained. An initial ^{1}H NMR spectrum was then obtained. The NMR tube was then

heated to the desired temperature (100, 110, 120, 130, 140 °C), using an oil bath such that the NMR tube was completely submerged in oil. The formation of 1-octanenitrile was monitored by analyzing the ^{1}H NMR spectrum against dioxane as the internal standard. To confirm reproducibility, all kinetic experiments were performed in triplicate.

3.10.2 Synthesis and Characterization

Ru(b^{i}Prpi)(PPh$_3$)Cl (5). THF (10 mL) was added to a 20 mL vial charged with biPrpi- K+ (81.6 mg, 0.194 mmol), $RuCl_2(PPh_3)_3$ (186 mg, 0.194 mmol), and a stir bar. The resulting solution was stirred at 70 °C for 20 h. THF was removed under vacuum. The crude product was extracted with DCM (20 mL), and the DCM was then removed under vacuum. The purple solid was washed with Et_2O (4 x 5 mL), and pentane (4 x 10 mL). Yield: 78 mg (52%). Crystals were obtained by allowing pentane to diffuse into a C_6H_6 solution. ^{1}H NMR (700 MHz, C_6D_6): δ 7.98 (m, 2H), 7.56 (d, J_{HH} = 7.9 Hz, 2H), 7.20 (t, J_{HH} = 7.6 Hz, 2H), 7.01 (m, 2H), 6.83 (t, J_{HH} = 8.6 Hz, 6H), 6.79 (t, J_{HH} = 7.2 Hz, 3H), 6.68 (t, J_{HH} = 7.4 Hz, 6H), 6.44 (d, J_{HH} = 7.3 Hz, 2H), 1.66 (d, J_{HH} = 6.4 Hz, 6H), 0.92 (d, J_{HH} = 6.3 Hz, 6H), −0.01 (p, J_{HH} = 6.5 Hz, 2H). ^{13}C{1H} NMR (700 MHz, C_6D_6): δ 170.2, 156.0, 153.3, 141.7, 135.5, 135.3, 135.1, 133.5, 133.4, 129.2, 128.6, 126.2, 120.4, 37.4, 25.1, 23.4. ^{31}P{1H} NMR (700 MHz, C_6D_6): δ 45.8 (s, PPh_3). IR (ATR, cm^{-1}): 3074, 1570, 1515, 1466, 1434, 1402, 1316, 1217, 1191, 1111, 1089, 850, 830, 807, 782, 748, 696. Anal. Calculated (Found): C, 64.57 (64.60); H, 5.03 (5.01); N, 8.96 (8.87).

HRu(bMepi)(PMe$_3$)$_2$ (1-PMe_3**).** PMe_3 (150 µL, 1.45 mmol) was added to a 20 mL vial charged with ClRu(bMepi)(PPh_3) (106 mg, 0.146 mmol) and THF (10 mL). The resulting solution stirred at room temperature for 20 h, resulting in a purple solid precipitate, [Ru(bMepi)(PMe_3) 2]Cl. The

solid was filtered and washed with THF (4 x 5 mL), then Et_2O (4 x 5 mL) and used without further purification. Yield: 72.7 mg (82%). This compound ([Ru(bMepi)(PMe_3)2]Cl; 15.4 mg, 0.025 mmol), was added to a 20 mL vial and charged with C_6H_6 (10 mL) followed by PMe_3 (0.004 mL, 0.039 mmol), and a stir bar. $NaHEt_3B$ (0.026 mL, 0.026 mmol) was added to the solution, and the reaction solution color changed from purple to green immediately. The reaction solution was allowed to stir for 1 h. The C_6H_6 solvent was removed under vacuum, and the crude product was extracted with pentane (4 × 5 mL). Evaporation of the volatiles under vacuum afforded the product as a green powder. Yield: 12.7 mg (88%). Crystals were obtained by cooling a pentane solution to −35 °C. ^{1}H NMR (400 MHz, C_6D_6): δ 8.48 (dd, J_{HH} = 5.6, 3.2 Hz, 2H), 7.78 (dd, J_{HH} = 8.0, 1.2 Hz, 2H), 7.35 (dd, J_{HH} = 5.6, 3.2 Hz, 2H), 7.11 (t, J_{HH} = 7.6 Hz, 2H), 6.63 (dd, J_{HH} = 7.2, 1.6 Hz, 2H), 3.17 (s, 6H), 0.27 (t, J_{HH} = 2.4 Hz, 18H), −10.77 (t, J_{PH} = 23.0 Hz, 1H). ^{13}C{1H} NMR (700 MHz, C_6D_6): 164.4, 160.9, 151.2, 142.9, 131.1, 128.6, 126.4, 120.9, 116.6, 35.3, 15.1 ^{31}P NMR (162 MHz, C_6D_6): δ 2.14 (d, J_{PH} = 22.7 Hz). IR (ATR, cm^{-1}): 3066, 2962, 2918, 2885, 2796, 2105, 1969, 1605, 1569, 1505, 1418, 1374, 1197, 1123, 772, 713, 683, 658. Anal. Calculated (Found): C, 53.79 (53.63); H, 6.08 (6.05); N, 12.06 (12.02).

HRu(bpi)(PPh_3)$_2$ (1-bpi). ClRu(bpi)(PPh_3)$_2$ (100 mg, 0.104 mmol) was dissolved in THF (10 mL) in a 20 mL vial charged with a stir bar. While stirring, $NaHEt_3B$ (110 µL, 0.110 mmol) was added to the solution, and the reaction solution color immediately changed from green to black. After stirring at room temperature for 30 minutes THF was removed under vacuum. The black solid was extracted with C_6H_6 (10 mL). C_6H_6 was removed under vacuum and the gray product was washed with pentane (4 x 10 mL), affording 62.4 mg (65%). ^{1}H NMR (700 MHz, C_6D_6): δ 8.61 (d, J_{HH} = 6.0 Hz, 2H), 8.39 (m, 2H), 7.37 (d, J_{HH} = 8.1 Hz, 2H), 7.30 (t, J_{HH} = 5.7 Hz), 14H), 6.82 (m, 16H),

6.68 (t, J_{HH} = 7.6 Hz, 2H), 5.34 (t, J_{HH} = 6.6 Hz, 2H), −10.77 (t, J_{PH} = 23.3 Hz, 1H). $^{13}C\{1H\}$ NMR (700 MHz, C_6D_6): δ 163.7, 158.8, 152.8, 142.6, 134.7 (t, JCP = 16.6 Hz, ipso-CP), 133.5, 131.5, 128.4, 120.6, 113.5. $^{31}P\{1H\}$ NMR (700 MHz, C_6D_6): δ 55.59 (s, PPh_3). IR, neat (cm^{-1}): 3048, 1842, 1545, 1499, 1435, 1379, 1311, 1286, 1194, 1114, 1089, 1006, 906, 769, 694. Anal. Calculated (Found): C, 70.12 (67.81); H, 4.69 (4.66); N, 7.57 (7.45).

In situ synthesis of Ru(-CH_2CH_3pi)(PPh_3)($NH_2C_8H_9$) (6). A 20 mL vial was charged with trimethylsilylmethyllithium (3.9 mg, 0.041 mmol) and THF (1 mL), and was cooled to −78 °C. A solution of 4-methylbenzylamine (5.3 µL, 0.042 mmol) in THF (1 mL) was added drop-wise to the trimethylsilylmethyllithium solution, and stirred for 30 minutes at −78 °C. This solution was then added to Ru(bMepi)(PPh_3)Cl (29.8 mg, 0.041 mmol) dissolved in THF (10 mL). After stirring at −78 °C for 15 minutes, THF was removed under vacuum. The dark green solid was extracted with C_6D_6 and ^1H and ^{31}P NMR spectra were obtained. Crystals were obtained by diffusion of pentane into a solution of C_6H_6, at −35 °C. ^1H NMR (500 MHz, C_6D_6): δ 8.49 – 8.47 (m, 1H), 8.42 – 8.41 (m, 1H), 7.79 (d, J_{HH} = 7.8 Hz, 1H), 7.59 (d, J_{HH} = 8.3 Hz, 1H), 7.29 (dd, J_{HH} = 5.4, 3.0 Hz, 2H), 7.22 (t, J_{HH} = 7.8 Hz, 1H), 7.05 (t, J_{HH} = 7.5 Hz, 1H), 6.96 (t, J_{HH} = 8.3 Hz, 6 H, PPh_3), 6.82–6.76 (m, 9H, PPh_3), 6.49 (d, J_{HH} = 7.7 Hz, 2H), 6.43 (d, J_{HH} = 6.3 Hz, 1H), 6.14 (d, J_{HH} = 7.1 Hz, 1H), 5.98 (d, J_{HH} = 7.8 Hz, 2H), 2.79 (s, 3H), 2.26 (t, J = 12.1 Hz, 2H), 1.98 – 1.87 (m, 1H), 1.86 (s, 3H), 1.81 – 1.71 (m, 1H), 1.51 (s, 2H). $^{31}P\{1H\}$ NMR (500 MHz, C_6D_6): δ 62.55 (s, PPh_3).

3.11 Notes and References

(1) Fleming, F. F. Nat. Prod. Rep. 1999, 16, 597.

(2) (a) Fleming, F. F.; Yao, L.; Ravikumar, P. C.; Funk, L.; Shook, B. C. J. Med. Chem. **2010**, 53, 7902. (b) Pollak, P.; Romeder, G.; Hagedorn, F.; Gelbke, H.-P. In Ullmann's

Encyclopedia of Industrial Chemistry, 6th ed.; Bailey, J. E.et al., Eds.; Wiley-VCH Verlag GmbH & Co. KGaA: Weinheim, **2000**; pp 252−265.

(3) (a) Srimani, D.; Feller, M.; Ben-David, Y.; Milstein, D. *Chem. Commun*. **2012**, 48, 11853. (b) Gunanathan, C.; Hoelscher, M.; Leitner, W. Eur. J. *Inorg. Chem.* **2011**, **2011**, 3381.

(4) (a) Murahashi, S.-I.; Imada, Y. In Transition Metals for Organic Synthesis; Beller, M., Bolm, C., Eds.; Wiley-VCH Verlag GmbH: Weinheim, **2008**; p 497. (b) Sheldon, R. A.; Kochi, J. K. Metal Catalyzed Oxidations of Organic Compounds; Academic Press: San Diego, 1981; p 387. (c) Green, G.; Griffith, W. P.; Hollinshead, D. M.; Ley, S. V.; Schroder, M. J. Chem. Soc., *Perkin Trans.* 1 1984, 0, 681. (d) Lee, J. B.; Parkin, C.; Shaw, M. J.; Hampson, N. A.; Macdonald, K. I. *Tetrahedron* 1973, 29, 751. (e) Clarke, T. G.; Hampson, N. A.; Lee, J. B.; Morley, J. R.; Scanlon, B. *Tetrahedron Lett*. 1968, 9, 5685. (f) Stojiljkovic, A.; Andrejevic´ , V.; Mihailovi, M. L.´ *Tetrahedron* **1967**, 23, 721.

(5) (a) Yamazaki, S.; Yamazaki, Y. Bull. Chem. Soc. Jpn. 1990, 63, 301. (b) Nicolaou, K. C.; Mathison, C. J. N. *Angew. Chem., Int. Ed.* **2005**, 44, 5992. (c) Griffith, W. P.; Reddy, B.; Shoair, A. G. F.; Suriaatmaja, M.; White, A. J. P.; Williams, D. J. J. Chem. Soc., *Dalton Trans.* **1998**, 0, 2819. (d) Porta, F.; Crotti, C.; Cenini, S.; Palmisano, G. J. Mol. Catal. 1989, 50, 333.

(6) (a) Ryland, B. L.; Stahl, S. S. *Angew. Chem., Int. Ed.* **2014**, 53, 8824. (b) Kim, J.; Stahl, S. S. *ACS Catal*. **2013**, 3, 1652. (c) Schumperli, M. T.; Hammond, C.; Hermans, I. *ACS Catal*. **2012**, 2, 1108. (d) Aiki, S.; Taketoshi, A.; Kuwabara, J.; Koizumi, T.-a.; Kanbara, T. J. Organomet. Chem. **2011**, 696, 1301. (e) Maeda, Y.; Nishimura, T.; Uemura, S. Bull. Chem. Soc. Jpn. **2003**, 76, 2399. (f) Yamaguchi, K.; Mizuno, N. *Angew. Chem., Int. Ed.* **2003**, 42, 1480. (g) Mori, K.; Yamaguchi, K.; Mizugaki, T.; Ebitani, K.; Kaneda, K. *Chem. Commun*. **2001**, 0, 461. (h) Bailey, A. J.; James, B. R. *Chem. Commun*. **1996**, 0, 2343. (i) Tang, R.; Diamond, S. E.; Neary, N.; Mares, F. J. Chem. Soc., *Chem. Commun*. 1978, 0, 562.

(7) Gunaathan, C.; Milstein, D. *Science* **2013**, 341, DOI: 10.1126/ science.1229712.

(8) Yoshida, T.; Okano, T.; Otsuka, S. J. Chem. Soc., *Chem. Commun*. 1979, 870.

(9) (a) Bernskoetter, W. H.; Brookhart, M. *Organometallics* **2008**, 27, 2036. (b) Wang, Z.; Belli, J.; Jensen, C. M. Faraday Discuss. **2011**, 151, 297. (c) Gu, X.-Q.; Chen, W.; Morales-Morales, D.; Jensen, C. M. J. Mol. Catal. A: Chem. 2002, 189, 119.

(10) (a) Nielsen, M.; Alberico, E.; Baumann, W.; Drexler, H.-J.; Junge, H.; Gladiali, S.; Beller, M. Nature (London, U. K.) **2013**, 495, 85. (b) Rodríguez-Lugo, R. E.; Trincado, M.; Vogt, M.; Tewes, F.; SantisoQuinones, G.; Grützmacher, H. Nat. Chem. **2013**, 5, 342. (c) Spasyuk, D.; Smith, S.; Gusev, D. G. *Angew. Chem., Int. Ed.* **2012**, 51, 2772. (d) Nielsen, M.; Junge, H.; Kammer, A.; Beller, M. *Angew. Chem., Int. Ed.* **2012**, 51, 5711. (e) Marr, A. C. *Catal. Sci. Technol.* **2012**, 2, 279. (f) Prades, A.; Peris, E.; Albrecht, M. *Organometallics* **2011**, 30, 1162. (g) Johnson, T. C.; Morris, D. J.; Wills, M. *Chem. Soc. Rev.* **2010**, 39, 81. (h) Dobereiner, G. E.; Crabtree, R. H. *Chem. Rev.* **2010**, 110, 681. (i) Tseng, K.-N. T.; Kampf, J. W.; Szymczak, N. K. *Organometallics* **2013**, 32, 2046. (j) Friedrich, A.; Schneider, S. ChemCatChem **2009**, 1, 72. (k) Bonitatibus, P. J., Jr.; Chakraborty, S.; Doherty, M. D.; Siclovan, O.; Jones, W. D.; Soloveichik, G. L. *Proc. Natl. Acad. Sci. U. S. A.* **2015**, 112, 1687. (l) Murahashi, S.; Naota, T.; Ito, K.; Maeda, Y.; Taki, H. *J. Org. Chem.* 1987, 52, 4319. (m) Zhang, J.; Leitus, G.; BenDavid, Y.; Milstein, D. *J. Am. Chem. Soc.* **2005**, 127, 10840. (n) Zhao, J.; Hartwig, J. F. *Organometallics* **2005**, 24, 2441.

(11) (a) Tseng, K.-N. T.; Rizzi, A. M.; Szymczak, N. K. *J. Am. Chem. Soc.* **2013**, 135, 16352. (b) Tseng, K.-N. T.; Szymczak, N. K. Synlett **2014**, 25, 2385.

(12) (a) Reguillo, R.; Grellier, M.; Vautravers, N.; Vendier, L.; SaboEtienne, S. *J. Am. Chem. Soc.* **2010**, 132, 7854. (b) Jung, C. W.; Fellmann, J. D.; Garrou, P. E. *Organometallics* 1983, 2, 1042.

(13) (a) He, L.-P.; Chen, T.; Gong, D.; Lai, Z.; Huang, K.-W. *Organometallics* **2012**, 31, 5208. (b) Bui-The-Khai; Concilio, C.; Porzi, G. J. Organomet. Chem. 1981, 208, 249. (c) Arcelli, A.; Bui-The-Khai; Porzi, G. J. Organomet. Chem. 1982, 231, C31. (d) Hollmann, D.; Baehn, S.; Tillack, A.; Beller, M. *Angew. Chem., Int. Ed.* **2007**, 46, 8291. (e) Hollmann, D.; Baehn, S.; Tillack, A.; Beller, M. *Chem. Commun.* **2008**, 3199. (f) Saidi, O.; Blacker, A. J.; Farah, M. M.; Marsden, S. P.; Williams, J. M. J. *Angew. Chem., Int. Ed.* **2009**, 48, 7375.

(14) (a) Zeng, G.; Sakaki, S.; Fujita, K.-i.; Sano, H.; Yamaguchi, R. *ACS Catal*. **2014**, 4, 1010. (b) Li, H.; Wang, X.; Huang, F.; Lu, G.; Jiang, J.; Wang, Z.-X. *Organometallics* **2011**, 30, 5233. (c) Gunanathan, C.; Milstein, D. *Acc. Chem. Res.* **2011**, 44, 588. (d) Li, H.; Zheng, B.; Huang, K.-W. Coord. *Chem. Rev.* **2015**, 293−294, 116. (e) Conley, B. L.; Pennington-Boggio, M. K.; Boz, E.; Williams, T. J. *Chem. Rev.* **2010**, 110, 2294.

(15) (a) Gunanathan, C.; Milstein, D. *Chem. Rev.* (Washington, DC, U. S.) **2014**, 114, 12024. (b) Khaskin, E.; Iron, M. A.; Shimon, L. J. W.; Zhang, J.; Milstein, D. *J. Am. Chem. Soc.* **2010**, 132, 8542.

(16) Tseng, K.-N. T.; Kampf, J. W.; Szymczak, N. K. *ACS Catal*. **2015**, 5, 5468.

(17) Siggelkow, B.; Meder, M. B.; Galka, C. H.; Gade, L. H. Eur. J. *Inorg. Chem.* **2004**, **2004**, 3424.

(18) The equilibrium constant for octylamine was calculated to be 0.125 M, corresponding to $\Delta G = -1.23$ kcal/mol for the ligand substitution of octylamine. Note that benzylamine was calculated at 1, 20, and 100 equiv of benzylamine with respect to 1, while octylamine was calculated at one concentration (100 equiv).

(19) (a) Rohmann, K.; Hoelscher, M.; Leitner, W. *J. Am. Chem. Soc.* **2016**, 138, 433. (b) Weymuth, T.; Couzijn, E. P. A.; Chen, P.; Reiher, M. J. Chem. Theory Comput. **2014**, 10, 3092. (c) Ahlquist, M. S. G.; Norrby, P.-O. *Angew. Chem., Int. Ed.* **2011**, 50, 11794.

(20) See SI for detailed benchmarking studies

(21) H^-D exchange between 1-octylamine and toluene-d8 was observed during kinetic experiments and found to occur ∼3 times faster than amine dehydrogenation, and thus, initial rates were measured based on appearance of 1-octanenitrile product

(22) At 4.2% completion, there is an H_2 pressure of 0.07 psi, which will not significantly affect the initial rate of reaction. See erence 11a for H_2 dependence studies

(23) A bridging amine can decrease the activation barrier to 41.8 kcal/mol. See SI for more details.

(24) Protonation of the imine functionality was observed to be the kinetic site of protonation for Ru-bpi complexes over the isoindoline nitrogen (see erence 16). For the mechanism shown

in Scheme 4, protonation of the isoindoline nitrogen was found to occur with a barrier of 52.2 kcal/mol. See SI for more details.

(25) Csonka, R.; Speier, G.; Kaizer, J. *RSC Adv.* **2015**, 5, 18401.

(26) A four-membered transition state was also considered with a lower barrier of 27.4 kcal/mol. However, the experimentally derived rate law is inconsistent with this pathway. See SI for details.

(27) An oxidative addition of the N−H bond was also investigated after dissociation of the pyridine arm, because an open coordination site becomes available. The oxidative addition was calculated to occur with a barrier between 48 and 57.5 kcal/mol, depending on the ligand geometry of the transition state. The high barriers for each of these pathways makes oxidative addition of the N−H bond unlikely. For full details, see the SI.

(28) Protonation of the hydride by the equatorial amine was investigated and found to occur with a lower barrier of 33.6 kcal/mol for the bMepi variant. However, the release of H_2 is a higher energy process (39.7 kcal/mol) with an equatorial amido ligand. Thus, the overall pathway following hydride protonation from the equatorial amine is less favorable. See details in the SI.

(29) Brookhart, M.; Green, M. L. H.; Parkin, G. *Proc. Natl. Acad. Sci. U. S. A.* **2007**, 104, 6908.

(30) Gas-phase calculations and solvation models do not take into account the temperature dependence of the solvation free energy, and thus, the computed entropies are expected to differ from the experimental values. For an extensive discussion, please see: Plata, R. E.; Singleton, D. A. *J. Am. Chem. Soc.* **2015**, 137, 3811.

(31) Wilkins, R. G. Kinetics and Mechanism of Reactions of Transition Metal Complexes; Wiley-VCH Verlag GmbH & Co. KGaA: **2003**; p 199.

(32) (a) Weinhold, F.; Landis, C. R. Valency and Bonding: A Natural Bond Orbital Donor-Acceptor Perspective; Cambridge University Press: Cambridge, UK, **2005**. (b) Reed, A. E.; Curtiss, L. A.; Weinhold, F. *Chem. Rev.* 1988, 88, 899.

(33) (a) Bader, R. F. W. *Chem. Rev.* 1991, 91, 893. (b) Johnson, E. R.; Keinan, S.; Mori-Sanchez, P.; Contreras-Garcia, J.; Cohen, A. J.; Yang, W. *J. Am. Chem. Soc.* **2010**, 132, 6498. (c)

Contreras-Garcia, J.; Johnson, E. R.; Keinan, S.; Chaudret, R.; Piquemal, J.-P.; Beratan, D. N.; Yang, W. J. Chem. Theory Comput. **2011**, 7, 625.

(34) Lane, J. R.; Contreras-Garcia, J.; Piquemal, J.-P.; Miller, B. J.; Kjaergaard, H. G. J. Chem. Theory Comput. **2013**, 9, 3263.

(35) See SI for AIM analysis

(36) Jensen, S. J. K.; Tang, T.-H.; Csizmadia, I. G. *J. Phys. Chem. A* **2003**, 107, 8975.

(37) Cambridge Structural Database, version 1.17, April **2016**; Cambridge Crystallographic Data Centre, 12 Union Road, Cambridge CB2 1EZ, U.K..

(38) Utsunomiya, M.; Kuwano, R.; Kawatsura, M.; Hartwig, J. F. *J. Am. Chem. Soc.* **2003**, 125, 5608.

(39) Bryndza, H. E.; Tam, W. *Chem. Rev.* 1988, 88, 1163.

(40) (a) Bryndza, H. E.; Fultz, W. C.; Tam, W. *Organometallics* 1985, 4, 939. (b) Chang, Y.-H.; Nakajima, Y.; Tanaka, H.; Yoshizawa, K.; Ozawa, F. *J. Am. Chem. Soc.* **2013**, 135, 11791.

(41) (a) Crochet, P.; Gimeno, J.; Garcia-Granda, S.; Borge, J. *Organometallics* **2001**, 20

(42) , 4369. (b) Temprado, M.; McDonough, J. E.; Mendiratta, A.; Tsai, Y.-C.; Fortman, G. C.; Cummins, C. C.; Rybak-Akimova, E. V.; Hoff, C. D. *Inorg. Chem.* **2008**, 47, 9380. (c) Khalimon, A. Y.; Farha, P.; Kuzmina, L. G.; Nikonov, G. I. *Chem. Commun*. **2012**, 48, 455.

(43) (a) Zhao, Y.; Truhlar, D. G. J. Chem. Phys. **2006**, 125, 194101. (b) Zhao, Y.; Truhlar, D. G. *Chem. Phys. Lett*. **2011**, 502, 1. (c) Zimmerman, P. M. *J. Chem. Phys.* **2013**, 138, 184102. (d) Zimmerman, P. J. J. *Chem. Theory Comput*. **2013**, 9, 3043. (e) Zimmerman, P. M. J. Comput. Chem. **2015**, 36, 601.

Chapter 4: Stereoretentive Deuteration of α-Chiral Amines with D_2O

Portions of this chapter have been published:
Hale, L. V. A.; Szymczak, N. K. Stereoretentive Deuteration of α-Chiral Amines with D_2O. *J. Am. Chem. Soc.* **2016**, 138, 13489-13492

4.1 Introduction

Deuterium- and tritium-labeled compounds are widely applied in the pharmaceutical industry to enhance the pharmacokinetic properties of a drug, as metabolic tracers, and as mass spectrometry standards.[1] For drug development, D/T labeling offers a powerful approach for further modifications based on the known characteristics of the protio molecule. As a result of the kinetic isotope effect, the C–D bond is more inert toward metabolic oxidation compared with the C–H isotopologue. Thus, improvements in pharmaceutical residence times can be achieved at low cost and with predictable outcomes.[1a] Since this concept was first applied to bioactive molecules,[2] a substantial effort has been devoted to prepare and patent deuterium-labeled pharmaceuticals.[1e, 3] However, labeled compounds are commonly prepared via multistep syntheses and require expensive labeled starting materials. As an alternative strategy, isotope exchange through C–H bond activation allows direct labeling and ideally may be used as a late-stage modification of a complex molecule.[4]

The primary amine unit is an important functional group found in a variety of pharmaceutical drugs and is commonly metabolized through oxidative deamination by amine

oxidase enzymes.[5] For such compounds, the in vivo efficacy can be significantly improved by deuterium incorporation at a C–H bond that is adjacent to the primary amine nitrogen atom. For example, the bioactive compounds tryptamine,[2] amphetamine,[6] and dopamine[7] have been targeted for deuterium incorporation at the α-C–H position to slow metabolic oxidation (Figure 4-1). However, the labeling protocols for these compounds require multistep syntheses, resolution techniques for α-chiral amines, and/or use expensive labeled starting materials. [6-8]

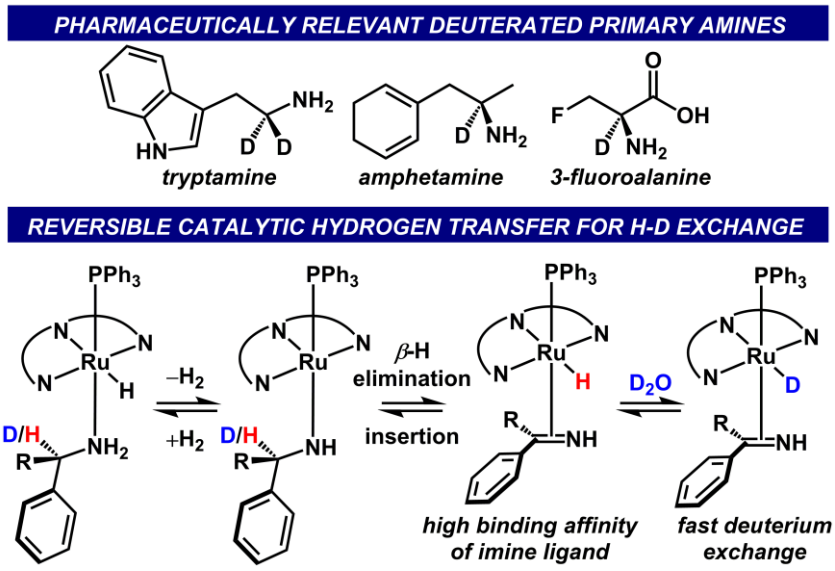

Figure 4-1. Select deuterated bioactive primary amines (top). Conceptual development of stereoretentive H/D exchange using hydrogen transfer (bottom).

A promising alternative strategy to incorporate deuterium into the amine unit is to employ catalytic hydrogen transfer using a ruthenium catalyst in D_2O.[9,10] This approach exploits reversible dehydrogenation/hydrogenation coupled with H/D exchange processes. However, the direct labeling of primary amines in this manner faces major challenges. (De)hydrogenation catalysts often facilitate transamination in the presence of primary amines, leading to a mixture of products.[9a,11] Furthermore, many bioactive compounds contain α-chiral amines, which can racemize through a prochiral imine intermediate during reversible β-hydride elimination.[12,13]

Finally, D_2 is commonly employed as the deuterium source, which is more expensive than D_2O and imposes additional operational challenges.[14] To overcome these limitations, we present a stereoretentive protocol for labeling primary amines that employs inexpensive D_2O.

We recently reported a series of Ru-bMepi complexes (bMepi = 1,3-(6′-methyl-2′-pyridylimino)isoindolate) that are excellent alcohol and amine dehydrogenation catalysts.[15] For amine dehydrogenation, imine intermediates remain coordinated to Ru following reversible *β*-hydride elimination from a Ru–amido intermediate (Figure 4-1).[16] This high binding affinity avoids the more commonly observed transamination reaction.[11] Due to the higher binding affinity of the imine vs the amine, we hypothesized that a chiral amine would retain its stereochemistry during a reversible *β*-hydride elimination process. This affinity could be exploited for stereoretentive deuteration if H/D exchange with the Ru–H occurs faster than reversible amine dehydrogenation.

4.2 Ruthenium-catalyzed H/D exchange with (*S*)-1-phenylethylamine and D_2O

To evaluate whether chiral amines retain their stereochemistry during the H/D exchange reaction, we selected (*S*)-1-phenylethylamine (7, Figure 4-2) as our model substrate. Notably, 7 is used as an advanced building block for syntheses of more complex molecules and is commercially available.[17] In a sealed vessel containing 1.24 mmol of (*S*)-1-phenylethylamine, 1 mol% **1** , and a 15:85 ratio of methylcyclohexane to D_2O, 71% deuterium incorporation was observed into the *α*-C–H position.[18] Significantly, H/D exchange proceeded with 90% ee.

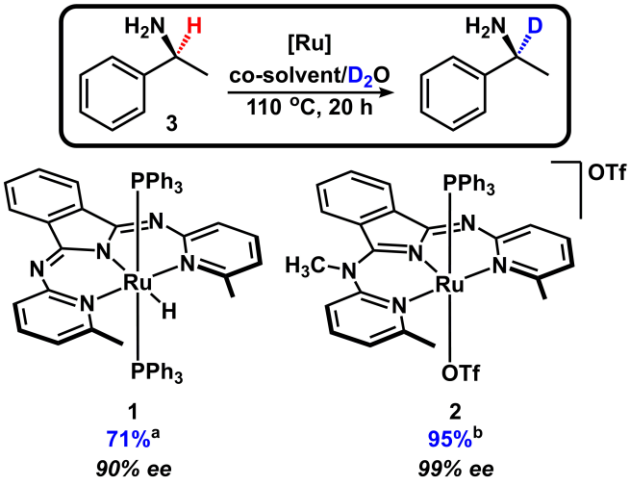

Figure 4-2. Stereoretentive deuterium incorporation of (*S*)-1-phenylethylamine with 1 and 2. [a]1 mol % 1 in methylcyclohexane. [b]2 mol % 2 in Me-THF.

The preservation of the stereochemistry in 7 is atypical in the absence of a chiral ligand. [19] Thus, we propose that two key factors influence stereoretention with **1**: (1) H/D exchange on ruthenium is fast in comparison to ligand (imine) exchange, and (2) the binding affinity of the imine intermediate is directly related to the retention of configuration for (*S*)-1-phenylethylamine. The Ru–H/Ru–D exchange reaction was evaluated using 1 by adding 3 equiv of D_2O to a solution of 1 in THF-d_8.[20] The appearance of HOD and H_2O after 10 min confirmed exchange of the Ru–H with D_2O. In contrast to amine dehydrogenation by 1, which requires at least 100 °C,[16] the H/D exchange of 1 with D_2O occurred at 35 °C. The facile exchange at low temperatures suggests that H/D scrambling of the Ru–H bond is much faster than amine dehydrogenation.[21]

To further mitigate racemization of chiral amine substrates, a more electrophilic Ru catalyst was selected to limit dissociation of the prochiral imine intermediate. The cationic complex $Ru(bMepi^{Me})(PPh_3)(OTf)_2$ (2, Figure 4-2)[22] was hypothesized to have a higher binding affinity for the imine ligand and, by extension, higher stereoretention compared to 1. Optimal conditions were

obtained by using a 15:85 ratio of 2-methyltetrahydrofuran (Me-THF) to D_2O in a sealed 3 mL tube,[23] with 2 mol% 2 for 20 h, which resulted in 95% deuterium incorporation with complete retention of stereochemistry (Figure 4-2).

4.3 Substrate Scope

Based on the limited number of amine deuteration procedures,[9,10,14] we applied our optimized conditions to a variety of chiral and achiral primary amines. For all substrates, high deuterium incorporation was identified at the α-carbon (Figure 4-3).[18] Notably, the presence of electron-withdrawing or -donating substituents on the substrate did not have a negative impact on the deuterium incorporation or enantiomeric purity. Substrates 8 and 9, which contain *para* -methoxy and *para* -chloro substituents, proceeded with complete retention of stereochemistry and 99 and 88% incorporation of deuterium, respectively. Deuterated bioactive compounds, such as dopamine[11,7] tryptamine[12,2] and *d*-amphetamine[13,6] as well as precursors to bioactive compounds[10,14,15,24] were obtained using our methodology. Importantly, a simple acidic workup removed the ruthenium catalyst, 2. For example, <4 ppm Ru was detected by ICP-OES after the isolation of the ammonium chloride salt of 4-methoxy-2-phenethylamine (6). The convenient workup and low level of Ru further highlights the potential to employ Ru-bMepi complexes for pharmaceutical applications.[25] The simple protocol for deuteration, coupled with the high deuterium incorporation, product recovery, and low residual metal content, demonstrates the broad utility of this catalytic deuteration method.

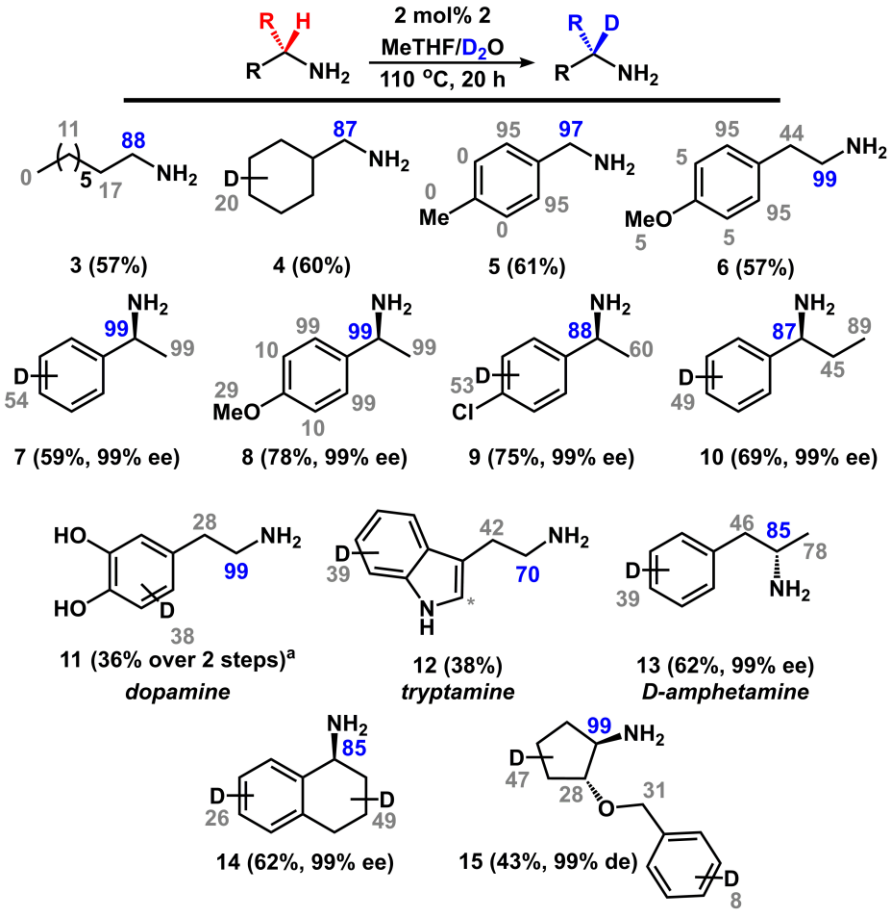

Figure 4-3. Deuteration of primary amines with 2 and D_2O. Deuterium incorporation was determined by ^2H NMR spectroscopy. Percent recovery shown in parentheses. [a]Formed from the deprotection of 3,4-dimethoxyphenylethylamine.

Many pharmaceutically relevant chiral amines contain heterocycles, amide, and ester functional groups. Such functional groups may erode the enantiomeric purity by competitive coordination during reversible hydrogen transfer. To evaluate this possibility, we examined the functional group tolerance and stereoretention of 7 in the presence of several common functional groups (Table 4-1).[26] In the presence of other L-type donor ligands, such as 2-butylthiophene (entry 1) and 3,5-lutidine (entry 2), the deuterium incorporation decreased to 55% and 24%; however, the enantiomeric purity was retained. Notably, additives such as esters and amides did not decrease deuterium incorporation or enantiomeric purity (entries 3 and 4). One limitation,

however, is the incompatibility with hydrogen acceptors such as 2-vinylnaphthalene (entry 5). The proposed mechanism for deuterium incorporation relies on a reversible hydrogen transfer process (Figure 4-1); hence, an additive that irreversibly removes hydrogen, such as an alkene, prevents deuterium incorporation. Overall, these results highlight the potential and limitations of Ru-bMepi complexes as late-stage stereoretentive deuteration catalysts with D_2O.

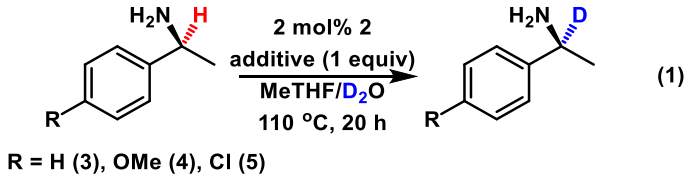

(1)

Entry	Additive	% D	% ee
1	2-butylthiophene	55	99
2	3,5-lutidine	24	99
3	methyl benzoate	85	99
4	*N*-methyl-*N*-phenylacetamide	95	99
5	2-vinylnaphthalene	0	N/A

Table 4-1. Deuteration of (*S*)-1-Phenylethylamine in the Presence of Common Functional Group Additives. Deuterium incorporation was determined by ^{2}H NMR spectroscopy using acetonitrile-d_3 as an internal standard

4.4 Rationalization for stereoretentive H/D exchange with *α*-chiral amines

The high binding affinity of the imine intermediate is proposed to be crucial to the stereoretention. This hypothesis was evaluated by comparing the dissociation energies of prochiral imine with analogous ketone intermediates (derived from alcohol precursors). Although the dissociation energy of benzaldimine is endergonic by 8.2 kcal/mol, acetophenone dissociation is exergonic by −3.9 kcal/mol (Figure 4-3).[16, 27] Consistent with these data, when (*S*)-1-phenylethanol

was subjected to conditions for H/D exchange, complete racemization was observed. The requirement for a coordinated imine intermediate is further supported by comparison with the known outer-sphere catalyst, Shvo's complex ([(η^5-$Ph_4C_4CO)_2H]Ru_2(CO)_4(\mu$-H)).[1] **3a**,[13d] We hypothesized that the % ee may erode with catalysts that operate through an outer-sphere mechanism due to face-to-face exchange of the imine π-bond. Accordingly, a reduction in % ee was observed with Shvo's catalyst, providing deuterium incorporation of 78% with 50% ee (Table 4-2, entry 2).

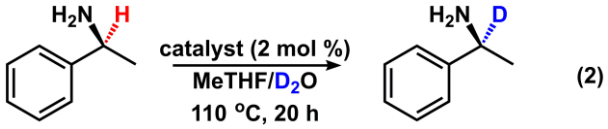

(2)

Entry	Catalyst	%D	%ee
1	**2**	95	99
2	[(η^5-$Ph_4C_4CO)_2H]Ru_2(CO)_4(\mu$-H))	78	50
3	[C_6H_3-2,6-($OP^tBu_2)_2$]IrHCl	7	NA
4	$Ru(PCy_3)_2(H)_2(H_2)_2$	61	65
5	$RuCl_2(PPh_3)_3$	94	68

Table 4-2. Deuteration of (*S*)-1-Phenylethylamine with known hydrogen transfer catalysts

Although an imine-bound intermediate appears to be a requirement for stereoretentive deuteration with 1 and 2, we propose additional features of the Ru-bMepi catalyst system that enable this transformation: (1) a reversible *β*-hydride elimination step, (2) a faster H/D exchange process on ruthenium than ligand exchange of the imine (vide supra), and (3) limited rotation of the *α*-chiral amine, which may be facilitated by *ortho*-CH_3 groups in complexes **1** and **2**. To assess the first point, we examined the iridium pincer complex [C_6H_3-2,6-($OP^tBu_2)_2$]IrH_2. This complex

is one of the few reported catalysts in addition to 1 that facilitates the double dehydrogenation of primary amines.[15c, 28] However, the mechanism is distinct from 1. Amine dehydrogenation by 1 occurs via a rate-determining hydride protonation step followed by fast and reversible *β*-hydride elimination of a Ru–amido species.[16] In contrast, $[C_6H_3\text{-}2,6\text{-}(OP^tBu_2)_2]IrH_2$ facilitates a reversible N–H bond oxidative addition followed by irreversible *β*-hydride elimination.[28a] When $[C_6H_3\text{-}2,6\text{-}(OP^tBu_2)_2]IrHCl$ was subjected to H/D exchange conditions,[29] deuterium incorporation of (*S*)-1-phenylethylamine provided only 7% deuterium incorporation (Table 4-2, entry 3).

The *ortho*-CH_3 groups may also contribute to high stereoretention by limiting rotation around the Ru–imine bond. Thus, we examined known inner-sphere (de)hydrogenation catalysts that have reported imine-bound ruthenium intermediates yet lack significant steric bulk around the ruthenium center (Table 4-2). The ruthenium catalyst $Ru(PCy_3)_2(H)_2(H_2)_2$[30] facilitates amine double dehydrogenation of 1-octylamine to 1-octanenitrile,[31] suggesting that this catalytic system may also promote H/D exchange with high enantiomeric purity. However, under our optimized conditions, we observed 61% deuterium incorporation into (*S*)-1-phenylethylamine, with only 65% ee (entry 4). Similarly, the inner-sphere catalyst $RuCl_2(PPh_3)_3$ resulted in 94% deuterium incorporation but only 68% ee (entry 5). These studies suggest that catalysts 1 and 2 have an additional feature that enables the retention of enantiomeric purity. We propose that the *ortho*-CH_3 substituents contribute to the high enantiomeric excess by preventing rotation of the *α*-chiral amine when coordinated to complexes 1 and 2.[32] Our analysis of known (de)hydrogenation catalysts highlights the unique role of the bMepi ligand. In the absence of chiral ligands, stereoretentive hydrogen transfers are not common.[14] We have identified the key features of Ru-bMepi complexes that enable stereoretention.

Limited examples of primary amine deuteration through C–H bond activation have been reported,[10] and even fewer exist for α-chiral amines.[14] Our study provides a new strategy to use an *achiral* hydrogen transfer catalyst for the stereoretentive H/D exchange of α-chiral amines—the first homogeneous catalyst to promote this transformation. We found that the highest stereoretention is achieved with a catalyst that tightly coordinates a prochiral imine intermediate, facilitates reversible β-hydride elimination, and fast Ru–H/Ru–D exchange. Overall, these studies provide a new method for stereoretentive C–H activation and will likely find application for late-stage deuteration as well as synthetic methodology.

4.5 Experimental

4.5.1 General Considerations

All manipulations involving the catalyst and catalysis were conducted under a nitrogen atmosphere using standard Schlenk technique, or in a glovebox unless otherwise stated. Amine reagents were purchased from commercial vendors, degassed, and used without further purification. If the amine was purchased as a hydrochloride salt or hemisulfate salt, the salt was dissolved in deionized water and NaOH was added. The aqueous solution was extracted with dichloromethane, and concentrated to obtain the freebase amine, which was then degassed and stored under nitrogen in the glovebox. The following compounds were synthesized according to literature methods: $HRu(bMepi)(PPh_3)_2$ (1),[1] $Ru(bMepi^{Me})(PPh_3)(OTf)_2$ (2),[2] $Ru(PCy_3)_2(H)_2(H_2)_2$,[3] and $[C_6H_3\text{-}2,6\text{-}(OP^tBu_2)_2]IrHCl$.[4] Toluene-$d_8$ was degassed using evacuation/refill cycles and then stored over 3 Å molecular sieves for at least 24 h in the glovebox prior to use. D_2O was degassed by sparging with nitrogen, and stored under nitrogen in the glovebox. Degassed, anhydrous solvents were obtained using a Glass Contour, SG Waters USA

solvent purification system or were distilled over CaH_2, degassed, and stored over 3 Å molecular sieves for at least 24 h in the glovebox prior to use. The 3 Å molecular sieves were dried at 250 °C under dynamic vacuum for 24 h. NMR spectra were recorded on Varian Inova 500, Varian MR400, Varian vnmrs 500 and Varian vnmrs 700 spectrometers at ambient temperature, unless otherwise stated. ^1H chemical shifts are reported in parts per million (ppm) relative to TMS. When ^1H NMR were obtained of ammonium hydrochloride salts in D_2O, $NaHCO_2$ was used as an internal reference (8.35 ppm in D_2O). ^2H NMR spectrum were obtained in CH_2Cl_2 or deionized H_2O, and ^2H chemical shifts are reported in parts per million (ppm) relative to TMS with a deuterated solvent as the internal standard (C_6D_6, CD_3CN, CD_2Cl_2, or CD_3OD). The enantiomeric excess for compounds 7-10, and 13-15 was determined using HPLC analysis with a DAICEL CHIRALPAK OD-H chiral stationary phase column, and a mobile phase of hexane/2-propanol dependent on the compound, and by comparing the samples with the appropriate racemic mixtures. ICP-OES was performed on a Perkin-Elmer Optima **2000** DV with Winlab software.

4.5.2 Initial observation and optimization of deuterium incorporation into 1-octylamine

Deuterium was incorporated into the α-carbon of 1-octylamine in the presence of toluene-d8 and $HRu(bMepi)(PPh_3)_2$ (1). When 1 mol% **1** was combined with 0.50 mmol 1-octylamine in toluene-d_8 solvent and heated at 120 °C for 1 h, both 1-octanenitrile (2%) and 1,1-d_2-octylamine (12%), were observed by ^1H and ^2H NMR spectroscopy. Deuterium incorporation to 1-octylamine was improved by employing D_2O, using methylcyclohexane as a co-solvent, and increasing the reaction time to 20 h. In a 5 mL sealed vessel containing 1.24 mmol 1-octylamine, 1 mol % **1**, and a 15:85 ratio of methylcyclohexane and D_2O, 60% deuterium incorporation was achieved after 20 hours.

4.5.3 General procedure for optimization of co-solvent, temperature, catalyst, and catalyst loading

A 8 mL microwave vial charged with amine (1.24 mmol), ruthenium catalyst 1 or 2, co-solvent (0.30 mL), D_2O (1.7 mL), and a stir bar was sealed and stirred (1000 rpm) at 110 °C for 20 hrs. After cooling to room temperature, the organic layer was removed and hexamethylbenzene (0.50 mL, 0.036M) was added as an internal standard. The deuterium incorporation was evaluated using ^1H NMR spectroscopy by comparing the integration of the remaining α-CH proton resonance to hexamethylbenzene.

4.5.4 Determination of a homogeneous or heterogeneous active catalytic species.

Nanoparticulate heterogeneous ruthenium catalysts have been reported to promote a selective H/D exchange reaction of amines using D_2, rather than D_2O, as the deuterium source.[5] To evaluate whether 2 serves as a precursor to an active heterogeneous catalyst, the catalytically active form of 2 was probed using catalyst poisoning experiments. Consistent with our previously reported homogeneous amine dehydrogenation,[6] the catalytic activity of 2 was minimally affected with the addition of 0.1 equivalent of phenanthroline, but complete poisoning was observed with the addition of 1 equivalent. This poisoning profile is consistent with a homogeneous, rather than a heterogeneous (nanoparticulate) catalyst for H/D exchange. Heterogenous catalysts are typically poisoned << 1 equiv poison.[7]

Procedure for poisoning experiments with phenanthroline.

A 8 mL microwave vial charged with amine (1.24 mmol), 2, Me-THF (0.30 mL), D_2O (1.7 mL), and a stir bar was sealed and stirred (1000 rpm) at 110 °C for 20 hrs. After 6 hours (36% deuterium incorporation at the α-CH position), the reaction was removed from heat, and

phenanthroline (0-2 equiv) was added. The reaction was heated for an additional 15 h. After cooling to room temperature, the organic layer was removed and hexamethylbenzene (0.50 mL, 0.036M) was added as an internal standard. The deuterium incorporation was evaluated using ^{1}H NMR spectroscopy by comparing the integration of the remaining α-CH to hexamethylbenzene.

4.5.5 Dependence on headspace volume of the reaction vessel.

A microwave vial (5, 8, or 32 mL) charged with amine (1.24 mmol), 2, Me-THF (0.30 mL), D_2O (1.7 mL), and a stir bar was sealed and stirred (1000 rpm) at 110 °C for 20 hrs. After cooling to room temperature, the organic layer was removed and hexamethylbenzene (0.50 mL, 0.036M) was added as an internal standard. The deuterium incorporation was evaluated using ^{1}H NMR spectroscopy by comparing the integration of the remaining α-CH proton resonance to hexamethylbenzene.

4.5.6 Deuterium exchange between HRu(bMepi)(PPh_3)$_2$ and D_2O

HRu(bMepi)(PPh_3)$_2$ (0.0075g, 0.0079 mmol) was dissolved in THF-d_8 (0.400 mL) in an NMR tube equipped with a J-Young valve. An initial ^{1}H NMR spectrum was obtained at 25 °C (A, Figure S1). A solution of hexamethylbenzene (0.28M, 0.0011 mmol) and D_2O (5.5M, 0.022 mmol) in THF-d_8 was then added and a second ^{1}H NMR spectrum was obtained in which an initial amount of HOD can be observed (B, Figure S1). Over 10 minutes at 35 °C a growth in HOD and H_2O can be observed (C and D, Figure S1), with a concomitant decrease in the Ru-H resonance.

4.5.7 General procedure for H/D exchange of amines with 2.

A 3 mL NMR tube, equipped with a J-Young valve, charged with amine (0.50 mmol), 2 (0.01 mmol, 2 mol %), Me-THF (0.115 mL), and D_2O (0.655 mL), was sealed and heated at 110 °C for

20 hrs. After cooling to room temperature, DCl (0.140 mL, 20% solution in D_2O) was added to the crude reaction to obtain the ammonium chloride salt. The D_2O layer was washed with dichloromethane (DCM, 6 x 1 mL). After the last DCM wash, the residual DCM was removed by rotary evaporation at room temperature (ca. 15 minutes). $NaHCO_2$ was then added as an internal standard and an ^1H NMR spectrum was obtained and compared against the reference (non-deuterated) ammonium salt in D_2O. NaOH (30 mg, 0.75 mmol) was added, and the organic layer was extracted with DCM (6 x 1 mL). The collected organic fractions were dried over Na_2SO_4, filtered, then concentrated to obtain a recovered mass of the freebase amine. A ^2H NMR spectrum was obtained in CH_2Cl_2 with a deuterated solvent as an internal standard, and compared against the ^1H NMR spectrum of the non-deuterated freebase amine in CD_2Cl_2. Deuterium incorporation was determined based on ^2H NMR integrations against the deuterated internal standard.

4.6 Notes and References

(1) (a) Gant, T. G. J. Med. Chem. **2014**, 57, 3595. (b) Tung, R. D. Future Med. Chem. **2016**, 8, 491. (c) Harbeson, S. L.; Tung, R. D. Annu. Rep. Med. Chem. **2011**, 46, 403. (d) Insa, R. ChemMedChem **2013**, 8, 336. (e) Timmins, G. S. Expert Opin. Ther. Pat. **2014**, 24, 1067. (f) Isin, E. M.; Elmore, C. S.; Nilsson, G. N.; Thompson, R. A.; Weidolf, L. Chem. Res. Toxicol. **2012**, 25, 532.

(2) Tryptamine was among the first drugs to be tested for an improved pharmacokinetic profile by incorporation of deuterium, and was previously prepared through the reduction of indole-3-acetamide with LiAlD4. See: Belleau, B.; Burba, J.; Pindell, M.; Reiffenstein, J. *Science* 1961, 133, 102.

(3) Halford, B. Chem. Eng. News **2016**, 94 ([27]), 32.

(4) Atzrodt, J.; Derdau, V.; Fey, T.; Zimmermann, J. *Angew. Chem., Int. Ed.* **2007**, 46, 7744.

(5) Mondovi, B.; Agro, A. F. Adv. Exp. Med. Biol. 1982, 148, 141.

(6) (a) Najjar, S. E.; Blake, M. I.; Lu, M. C. J. Labelled Compd. Radiopharm. 1978, 15, 71. (b) Najjar, S. E.; Blake, M. I.; Benoit, P. A.; Lu, M. C. J. Med. Chem. 1978, 21, 555. (c) Foreman, R. L.; Siegel, F. P.; Mrtek, R. G. J. Pharm. Sci. 1969, 58, 189.

(7) (a) Kańska, M.; Pająk, M. J. Radioanal. Nucl. Chem. **2009**, 281, 365. (b) Perel, J. M.; Dawson, D. K.; Dayton, P. G.; Goldberg, L. I. J. Med. Chem. 1972, 15, 714.

(8) Gynther, J.; et al. Acta Chem. Scand. 1988, B42, 433.

(9) (a) Neubert, L.; Michalik, D.; Baehn, S.; Imm, S.; Neumann, H.; Atzrodt, J.; Derdau, V.; Holla, W.; Beller, M. *J. Am. Chem. Soc.* **2012**, 134, 12239. (b) Alexakis, E.; Hickey, M. J.; Jones, J. R.; Kingston, L. P.; Lockley, W. J. S.; Mather, A. N.; Smith, T.; Wilkinson, D. J. *Tetrahedron Lett*. **2005**, 46, 4291.

(10) Takahashi, M.; Oshima, K.; Matsubara, S. Chem. *Lett*. **2005**, 34, 192.

(11) Dobereiner, G. E.; Crabtree, R. H. *Chem. Rev.* **2010**, 110, 681.

(12) Conley, B. L.; Pennington-Boggio, M. K.; Boz, E.; Williams, T. J. *Chem. Rev*. **2010**, 110, 2294.

(13) (a) Ahn, Y.; Ko, S.-B.; Kim, M.-J.; Park, J. Coord. *Chem. Rev.* **2008**, 252, 647. (b) Macgregor, S. A.; Vadivelu, P. *Organometallics* **2007**, 26, 3651. (c) Zhao, J.; Hesslink, H.; Hartwig, J. F. *J. Am. Chem. Soc.* **2001**, 123, 7220. (d) Warner, M. C.; Backvall, J.-E.¨*Acc. Chem. Res.* **2013**, 46, 2545. (e) Stark, G. A.; Gladysz, J. A. *Inorg. Chem.* **1996**, 35, 5509. (f) Bornschein, C.; Gustafson, K. P. J.; Verho, O.; Beller, M.; Backvall, J.-E.¨*Chem. - Eur. J.***2016**, 22, 11583.

(14) (a) Taglang, C.; Perato, S.; Sam Lone, A.; Puente, C.; Dugave, C.; Rousseau, B.; Pieters, G.; Martinez-Prieto, L. M.; del Rosal, I.; Maron, L.; Poteau, R.; Chaudret, B.; Philippot, K. *Angew. Chem., Int. Ed.* **2015**, 54, 10474. (b) Using electrolysis of D_2O to form D2 in situ: Bhatia, S.; Spahlinger, G.; Boukhumseen, N.; Boll, Q.; Li, Z.; Jackson, J. E. Eur. *J. Org. Chem.* **2016**, **2016**, 4230.

(15) (a) Tseng, K.-N. T.; Kampf, J. W.; Szymczak, N. K. *Organometallics* **2013**, 32, 2046. (b) Tseng, K.-N. T.; Rizzi, A. M.; Szymczak, N. K. *J. Am. Chem. Soc.* **2013**, 135, 16352. (c) Tseng, K.-N. T.; Szymczak, N. K. Synlett **2014**, 25, 2385. (d) Tseng, K.-N. T.; Kampf, J. W.; Szymczak, N. K. *ACS Catal*. **2015**, 5, 5468. (e) Tseng, K.-N. T.; Lin, S.; Kampf, J. W.; Szymczak, N. K. *Chem. Commun*. **2016**, 52, 2901.

(16) Hale, L. V. A.; Malakar, T.; Tseng, K.-N. T.; Zimmerman, P. M.; Paul, A.; Szymczak, N. K. *ACS Catal*. **2016**, 6, 4799.

(17) Nogradi, M. Stereoselective Synthesis: A Practical Approach, 2nd ed.; VCH: Weinheim, 1995.

(18) Deuterium incorporation was also observed at other C−H positions. See SI and Figure 4-3 for full details.

(19) For a representative example, see: Bizet, V.; Pannecoucke, X.; Renaud, J.-L.; Cahard, D. *Angew. Chem., Int. Ed.* **2012**, 51, 6467.

(20) Note that a ruthenium−imine species could not be isolated; thus, PPh_3 was employed as an alternative L-type ligand.

(21) For a similar H/D exchange reaction with a ruthenium hydride, see: Frost, B. J.; Mebi, C. A. *Organometallics* **2004**, 23, 5317.

(22) Tseng, K.-N. T.; Kampf, J. W.; Szymczak, N. K. *ACS Catal*. **2015**, 5, 411.

(23) The incorporation of deuterium is affected by the volume of the reaction vessel. See SI for details.

(24) (a) Thalen, L. K.; Zhao, D.; Sortais, J.; Paetzold, J.; Hoben, C.;` Backvall, J.-E.¨ *Chem. - Eur. J.***2009**, 15, 3403. (b) Knight, A.; Hemmings, J. L.; Winfield, I.; Leuenberger, M.; Frattini, E.; Frenguelli, B. G.; Dowell, S. J.; Lochner, M.; Ladds, G. J. Med. Chem. **2016**, 59, 947. (c) Giardina, G. A. M.; Sarau, H. M.; Farina, C.; Medhurst, A. D.; Grugni, M.; Foley, J. J.; Raveglia, L. F.; Schmidt, D. B.; Rigolio, B.; Vassallo, M.; Vecchietti, V.; Hay, D. W. P. J. Med. Chem. **1996**, 39, 2281.

(25) Dunn, P. J., Hii, K. K., Krische, M. J., Williams, M. T., Eds. Sustainable Catalysis: Challenges and Practices for the Pharmaceutical and Fine Chemical Industries; John Wiley & Sons, Inc.: New York, **2013**.

(26) Collins, K. D.; Glorius, F. Nat. Chem. **2013**, 5, 597.

(27) The binding affinity of *α*-methylbenzylidenimine is expected to be higher than that of benzaldimine. As an analogy, ketones typically have a higher binding affinity than aldehydes. See: Sanders, J. K. M.; Williams, D. H. *J. Am. Chem. Soc.* 1971, 93, 641.

(28) (a) Bernskoetter, W. H.; Brookhart, M. *Organometallics* **2008**, 27, 2036. (b) Wang, Z.; Belli, J.; Jensen, C. M. Faraday Discuss. **2011**, 151, 297.

(29) $[C_6H_3\text{-}2,6\text{-}(OP^tBu_2)_2]IrH_2$ was generated in situ using 10 mol% NaO^tBu.

(30) Chaudret, B.; Poilblanc, R. *Organometallics* **1985**, *4*, 1722.

(31) 1-Octylamine dehydrogenation to 1-octanenitrile (9% GC yield) occurred using Ru(PCy3)2(H)2(H_2)2 (1 mol%). See SI.

(32) Ru(bpi)(Cl)(PPh_3)2 is inactive for amine dehydrogenation as well as H/D exchange. See 16 for more details.

Chapter 5: Intercepting Ketenimines from *α,β*-Unsaturated Nitriles During Catalytic Hydrogen Transfer

5.1 Introduction

Ketenimines are a diverse class of synthetic intermediates for highly functionalized chemicals, including synthetically challenging quaternary carbon centers and complex heterocycles.[1] Transformations from ketenimines encompass both electrophilic and nucleophilic additions, as well as cycloaddition and sigmatropic rearrangements. The synthetic versatility of ketenimines is possible due to three resonance structures that represent the charge delocalization across the heterocumulene unit (**a-c**, Figure 5-1). While the central carbon of a ketenimine is electrophilic, the nitrogen and terminal carbon exhibit nucleophilic character. Harnessing the ketenimine to react as a nucleophile or electrophile depends on influencing the electronic character of substituents R_1, R_2, and R_3.

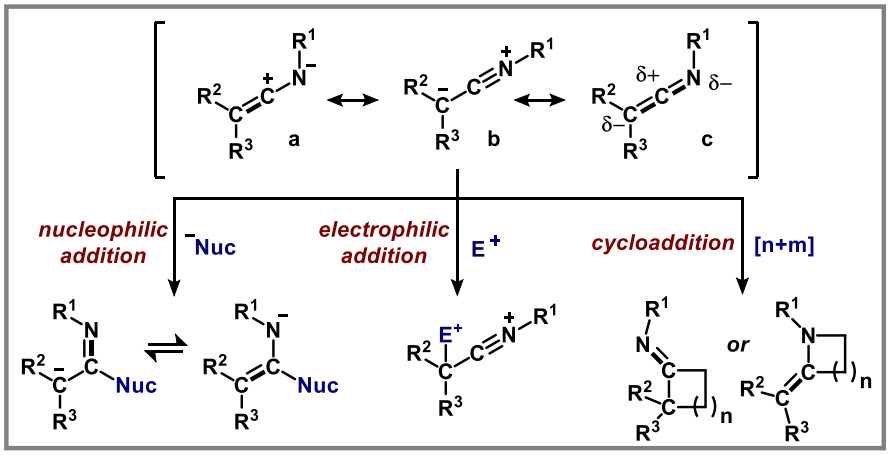

Figure 5-1. Resonance structures and reaction diversity of ketenimines

Despite their broad synthetic utility, a limited number of catalytic methods utilize ketenimines (Figure 5-2). This is due to a narrow scope of organic precursors that are available for predictable *in situ* generation of a ketenimine intermediate.[2,3] For example, *N*-allyl ynamides are tailored for Pd(0) catalysts, and the ketenimine is only accessible following a 1,3-metallotropic shift to form a Pd-allyl species (Figure 5-2a).[4,5] Alternatively, copper catalysts may generate ketenimines from highly reactive azides and alkynes under basic conditions (Figure 5-2b).[6] For catalytic methods based on Cu and Pd, the resulting ketenimine necessarily has a stabilizing substituent (R1) at nitrogen.[7-9] Transition-metal ketenimines may also be formed *via* stoichiometric deprotonation of alkyl nitriles; however, catalytic examples are limited to acetonitrile or benzylic nitriles (Figure 5-2c).[8]

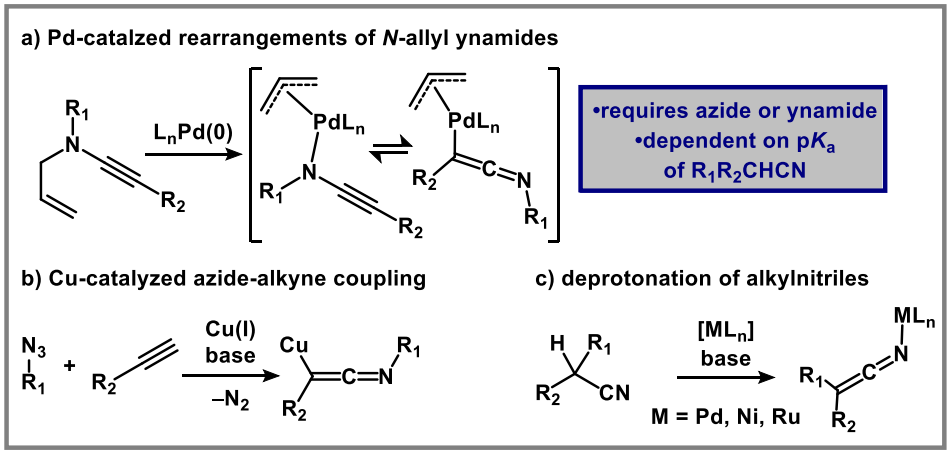

Figure 5-2. Catalytic formation of ketenimines

Catalysis involving transition-metal hydrides offer an alternative entry point for accessing ketenimine intermediates through insertion reactions. Nitriles commonly undergo insertion into metal-hydrides to afford imine type products. However, if the nitrile contains another site of unsaturation, isomerization to a ketenimine is possible. α,β-Unsaturated nitriles represent an ideal building block because they can be easily accessed from the corresponding ketone, aldehyde, or

alkene in a single step.[10,11] Despite their potential for rapid multi-functionalization, there have been no reports that demonstrate this approach.[12] If generated as a catalytic intermediate, ketenimines may undergo tandem functionalization through nucleophilic, electrophilic, or cycloaddition reactions.[13,14]

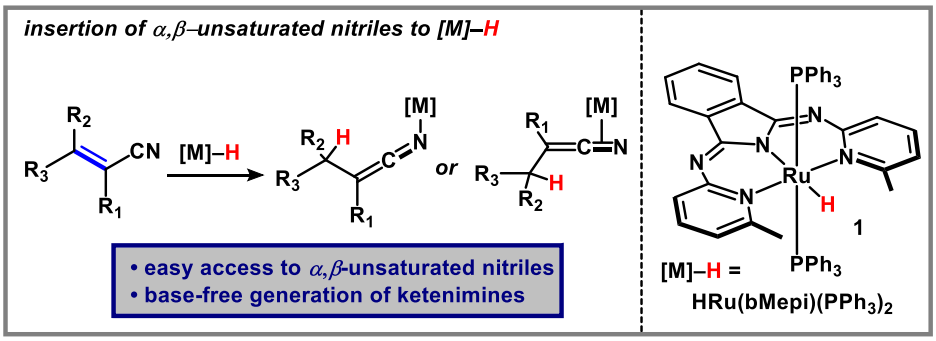

Figure 5-3. *In situ* formation of ketenimines for *via* the insertion of *α,β*-unsaturated nitriles into M–H.

5.2 Capture of *N*-Metalated Ketenimines via Hydride Insertion

We previously reported that $HRu(bMepi)(PPh_3)_2$ (**1**) is an excellent catalyst for reversible hydrogen transfer reactions of alcohols and amines.[15-18] For nitrile substrates, hydride insertion readily occurs to form imine coordinated species, and the catalytically active Ru–H can be directly (re)generated from H_2. **1** exhibits unique reactivity with amines and nitriles and has a high binding affinity for the intermediate imine.[18,19] We hypothesized that this unique reactivity would provide an entry point to partially saturated insertion products, such as ketenimines.

When *α*-phenylcinnamonitrile (**2**) (1.3 equiv) was added to a toluene-d_8 solution of **1** at room temperature, quantitative conversion to a new species occurred within 5 minutes. ^{31}P NMR spectroscopy confirmed the disappearance of **1** (51 ppm), concomitant with the appearance of free PPh_3 and a new resonance at 39 ppm. **1** was also absent in the ^1H NMR spectrum, with no detectable H_2, consistent with a hydride insertion reaction. A phase sensitive ^1H–^{13}C correlation

experiment (HSQC) revealed the presence of a –CH_2 group (^{1}H δ: 3.20; ^{13}C δ: 34.7), consistent with hydride addition to the least substituted carbon of *α*-phenylcinnamonitrile (Figure 5-4).

X-ray diffraction unambiguously confirmed the insertion product as the Ru-ketenimine complex **3a**. The *N*-metalated ketenimine has a C1−N1 bond length of 1.190(7) Å and a C1–C2 bond length of 1.369(7) Å, which are lengthened and shortened, respectively, compared to the typical bonds lengths of –C≡N (avg. 1.14 Å) and C–C (avg. 1.54 Å) groups. These bond distances are consistent with known metal-ketenimine complexes and reflect electronic delocalization from the partially negative C2 atom into the adjacent –CN group. All reported *N*-metalated Ru-ketenimine complexes exhibit nearly linear coordination modes (Ru–N–C1 Avg. 173°). However, the Ru–N1–C1 angle in **3a** is bent (= 141°), which is unusual for metalated ketenimines — only four structurally characterized ketenimine complexes have M–N–C angles <145°.[20-24] This deviation from linear binding is consistent with sp^2 rather than sp-hybridization at nitrogen.[25]

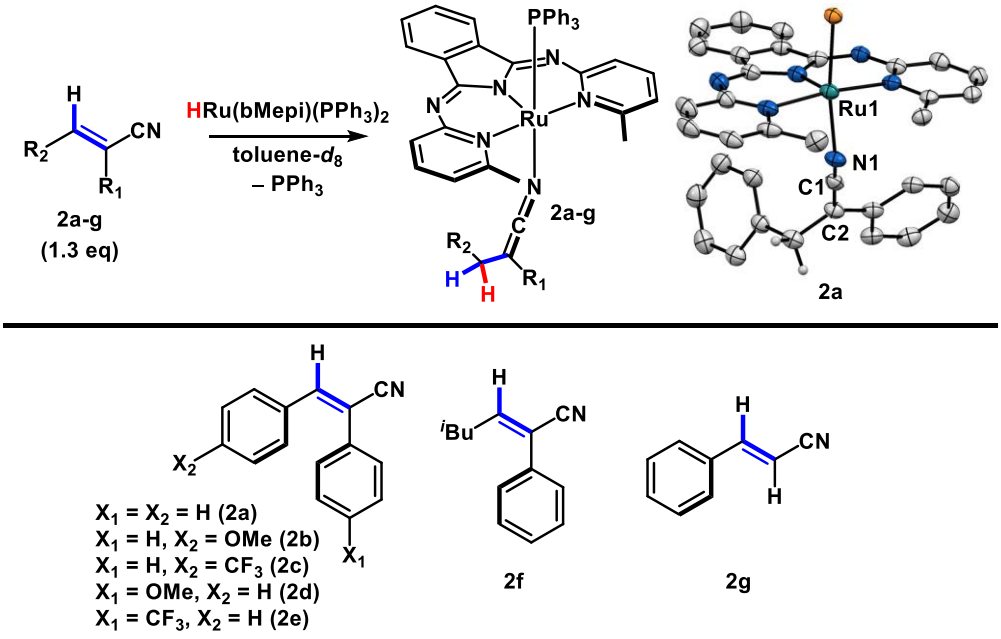

Figure 5-4. Formation of Ru-ketenimine complexes from 1 and *α,β*-unsaturated nitriles.

The stability of **3a** was evaluated by NMR spectroscopy at temperatures ranging from −40 °C to 70 °C. While a single compound was observed at temperatures < 70 °C, broadening of PPh_3 and minor decomposition products were observed > 70 °C. The quantitative formation of **3a** coupled with its high stability suggested that H^- insertion from 1 occurs *irreversibly* to capture the ketenimine derived from *α*-phenylcinnamonitrile. Computational analysis using Density Function Theory (DFT; rb3lyp/6-31g(d,p)) of the insertion reaction between 1 and *α*-phenylcinnamonitrile provided an exergonic Gibbs free energy of −20.1 kcal/mol to form **3a**. The facile formation and high stability of **3a** is attributed in part to the presence of the *α*-phenyl substituent, which forms a conjugated network across Ph–C=C=N. A depiction of the HOMO (−4.042 eV) for **3a** illustrates the extent of conjugation with the alignment of orbitals between the aromatic π-system and ketenimine moiety (Figure 5-5).

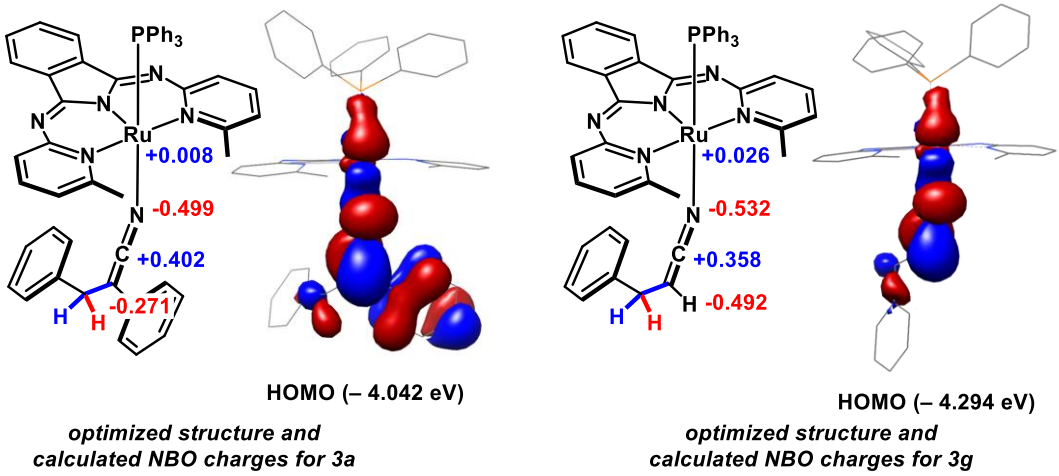

Figure 5-5. Optimized geometries of 3a and 3g with HOMO/LUMO depictions and NBO charge.

Hydride insertion to afford Ru-coordinated ketenimines was general to other *α*-phenyl substituted alkenyl nitriles. For instance, varying the *para* substituent of either phenyl group with OMe or CF_3 quantitatively provided Ru-ketenimine products with similar ^{1}H, ^{31}P, and ^{13}C signals

to **3a**. Replacing the *β*-phenyl substituent with an isobutyl group also resulted in similar spectroscopic features; however, an elevated reaction temperature of 70 °C in toluene-d_8 was required to initiate the insertion reaction, consistent with a higher barrier toward H^- transfer using electron rich alkenes. In contrast to alkenyl nitrile compounds with *α*-phenyl groups, addition of cinnamonitrile resulted in multiple species as assessed by ^{31}P NMR spectroscopy. Although the disappearance of the hydride resonance in the ^1H NMR spectrum suggested an insertion process of cinnamonitrile with **1**, neither *N* or *C*-coordinated products could be distinguished using 1D NMR spectroscopy.

The Ru-ketenimine derived from cinnamonitrile (**3g**) was evaluated through computational analysis. Similar to **3a**, formation of **3g** via H^- insertion from **1** is exergonic ($\Delta G = -13.1$ kcal/mol). Additionally, both ketenimines **3g** and **3a** display similar geometry and bond metrics; the cinnamonitrile derived ketenimine coordinates to Ru with a Ru–N–C*α* angle of 135°, and bond lengths of 1.211 Å and 1.338 Å for N–C*α* and C*α*–C*β*. Overall, experimental and theoretical analysis of **3a** and **3g** suggest that Ru-ketenimines are both thermodynamically and kinetically stable complexes.

The advantage of *base-free* hydride transfer to capture ketenimines was emphasized when the corresponding alkyl nitriles were employed as precursors to **3a** and **3g**. Deprotonation of acidic *α*-cyano C–H groups is a common approach to form metalated nitriles or ketenimines. Upon addition of 2a′ (5 equiv) to 1 in toluene-d_8 at room temperature, **3a** was generated in 38% conversion, relative to **1**. Although H_2 was not observed by NMR spectroscopy, the formation of **3a** from 2a′ likely occurs through deprotonation of the acidic *α*-C–H bond by Ru–H. Thus, in addition to hydride *insertion*, hydride *protonation* is a viable entry point to Ru-ketenimine

complexes. However, this approach is dependent on the pK_a of the saturated nitrile and limited to alkyl nitriles with highly acidic α-CH groups. No reaction occurred in the presence of the non-activated nitrile 2g′.

The electronic influence imparted by substituents at N and C2 dictates the reactivity of ketenimines. Natural Bond Order (NBO) analysis was performed for **3a** and **3g** to provide detailed charge distributions for the ketenimine units (Figure 5-5). **3a** exhibits partial negative charges located on N (−0.499) and C2 (−0.271), and a positive charge at C1 (+0.402). When the NBO analysis of **3g** was repeated after replacing –Ph with –H, we noted an increase in negative charge at C2 to −0.429, in line with the absence of an electron withdrawing α-substituent. Notably, the C1=N bond of **3g** is nearly twice as polarized (ΔN-C1 = 0.174) compared to that of **3a** (ΔN-C1= 0.097).

5.3 Hydrogenation Reactivity of 3a with H_2

Despite the relative solution stability of **3a**, the bent geometry and polarized charge of the C2=C1=N unit suggest the ketenimine is primed to react through two distinct pathways. While electrophilic reagents may initiate transformations at the negatively charged C2 position, nucleophilic species would target the polarized –CN group. To evaluate potential catalytic methods based on either reactant class, we considered conditions in which the Ru–H bond could be regenerated. Because **1**is capable of facile reversible hydrogenation, we began reactivity studies using H_2. Following H^- transfer to form the Ru-ketenimine, deprotonation of a Ru–(η^2-H_2) intermediate could occur by either the negatively charged carbon or nitrogen of the ketenimine, and simultaneously reform the Ru–H bond.

In the presence of H_2 (100 psig) and 1 mol % **1**, hydrogenation of **3a** occurred at 70 ºC in 96% conversion to a mixture of nitrile and amine products after 15 h (Figure 5-6). 2,3-diphenylpropanenitrile (2a′) was found as the major product (44%). The remaining products consisted of a mixture of semi-hydrogenated species, (4a and 4a′, 31%), and the fully hydrogenated primary amine (5a, 13%). Based on the ^{1}H NMR chemical shifts of the olefin signals, 4a (6.69 (t), J_{HH} = 9.5 Hz) and 4a′ (6.05 (t), J_{HH} = 8.5) were assigned as the enamine-imine tautomer. When the hydrogenation reaction was stopped at an earlier timepoint (2.5 h) or conducted at lower temperatures (25 – 50 °C), only the saturated nitrile 2a′ was observed. These results suggest that H^+ transfer to C2 is kinetically favored from **3a**; however, competing hydrogen transfer events to the –CN group become operative at higher temperatures and/or longer reaction times. The primary enamine (4a) and imine (4a′) products were calculated to be 2.4 kcal/mol and 0.5 kcal/mol thermodynamically downhill from 2,3-diphenylpropanitrile. A primary allylic amine was also considered as a possible product; however, computations show that this species is 3.8 kcal/mol *uphill* than 2,3-diphenylpropanitrile (2a′), suggesting this product is neither thermodynamically favored or kinetically accessible.

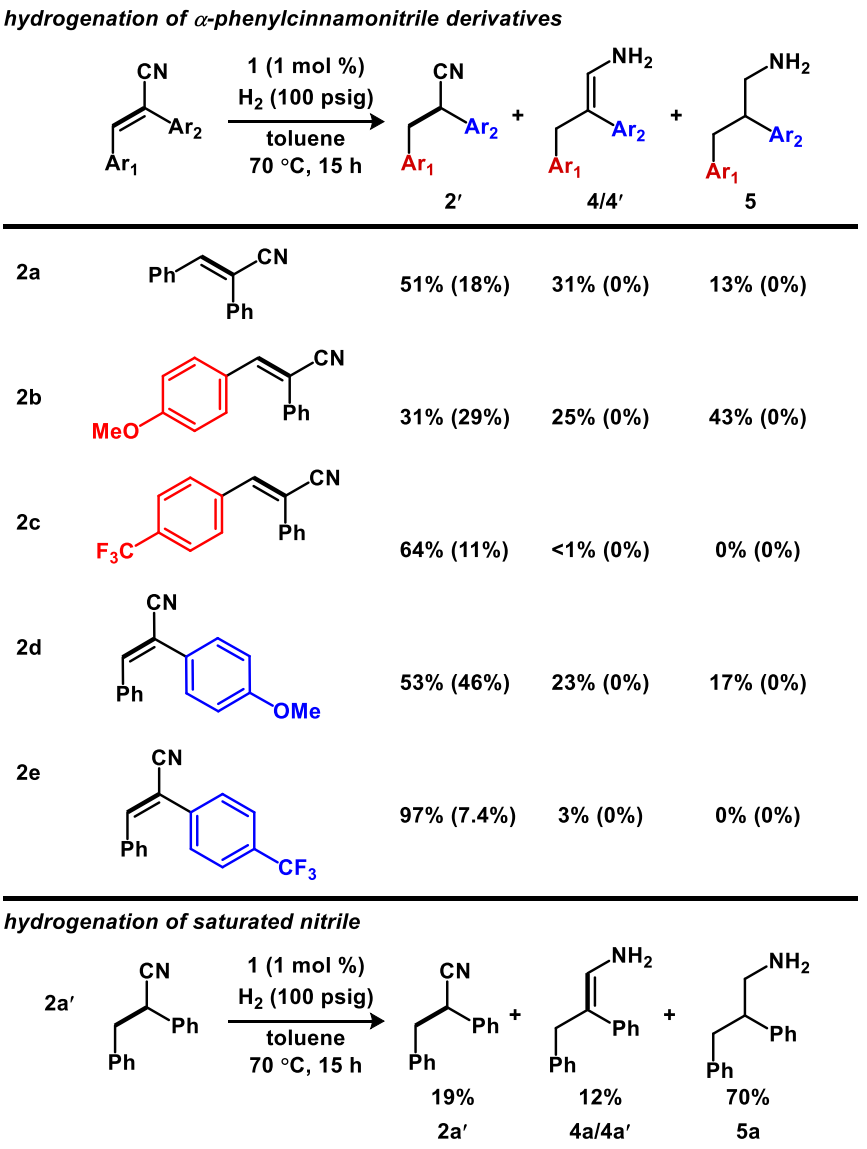

Figure 5-6. Product distribution depends on reaction time and substrate electronics. % NMR yields are based on an PhTMS as the internal standard and 15h. Values in parentheses are % NMR yields at 2.5 h.

5.4 Enamine-Imine Tautomers are Intercepted from Alkyl Nitriles

To probe the electronic influence of the substrate on the formation of 4a and 4a′, *α,β*-unsaturated nitriles 2a-2e were evaluated under hydrogenation conditions at 2.5 and 15 h (Figure 5-6. For all substrates, the nitrile 2a′-2e′, was the only product formed at 2.5 h, with NMR yields

ranging from 7 – 46%. Electron-rich alkenyl nitriles with *para*–OMe_3 substituents (2b and 2d) provided higher conversion to the corresponding saturated nitriles (29% for 2b′ and 46% for 2d′), compared to 18% obtained from 2a at 2.5 h. In contrast, electron deficient substrates 2c and 2e, gave only 11 and 7% yield of 2c′ and 2e′, respectively. Combined with the observation that the Ru-ketenimine intermediate is the resting state in the presence of H_2, and NBO analysis that highlights the sensitivity of C2 toward electronic perturbations, these data strongly support that protonation of the C2 position from H_2 is kinetically favored over H^+ addition to the coordinated nitrogen.

Longer reaction times (15 h) with electron rich substrates resulted in a mixture of hydrogenated products. While electron-donating –OMe groups promoted the formation of semi- and fully-hydrogenated amine products (4/4′ and 5), electron withdrawing $–CF_3$ groups completely hindered the production of amine products. We propose the formation of enamine/imine products is dependent on: 1) the basicity of the nitrogen atom, consistent with higher production of amine using more electron rich substrates, and 2) the equilibrium constant (K_{eq}) for the formation of a Ru-ketenimine via deprotonation of the alkyl nitrile. Because formation of **3a** is *reversible* from activated α-cyano groups, the thermodynamically more stable imine/enamine product can form. To test this hypothesis, 2a′ was subjected to catalytic hydrogenation conditions (Figure 5-6, bottom). After 15 h, hydrogenation to 82% conversion gave a mixture of 5a (70%), and 4a/4a′ (12%).

5.5 Hydroboration of Ru-Ketenimine Intercepts Enamine-Imine Tautomers

To determine if selective nucleophilic reactivity could be achieved at the C1 site, rather than electrophilic (H^+) addition to C2, we explored the addition of exogenous hydride sources.

When pinacolborane (HBpin, 1.1 equiv) was added to a mixture of 2a and **1**(1 mol%) in toluene-d_8, the blue solution turned to light green within minutes, suggesting a fast reaction of **3a** with HBpin. The ^{31}P NMR spectrum of the reaction mixture showed complete consumption of the ketenimine (39 ppm), and a new species at 36 ppm. Additionally, a distinct downfield resonance appeared in the ^{1}H spectrum as a broad singlet at 5.5 ppm and integrated as a single proton relative to the six *ortho*-CH_3 protons of the bMepi ligand (s, 1.51 ppm) and twelve –CH_3 signals assigned to BPin (s, 0.70 ppm). These chemical shifts are proposed to correspond to a metalated *enamine* intermediate that results from the addition of H^- (Figure 5-7).

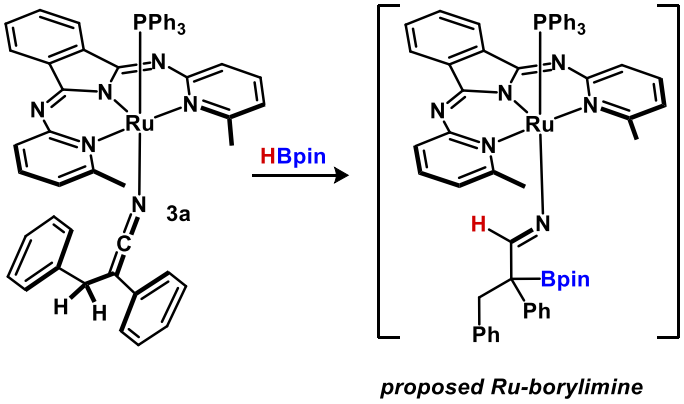

Figure 5-7. Hydroboration of 3a with HBpin to form an *α*-borylimino complex

Heating the reaction mixture to 70 °C in the absence of H_2 resulted in the poor conversion (17%) of 2a over two days. However, in the presence of H_2 (30 psig), *complete conversion* to form a mixture of products occurred. We hypothesize that this mixture consists of products derived from the proposed *C*-boryl Ru-imine intermediate (Figure 5-7). Notably, hydrogenation of 2a is suppressed, forming 2a′ in only 17% when H_2 is present, likely due to the background reaction described above.

Two reaction pathways are proposed following the formation of a Ru-imine intermediate: 1) a second addition of HBpin, which would provide an *N*,*C*-diboryl imine, and 2) hydrogenation of the Ru-imine intermediate to form a *C*-boryl aldimine. The higher reaction conversion observed with the addition of H_2 points toward the latter scenario. We note that boryl imines may undergo enamine-imine tautomerization, and thus provide more stable enamine isomers N-borylenamines). The Gibbs free energy resulting from *α,β*-unsaturated nitrile (2a), HBpin, and/or H_2, was calculated for each product (b3lyp/631g(d,p) level of theory). The enamine isomers are downhill in energy from 2a by 33.3 and 36.5 kcal/mol, depending on whether a double hydroboration (top reaction, Figure 5-8) or a tandem hydroboration/hydrogenation is operative (bottom reaction, Figure 5-8).

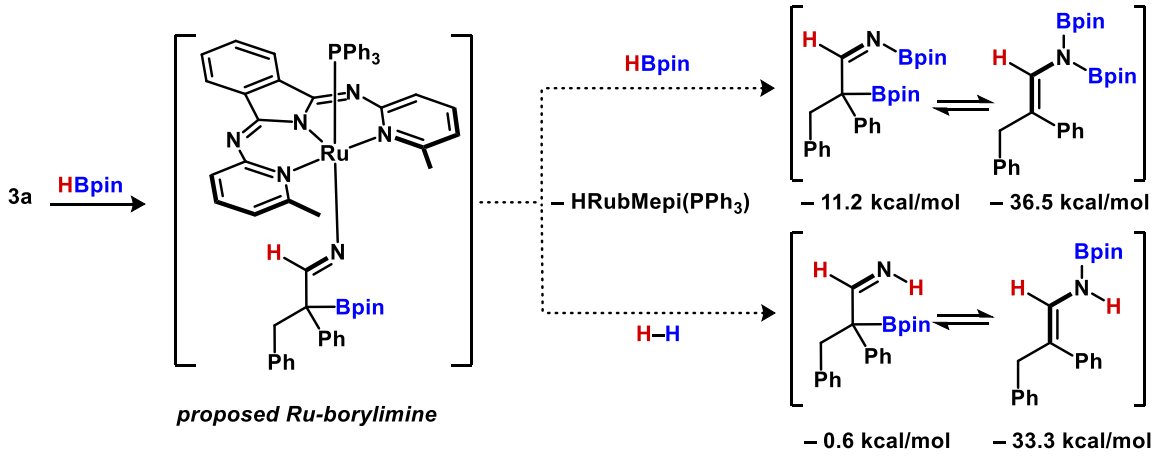

Figure 5-8. Double hydroboration versus a tandem hydroboration/hydrogenation reaction

5.6 Hydrocarbonylation of Ru-Ketenimines with Boc_2O

The electrophilic addition of di-*tert*-butyl dicarbonate (Boc_2O) to 2a was achieved in high conversion and moderate selectivity in the presence of **1** (1 mol %), LiO^tBu (10 mol%) and H_2 (100 psig) in toluene at 80 °C (Table 5-1). The presence of an alkali metal base was crucial for achieving high selectivity of the *α*-cyanoboryl product. Although complete consumption of 2a was seen without the presence of base, a complex mixture of hydrogenated products was observed.

Employing the Li^+, Na^+, or K^+ *tert*-butoxide bases (10 mol %) resulted in only products 7 and 2a′. A decreased overall conversion of 2a was noted with NaO^tBu (86% conversion) compared to KO^tBu (96%) and LiO^tBu (99%). The best selectivity for 7 was achieved using LiO^tBu (53%, entry 5), while K^+ and Na^+ were 45% selective for 7 (entries 2 and 3).

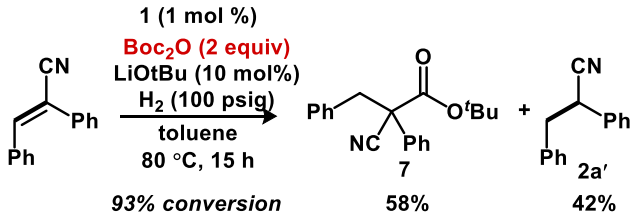

Entry	Base (10 mol%)	Additive	Total Conversion	Selectivity for 7
1	none	none	99	complex mixture
2	KO^tBu	none	96	45
3	NaO^tBu	none	86	46
4	LiO^tBu	none	100	53
5	LiO^tBu	PPh_3 (10 mol%)	88	61
6	LiO^tBu	Boc_2O (2 equiv)	93	62

Table 5-1. Alkali metal *tert*-butoxide bases promote selective Boc addition to 2a. Conversion was established using ^1H NMR spectroscopy.

Further optimization of the reaction conditions led to identifying a beneficial role of added PPh_3, and/or excess Boc_2O. The addition of either exogeneous PPh_3 (10 mol%) *or* an extra equivalent of Boc_2O, combined with LiO^tBu (10 mol%) provided 7 with selectivity > 60% (entry 5 and 6, Table 5-1). These studies point toward the potential role of Lewis acidic interactions in Ru-ketenimine chemistry. *N*-lithiated ketenimines are well-documented, and a weak non-covalent

interaction of Li^+ with **3a** and/or Boc_2O could promote ketenimine dissociation to initiate addition of the anhydride.

The large effect of substrate electronics on product distribution was by established by comparing the Boc_2O addition reactions of 2a and 2g. Under identical reaction conditions, the more electron rich alkenyl nitrile (2g), provided only the saturated nitrile, 2g′, and carbamate, 7. The absence of an α-cyano-Boc product is consistent with competing hydrogenation to form the fully saturated primary amine, which is followed by protection from Boc_2O (Figure 5-9). Given the number of parameters that may affect the product distribution beyond the electronics of the substrate (i.e. Lewis acid/base additives, H_2 pressure, solvent, etc.), further evaluation necessary. The development of distinct reaction conditions that would promote divergent reactivity from α,β-unsaturated nitriles is an appealing synthetic strategy if high selectivity can be achieved.

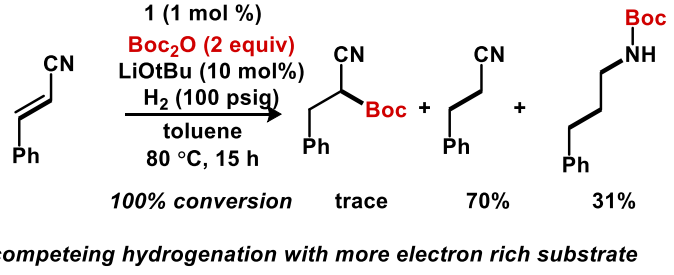

Figure 5-9. Competing hydrogenation over acylation with more electron rich cinnamonitrile substrate

5.7 An *N*-Silyl-ketenimine is Intercepted with Ph_3SiH During Hydrogenation

The addition of Ph_3SiH to a mixture of 2a and **1** under hydrogenation conditions resulted in formation of a single new product with ^{13}C NMR resonances at δ 189 (C1), 56.5 (C2), and 32 (–CH_2) ppm. These are indicative of an *N*-silylketenimine product (Figure 5-10). No reaction occurred in the absence of H_2.

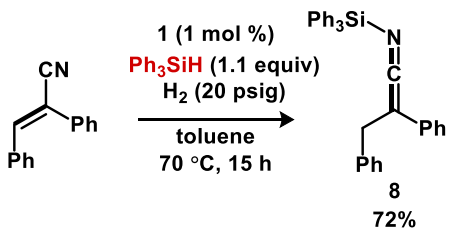

Figure 5-10. Synthesis of an *N*-silylketenimine from α-phenylcinnamonitrile and Ph_3SiH

5.8 Conclusions

The hydride insertion of $HRubMepi(PPh_3)_2$ with *α,β*-unsaturated nitriles affords ketenimines quantitatively under *base-free conditions*. This work identified the structural features of Ru(bMepi)-ketenimines using spectroscopic, X-ray crystallography, and NBO analysis. The bent coordination mode of **3a** combined with the polarized bonds across N=C1=C2 enable divergent site-selective reactions under hydrogenation conditions. In the absence of H_2, reactions from the Ru-ketenimine **3a** are slow. The results of this study offer a new route to synthetically diverse intermediates.

5.9 Experimental

5.9.1 General Considerations

All manipulations involving the catalyst and catalytic reactions were conducted under a nitrogen atmosphere using standard Schlenk technique, or in a glovebox unless otherwise stated. *α,β*-unsaturated nitriles were purchased from commercial sources, or synthesized according to literature procedure. $HRu(bMepi)(PPh_3)_2$ was synthesized according to literature procedure. Toluene-d_8 was degassed using evacuation/refill cycles and then stored over 3 Å molecular sieves for at least 24 h in the glovebox prior to use. Degassed, anhydrous solvents were obtained using a Glass Contour, SG Waters USA solvent purification system or were distilled over CaH_2, degassed,

and stored over 3 Å molecular sieves for at least 24 h in the glovebox prior to use. The 3 Å molecular sieves were dried at 250 °C under dynamic vacuum for 24 h. NMR spectra were recorded on Varian Inova 500, Varian MR400, Varian vnmrs 500 and Varian vnmrs 700 spectrometers at ambient temperature, unless otherwise stated. ^{1}H chemical shifts are reported in parts per million (ppm) relative to TMS. Calculations were performed with the Gaussian 09 suite of programs. All atoms underwent geometry optimization using the rb3lyp functional and 6-31G(d,p) basis set, with the exception of ruthenium, which was optimized using used the SDD basis set. The polarizable continuum model (PCM) solvent model for benzene was used in all cases.

General Reaction Protocol (A) for Hydrogenations Performed in a Parr bomb

Stock solutions of α-phenylcinnamonitrile (1M) and **1** (0.01 M) were prepared prior to each set of reactions in either toluene or toluene-d_8. An 8 mL vial with a stir bar was charged with alkenyl nitrile (250 µL, 0.25 mmol), and **1** (250 µL, 0.003 mmol). The reaction mixture was further diluted with the appropriate solvent to a total of 2 mL, sealed with a septa lined cap, and pierced with an 12g needle. The reaction(s) were set into the Parr bomb, which was sealed and heated to the specified temperature prior to addition of H_2.

General Reaction Protocol (B) for Hydrogenations Performed in sealed NMR vessel

Stock solutions of α-phenylcinnamonitrile (1M) and **1** (0.01 M) were prepared prior to each set of reactions in toluene-d_8. A 20 mL vial was charged with alkenyl nitrile (250 µL, 0.25 mmol), **1** (250 µL, 0.003 mmol), and phenyltrimethylsilane (PhTMS) as an internal standard. The reaction mixture was further diluted with toluene-d_8 to a total of 750 µL and transferred to a sealed NMR tube, which was charged with H_2 using the stated psig.

5.9.2 Synthesis and characterization of Ru-ketenimine 3a

A 20 mL vial was charged with HRu(bMepi)(PPh_3)$_2$ (10 mg, 0.01 mmol), α-phenylcinnamonitrile (10 mg, 0.05 mmol), and 750 µL C_6D_6. The solution was transferred to a sealed NMR tube and analyzed by ^{1}H, ^{31}P, and ^{13}C NMR spectroscopy. The same reaction could be reproduced using toluene-d_8 or THF as a solvent. Crystals suitable for X-ray diffraction were grown by layering the reaction solution in THF with pentane at −70 °C.

^{1}H NMR (500 MHz, Benzene-d_6) δ 7.97 (s, 2H), 7.63 (d, J = 8.5 Hz, 1H), 7.22 (s, 1H), 6.96 (d, J = 7.3 Hz, 2H), 6.90 (d, J = 7.5 Hz, 2H), 6.84 (s, 1H), 6.46 (s, 1H), 6.35 (s, 1H), 3.21 (s, 1H), 1.53 (s, 2H); ^{31}P NMR (162 MHz, Benzene-d_6): 39; ^{13}C NMR (126 MHz, THF-d_8) δ 159.01, 155.22, 152.37, 141.35, 134.76, 127.58, 126.79, 34.32, 22.73.

5.9.3 Hydrogenation of 2a catalyzed by 1

Protocol (A) was using 100 psig H_2. After heating at 70 °C for 2.5 or 15 h the pressure vessel was cooled to room temperature, degassed and the solvent was removed by rotary evaporation. $CDCl_3$ and PhTMS was added directly to the crude reaction mixture for product analysis by ^{1}H NMR spectroscopy. The phenyl protons were not assigned in the crude reaction mixture due to significant signal overlap in the aromatic region.

2,3-diphenylpropanenitrile (2a′):

^{1}H NMR (500 MHz, $CDCl_3$) δ: 3.97 (dd, $^3J_{HH}$ = 8.2, 6.6 Hz, 1H, -C**H**), 3.18 (dd, $^2J_{HH}$ = 14.0 Hz, $^3J_{HH}$ = 8.3 Hz, 2H (-C**H**H), 3.12 (dd, $^3J_{HH}$ = 13.6 Hz, $^3J_{HH}$ = 6.4 Hz, 2H, -CH**H**)

2,3-diphenylpropenamine (4a):

^{1}H NMR (500 MHz, $CDCl_3$) δ: δ 6.69 (*t*, $^3J_{HH}$ = 9.5 Hz, 1H, =C**H**), 3.79 (s, 2H, -C**H**$_2$,), 3.33 (*t*, $^3J_{HH}$ = 9.4 Hz, 2H, -N**H**$_2$).

3-phenylpropanimine (4a′):

^{1}H NMR (500 MHz, $CDCl_3$) δ: 6.05 (t, $^{3}J_{HH}$ = 8.5 Hz, 1H, =C**H**), 4.28 (s, 1H, -C**H**), 3.61 (s, 2H, -C**H$_2$**).

3-phenylpropanamine (5a):

^{1}H NMR (500 MHz, $CDCl_3$) δ: 2.93 (m, 5H, -C**H$_2$**C**H**C**H$_2$**), 1.25 (bs, 2H, -N**H$_2$**)

5.9.4 Hydrocarbonylation of 2a with Boc_2O

Protocol (A) was followed using 100 psig H_2. After heating at 80 °C for 2.5 or 15 h the pressure vessel was cooled to room temperature, degassed and the solvent was removed by rotary evaporation. $CDCl_3$ and PhTMS was added directly to the crude reaction mixture for product analysis by ^{1}H NMR spectroscopy. In addition to 2a′, *tert*-butyl-2-cyano-3-phenylpropanoate (7) was identified in the reaction mixture.

tert-butyl-2-cyano-3-phenylpropanoate (7): ^{1}H NMR (500 MHz, Chloroform-d): δ 7.52 (d, J = 6.9 Hz, 2H), 7.38 (d, J = 7.6 Hz, 3H), 7.25 (dd, J = 6.0, 3.6 Hz, 5H), 7.21 – 7.05 (m, 3H), 3.66 (d, J = 13.6 Hz, 1H), 3.27 (d, J = 13.6 Hz, 1H).

5.9.5 Interception of Silyl-ketenimine During Hydrogenation of 2a with Ph_3SiH

Protocol (B) was followed using 20 psig H_2. After heating at 70 C for 15 h, the crude reaction mixture was analyzed by ^{1}H and ^{13}C NMR spectroscopy. The phenyl protons were not assigned in the crude reaction mixture due to significant signal overlap in the aromatic region.

2,3-diphenyl-N-(triphenylsilyl)propenimine (8): ^{1}H NMR (500 MHz, Toluene-d_8) δ 3.51 (s, 2H). ^{13}C NMR (126 MHz, Toluene-d_8) δ 189.35, 141.55, 132.42, 126.36, 123.33, 56.52, 32.59.

5.10 Notes and References

(1) Yang, X.; Fleming, F. F. C- and N-Metalated Nitriles: The Relationship between Structure and Selectivity Accounts of Chemical Research **2017**, *50*, 2556-2568.

(2) E., D. S.; W., W. T. Silyl Ketene Imines: Highly Versatile Nucleophiles for Catalytic, Asymmetric Synthesis *Angew. Chem. Int. Ed.* **2012**, *51*, 9980-9992.

(3) H., M. A.; C., F. G. Nucleophile-Catalyzed Asymmetric Acylations of Silyl Ketene Imines: Application to the Enantioselective Synthesis of Verapamil *Angew. Chem. Int. Ed.* **2005**, *44*, 949-952.

(4) DeKorver, K. A.; Li, H.; Lohse, A. G.; Hayashi, R.; Lu, Z.; Zhang, Y.; Hsung, R. P. Ynamides: A Modern Functional Group for the New Millennium *Chem. Rev.* **2010**, *110*, 5064-5106.

(5) H., D. R.; Kevin, C. Ketenimines Generated from Ynamides: Versatile Building Blocks for Nitrogen-Containing Scaffolds Chemistry – A European Journal **2018**, *24*, 2297-2304.

(6) Bae, I.; Han, H.; Chang, S. Highly Efficient One-Pot Synthesis of N-Sulfonylamidines by Cu-Catalyzed Three-Component Coupling of Sulfonyl Azide, Alkyne, and Amine *J. Am. Chem. Soc.* **2005**, *127*, 2038-2039.

(7) Arseniyadis, S., Kyler, K. S.; Watt, D. S. Addition and Substitution Reactions of Nitrile-Stabilized Carbanions. In *Organic Reactions.* (Ed.). doi:10.1002/0471264180.or031.01

(8) Rosa, L.; Claudio, P. Cyanoalkylation: Alkylnitriles in Catalytic C□C Bond-Forming Reactions *Angew. Chem. Int. Ed.* **2015**, *54*, 13170-13184.

(9) Yin, L.; Kanai, M.; Shibasaki, M. Nucleophile Generation Via Decarboxylation: Asymmetric Construction of Contiguous Trisubstituted and Quaternary Stereocenters through a Cu(I)-Catalyzed Decarboxylative Mannich-Type Reaction *J. Am. Chem. Soc.* **2009**, *131*, 9610-9611.

(10) Gao, D.-W.; Vinogradova, E. V.; Nimmagadda, S. K.; Medina, J. M.; Xiao, Y.; Suciu, R. M.; Cravatt, B. F.; Engle, K. M. Direct Access to Versatile Electrophiles Via Catalytic Oxidative Cyanation of Alkenes *J. Am. Chem. Soc.* **2018,** *140*, 8069–8073.

(11) D'Sa, B. A.; Kisanga, P.; Verkade, J. G. Direct Synthesis of A,B-Unsaturated Nitriles Catalyzed by Nonionic Superbases The Journal of Organic Chemistry **1998**, *63*, 3961-3967.

(12) Zhou, Y.; Bandar, J. S.; Liu, R. Y.; Buchwald, S. L. Cuh-Catalyzed Asymmetric Reduction of A,B-Unsaturated Carboxylic Acids to B-Chiral Aldehydes *J. Am. Chem. Soc.* **2018**, *140*, 606-609.

(13) The closet example is a proposed ketene intermediate derived from Cu–H and related α,β-unsaturated aldehydes.

(14) Lu, P.; Wang, Y. The Thriving Chemistry of Ketenimines *Chem. Soc. Rev.* **2012**, *41*, 5687-5705.

(15) Allen, A. D.; Tidwell, T. T. Ketenes and Other Cumulenes as Reactive Intermediates *Chem. Rev.* **2013**, *113*, 7287-7342.

(16) Tseng, K.-N. T.; Kampf, J. W.; Szymczak, N. K. Base-Free, Acceptorless, and Chemoselective Alcohol Dehydrogenation Catalyzed by an Amide-Derived NNN-Ruthenium(II) Hydride Complex *Organometallics* **2013**, *32*, 2046-2049.

(17) Tseng, K.-N. T.; Rizzi, A. M.; Szymczak, N. K. Oxidant-Free Conversion of Primary Amines to Nitriles *J. Am. Chem. Soc.* **2013**, *135*, 16352-16355.

(18) Tseng, K.-N. T.; Lin, S.; Kampf, J. W.; Szymczak, N. K. Upgrading Ethanol to 1-Butanol with a Homogeneous Air-Stable Ruthenium Catalyst *Chem. Commun.* **2016**, *52*, 2901-2904.

(19) Hale, L. V. A.; Szymczak, N. K. Stereoretentive Deuteration of A-Chiral Amines with D2o *J. Am. Chem. Soc.* **2016**, *138*, 13489-13492.

(20) Hale, L. V. A.; Malakar, T.; Tseng, K.-N. T.; Zimmerman, P. M.; Paul, A.; Szymczak, N. K. The Mechanism of Acceptorless Amine Double Dehydrogenation by N,N,N-Amide Ruthenium(Ii) Hydrides: A Combined Experimental and Computational Study *ACS Catal.* **2016**, *6*, 4799-4813.

(21) Cambridge Structural Database, version 5.38, August 2018

(22) Becker, L.; Haehnel, M.; Spannenberg, A.; Arndt, P.; Rosenthal, U. Reactions of Group 4 Metallocenes with Monosubstituted Acetonitriles: Keteniminate Formation Versus C-C Coupling *Chemistry – A European Journal* **2015**, *21*, 3242-3248.

(23) Culkin, D. A.; Hartwig, J. F. Synthesis, Characterization, and Reactivity of Arylpalladium Cyanoalkyl Complexes: Selection of Catalysts for the α-Arylation of Nitriles *J. Am. Chem. Soc.* **2002**, *124*, 9330-9331.

(24) Chainok, K.; Neville, S. M.; Forsyth, C. M.; Gee, W. J.; Murray, K. S.; Batten, S. R. Supramolecular Architecture of Silver(I) Coordination Polymers Containing Polydentate N-Donor Ligands *CrystEngComm* **2012**, *14*, 3717-3726.

(25) Jing-Min Shi, W. X., Su-Qiao Lu, Chang-Ju Wu, Jie-Chao Ge, Zhi-De Zhang Synthesis and Crystal Structure of Complex {[Cu(N-Men)2(Cda)2]·[Cu(N-Men)2]((Clo4)2}(N-Men = N-Methylethylenediamine, Cda = Carbamyldicyanomethanide Anion) *Chinese Journal of Structural Chemistry* **2002**, 640-642.

(26) For comparison, N-aryl and N-alkyl ketenimines typically have C–N–R (R = Ar or alkyl) bond angles between 117-129°

(27) Tseng, K.-N. T.; Kampf, J. W.; Szymczak, N. K. Mechanism of N,N,N-Amide Ruthenium(Ii) Hydride Mediated Acceptorless Alcohol Dehydrogenation: Inner-Sphere B-H Elimination Versus Outer-Sphere Bifunctional Metal–Ligand Cooperativity *ACS Catal.* **2015**, *5*, 5468-5485.

(28) Pitta, B. R.; Steward, O. W.; Fleming, F. F. Electrophile-Dependent Alkylations of Lithiated 4-Alkoxyalk-4-Enenitriles *J. Org. Chem.* **2018**, *83*, 2753-2762.

(29) See SI for complete details about hydrogenation

Chapter 6: Catalyst Designs for Hydrogen Transfer – Future Directions

6.1 Derivatives of the Bis(pyridylimino)isoindoline Ligand

The electronic and steric characteristics imparted by bpi-type ligands are crucial to reactivity, and the requirements vary depending on substrate class and desired direction of hydrogen transfer (hydrogenation or dehydrogenation). Our mechanistic analysis of alcohol and amine hydrogen transfer reactions established two key catalyst design criteria. First, the kinetic barriers toward transfer of H^+ and/or H^- between catalytic intermediates are high in energy. Thus, the σ-donating or withdrawing parameters of the ligand *trans* to Ru–H or Ru–(η^2-H_2) is crucial. The second major influence on catalytic hydrogen transfer, especially in the case of primary amines, is the steric profile resulting from the *ortho*-pyridyl substituents. Bulky groups such as Me and ^{i}Pr provide the necessary stabilization to the transition-states of 5-coordinate Ru-alkoxide and Ru-amido substrates during hydrogen transfer. Throughout the course of this work, we envisioned a variety of strategies based on our mechanistic findings to regulate hydrogen transfer reactivity through catalyst (re)design (Figure 6-1). These strategies include modification of: 1) the atoms *cis* and *trans* to the hydride or η^2-H_2 ligand; 2) overall charge of the complex; 3) the pK_a of a cooperative ligand and/or exogeneous additive; and 4) the steric profile of the pincer ligand. Depending on the desired transformation and substrate class, use of one or more of these approaches may improve the rates of H^+ and/or H^- transfer.

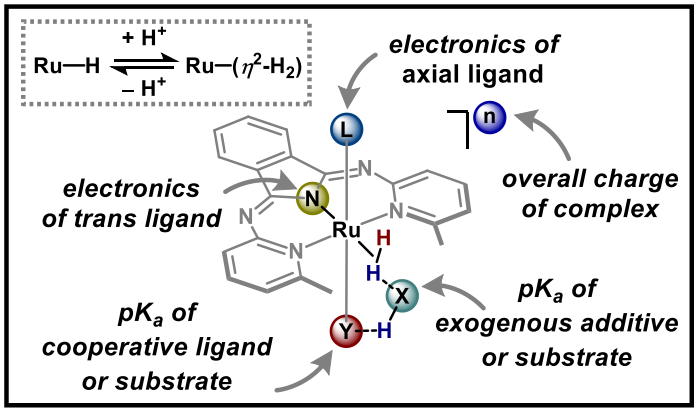

Figure 6-1. Strategies for tuning the reactivity of a Ru(bMepi)(η^2-H_2) complex

6.1.1 Steric Modifications

Common synthetic routes for generating HbRpi ligands and the corresponding Ru complexes are shown in Figure 6-2. Steric modifications of the *ortho*-pyridyl position could be achieved by varying the 2-amino-6-R-pyridine reagent, where R = H, Me, Et, ^{i}Pr, and ^{t}Bu. However, increasing the steric profile of the bRpi ligand has unfortunate drawbacks for ligand synthesis – impeding *ortho*-groups require longer reaction times and higher temperatures to form the HbRpi ligand. Similarly, deprotonation with KHMDS and the following metalation to form tridentate complexes becomes more challenging with the increase in steric bulk. Hb^{t}Bupi, for example, did not coordinate to Ru using the stepwise deprotonation and metalation route reported for the Me and ^{i}Pr variants.

In addition to providing steric protection for coordinatively unsaturated Ru-species, large *ortho*-groups can promote κ^2 (bidentate) over κ^3 (tridentate) coordination of the bpi framework. While we found that a hemi-labile type mechanism is not necessary to mediate (de)hydrogenation reactions of amines and alcohols, the advantages or disadvantages of this coordination mode in

other catalytic reactions have not been well-established. In the case that a κ^2-coordination mode is proposed to be catalytically relevant, the ^{i}Pr and ^{t}Bu derivatives may be worthy ligands to employ.

The neutral bMepi^{Me} ligand also provide a synthetic route to κ^2-coordination modes. For example, the Fe(bMepi^{Me})(Br)$_2$ complex (Figure 6-3) displays a four-coordinate pseudo-tetrahedral geometry at iron due to the bidentate bMepi^{Me} ligand. Analogous 5-coordinate Ru-κ^2-bMepi^{Me} species may also exist. Attempted synthesis of [HRu(bMepi^{Me})(PPh$_3$)$_2$]OTf from [Ru(bMepi^{Me})(PPh$_3$)(OTf)]OTf and various hydride sources (i.e. NaBHEt$_3$ or H_2 with added base) resulted in complex product mixtures of fluxional Ru–H species in solution. Variable temperature NMR experiments suggest that the coordination mode of bMepi^{Me} changes from κ^2 (high T) to κ^3 (low T). The identification of these putative Ru-κ^2-(bMepi^{Me}) species may have important implications for understanding and expanding Ru-catalyzed H/D exchange developed in Chapter 4.

The final modification considered based on the bpi framework was the replacement of *ortho*-CH$_3$ groups with –CF$_3$. The electron deficient substituents would impose a slightly larger steric profile to Ru-bpi type complexes, in addition to acting as potential H-bond acceptors. The typical condensation route between 2-amino-6-CF$_3$-pyridine and phthalonitrile readily provided the HbCF$_3$pi ligand. However, metalation of HbCF$_3$pi with RuCl$_2$(PPh$_3$)$_2$ to form ClRu(bCF$_3$pi)(PPh$_3$) was unsuccessful, likely due to the increased size of the –CF$_3$ group compared to –CH$_3$.

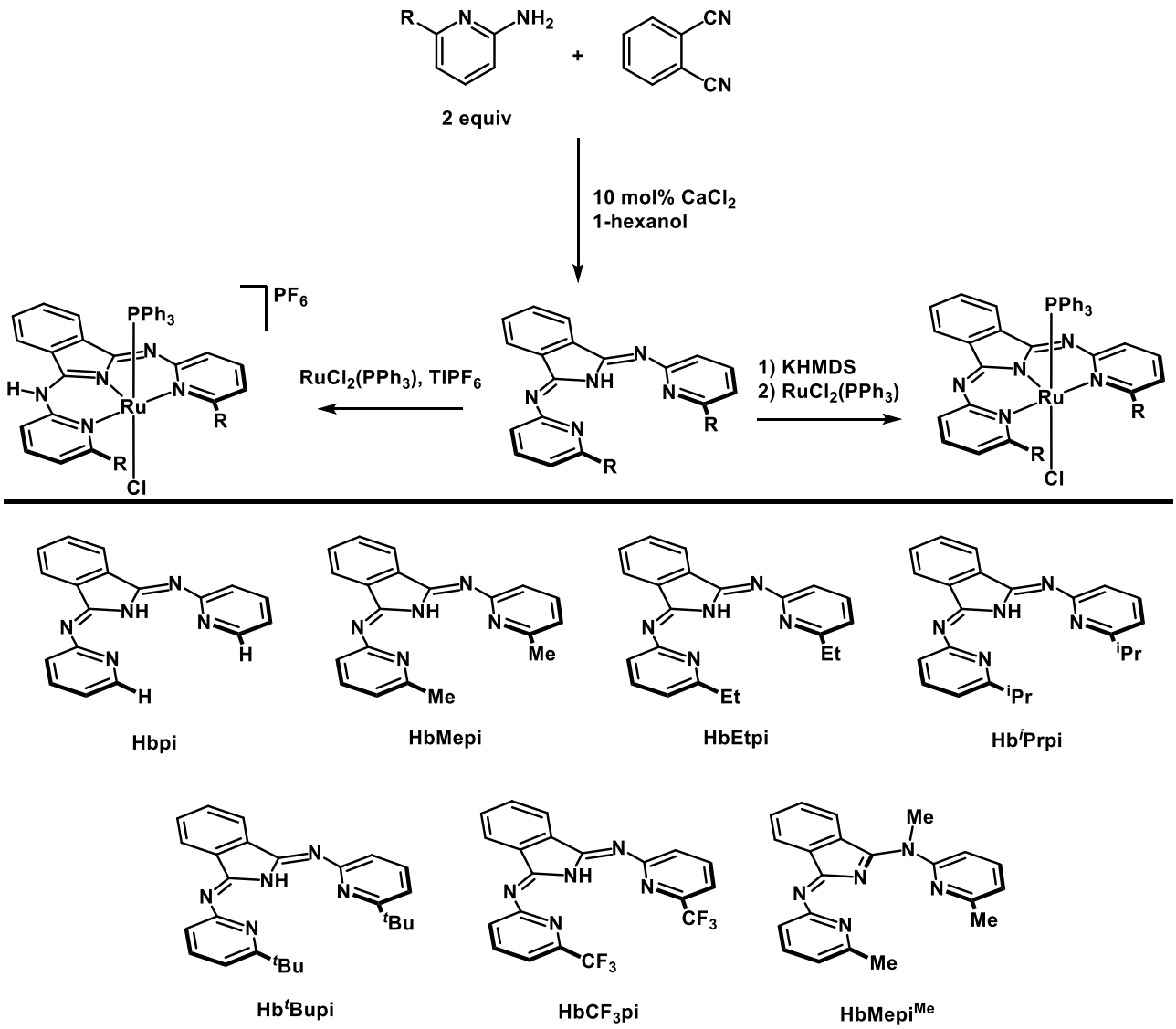

Figure 6-2. Modifications of bpi-type ligands

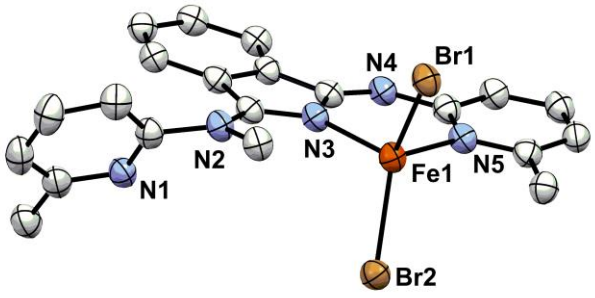

Figure 6-3. κ^2-binding of the Fe(bMepi)Br$_2$

6.1.2 Hydricity and pK_a Considerations for Ru-bpi Hydrogen Transfer Catalysts

Should the *hydricity* or pK_a of Ru–H dictate the future design of hydrogen transfer catalysts? Studies reported in Chapters 3-5 suggest acid-base equilibria govern the reactions of polar functional groups catalyzed by Ru-bpi type complexes. Chapter 3 delineated the ionic dehydrogenation mechanism specific to primary amines with Ru-bpi type catalysts, and additionally drew parallels between amine and related alcohol dehydrogenations. The mechanisms between the two substrate classes are fundamentally similar; both amine and alcohol dehydrogenation involve high energy kinetic barriers toward protonation of the of the Ru–H bond to form a transient Ru−(η^2-H_2) intermediate. However, H^- transfer events such as β–H elimination can be rate-limiting with high concentrations of acidic substrates (i.e. benzylalcohol). Although hydricity and pK_a are often correlated, where a high ΔG_{H^-} of M–H corresponds to a low pK_a of M−(η^2-H_2) and *vice versa* (Figure 6-4), the distinction is crucial for designing effective hydrogen transfer catalysts. In particular, the relationship between the electronics of the supporting ligand and the overall charge of the complex can complicate direct correlations of hydricity and pK_a. This section contextualizes the hydrogen transfer chemistry of Ru-bpi type catalysts as reversible acid-base reactions and outlines guidelines for future catalyst design. Ideally, the concepts discussed in this section will apply to transformations beyond primary amine and alcohol dehydrogenation, such as asymmetric hydrogen transfer and hydrogen borrowing methodologies with Ru-bpi type catalysts.

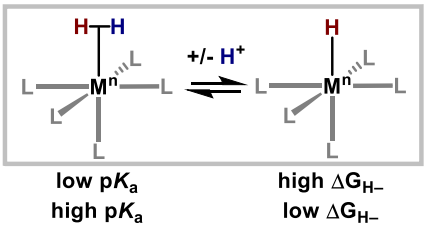

Figure 6-4. The relationship between hydricity and p*K*$_a$

6.1.2.1 Hydricity of Ru–H

The relative hydricities were established for select Ru–H complexes shown in Figure 6-5. The following analysis of $[HRu(\mathbf{L})(PPh_3)_2]^m$ using Density Functional Theory evaluates ΔG_{H^-} in relation to: 1) the *trans* influence imparted by **L** 2) the overall charge of the complex (m) 3) the presence of *ortho*-CH_3 vs *ortho*-H pyridyl groups, and 4) the identity of backbone linker (i.e. C=N, N–CH_2, C=CH, or C–N(CH_3)).

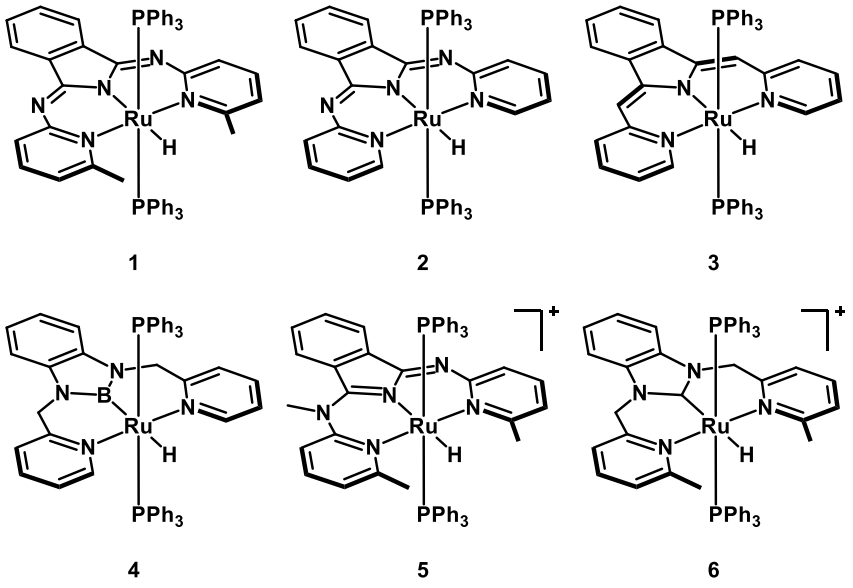

Figure 6-5. Ruthenium-hydride complexes targeted for evaluating changes in ΔG_{H^-}

Ruthenium-hydride complexes 1-6 and the corresponding 5-coordinate $[Ru]^+$ species were optimized using the rb3lyp functional, and 6-31g(d,p) basis set for all atoms except Ru, which used

the SDD basis set. The relative hydricities were established by calculating the energy of H^- transfer from Ru–H to BH_3 to provide $[BH_4]^-$ and a 5-coordinate $[Ru]^+$ or $[Ru]^{2+}$ species (Table 6-1). Larger ΔG_{H-} values correspond to a higher energy needed for H^- transfer, and thus a lower hydricity, while small ΔG_{H-} values correspond to a more hydridic Ru–H species. For this analysis, the σRu−H orbitals were also identified (those which included a σ-donor contribution from the *trans* group), in addition to the Ru–H bond length calculated for each complex (Table 6-1).

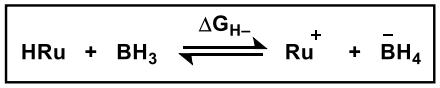

[HRu]	Ru–H (Å)	**HOMO-n (eV)**	ΔG_{H-} (kcal/mol)
(1) HRu(bMepi)$(PPh_3)_2$	1.60	HOMO-6 (−6.199)	25
(2) HRu(bpi)$(PPh_3)_2$	1.63	HOMO-6 (−6.300)	34
(3) HRu(bpm)$(PPh_3)_2$	1.63	HOMO-6 (−6.215)	30
(4) HRu(NBN)$(PPh_3)_2$	1.75	HOMO-2 (−4.415)	0.88
(5)$[HRu(bMepi^{Me})(PPh_3)_2]^+$	1.59	HOMO-8 (−7.712)	61
(6)$[HRu(2\text{-}Me\text{-}NCN)(PPh_3)_2]^+$	1.63	HOMO-3 (−7.309)	51

Table 6-1. Calculated ΔG_{H-} for hydride transfer from Ru–H to BH_3

The parent complex, HRubMepi$(PPh_3)_2$ (**1**), is the most hydridic species (ΔG_{H-} = 25 kcal/mol) among complexes with an anionic amido group *trans* to the hydride (**1-3**). Modifications to the *ortho*-substituents and backbone linkers resulted in minor changes to ΔG_{H-}. In general, bulky *ortho*-pyridyl substituents and methylene linkers (in place of imine linkers) provide slightly more hydridic catalysts. The σRu−H orbital is the low-lying HOMO−6 for each complex, with minimal variation in energy (−6.199, −6.300, and −6.215 eV for **1**, **2**, and **3**, respectively).

Replacing the central anionic amido with an anionic boryl group resulted in a significant enhancement in hydricity. The ΔG_{H^-} required for **4** to transfer a hydride to BH_3 was calculated as 0.88 kcal/mol, indicating that a Ru-boryl hydride species would be almost as hydridic as the widely used $[BH_4]^-$ reagent. Additionally, the energy of the σRu−H orbital for **4** (HOMO-2) was higher in energy at −4.415 eV, compared to −6.300 eV (HOMO-6) for **2**. In contrast, the cationic hydride complex, **5**, with a neutral *N*-heterocyclic carbene (NHC) group, is inert toward H^- transfer to BH_3 (ΔG_{H^-} = 51 kcal/mol), despite NHC ligands being known as exceptional σ-donor and π-acceptor ligands.

6.1.2.2 Influence of overall charge: *intra*molecular vs. *inter*molecular H^+ transfer

The poor hydricity of NCN-type complexes is surprising given that NHCs are good σ-donor/π-acceptor ligands. The increased σ-donating ability of the carbene donor compared to the amido donor of the bpi-type ligand is apparent in the complex $[ClRu(NCN)(PPh_3)_2]PF_6$, which has a lengthened Ru–Cl bond (2.511 Å) compared to $ClRu(bpi)(PPh_3)_2$ (2.478 Å) (Figure 6-6). However, due to the difference in overall charge between the neutral bpi- and cationic NCN-type complexes, further experimental and theoretical investigations are necessary to determine whether NCN or bpi-type complexes will have increased hydricity.

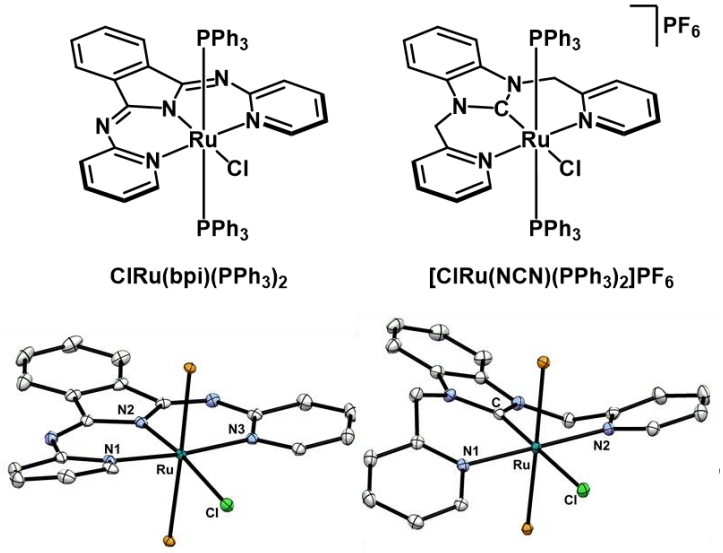

Figure 6-6. Crystal structures of ClRubpi(PPh_3)$_2$ and ClRu(NCN)(PPh_3)$_2$ complexes. Thermal ellipsoids are depicted at 50% probability. For clarity the hydrogen atoms and Ph groups of PPh_3 have been removed.

The NCN ligand is an example of a ligand with competing electronic effects of the inner-sphere and overall charge of the complex. Determining which effect is dominant depends on whether an intermolecular vs. intramolecular proton transfer events occurs. In the first scenario, the overall positive charge of the complex changes by one unit, while the complex in the latter scenario maintains the same overall charge (Figure 6-7).

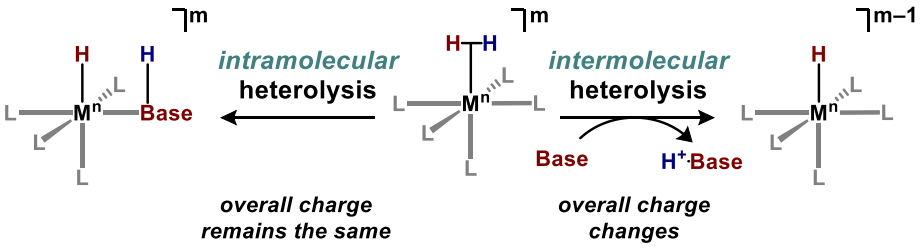

Figure 6-7. Intramolecular vs. intermolecular H^+ transfer and effect on overall charge

An intramolecular H^+ transfer process can be assessed using the 5-coordinate bis-phosphine complexes of the general formula [Ru(**L**)(PPh_3)$_2$]$^{\mathbf{m}}$, where **m** is the overall charge of the complex, and **L** is an anionic X-type (i.e. bpi, bMepi, or NBN) or neutral L-type ligand (i.e.

NCN or bMepi^{Me}). Intermolecular H^+ transfer involves coordination of H_2 to form [Ru(**L**)(η^2-H_2)$(PPh_3)_2]^{\mathbf{m}}$, followed by deprotonation of the H_2 ligand by an exogenous base. Additionally, intermolecular deprotonation results in formation of the conjugate acid of the added base and [Ru(**L**)(H)$(PPh_3)_2]^{\mathbf{m-1}}$ with a decreased net charge (**m−1**). The important orbital interactions of the Ru–H and Ru−(η^2-H_2) intermediates involve metal-based *d*-orbitals for π-backbonding and σ-interactions. The molecular orbitals having the appropriate symmetry for interacting with H_2 are visualized with the 5-coordinate cationic complexes, [Ru(bMepi)$(PPh_3)_2]^+$, [Ru(bMepi^{Me})$(PPh_3)_2]^{2+}$, and [Ru(2-Me-NCN)$(PPh_3)_2]^{2+}$ (Figure 6-8).

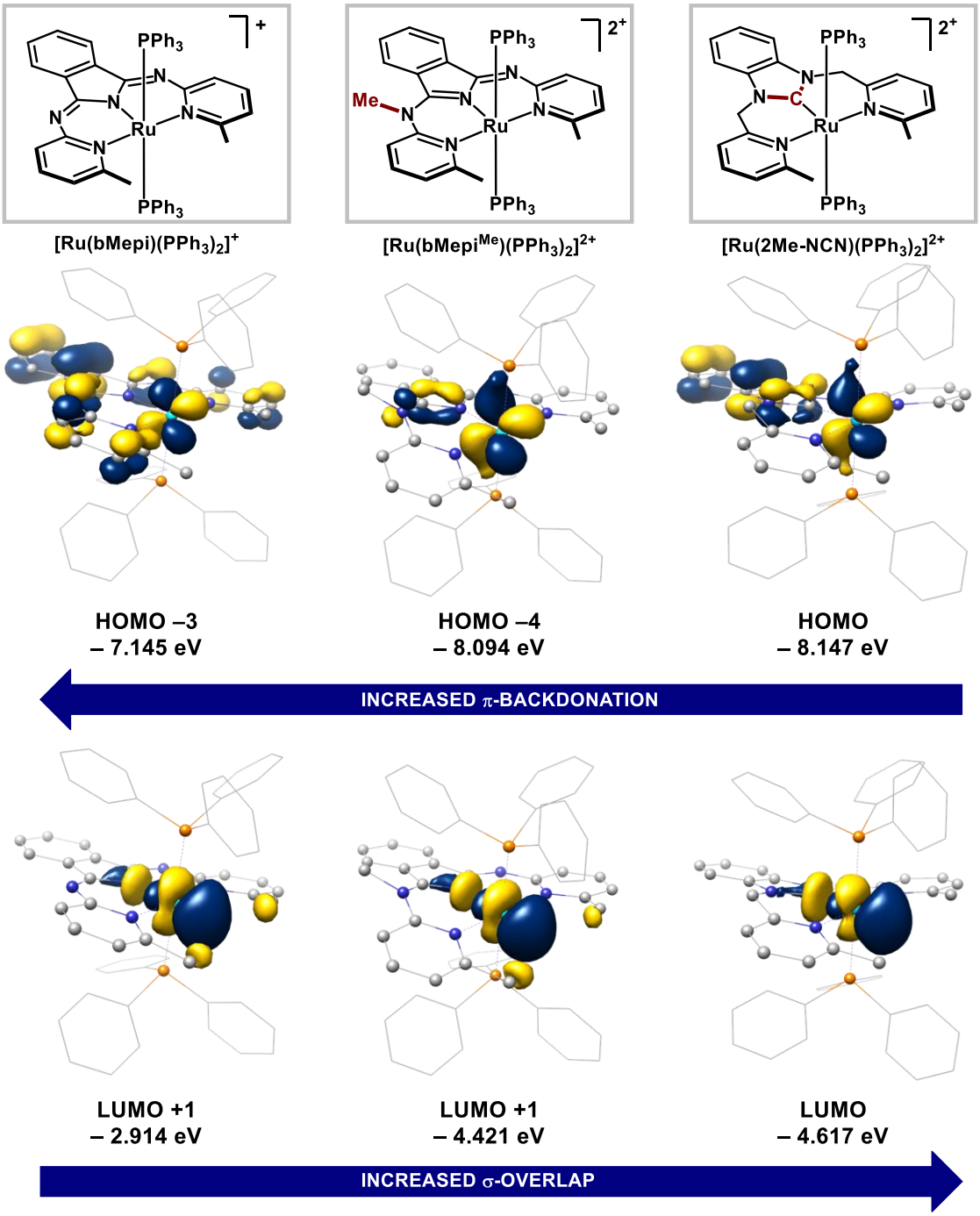

Figure 6-8. Depiction of the molecular orbitals capable of interacting with H_2 for $[Ru(bMepi)(PPh_3)_2]^+$, $[Ru(bMepi^{Me})(PPh_3)_2]^{2+}$, and $[Ru(2\text{-}Me\text{-}NCN)(PPh_3)_2]^{2+}$

Based on the changes in energies of the molecular orbitals depicted in Figure 6-8, we hypothesize the overall charge of the complex will have a large influence over H_2 coordination

and *inter*molecular activation. To bind H_2, the LUMO+1 orbital of $[Ru(bMepi)(PPh_3)_2]^+$ (− 2.914 eV) (Figure 6-8, bottom left) can accept electron density from the σ-bond of H_2 (HOMO, − 11.730 eV). π-Backdonation into the antibonding orbital of H_2 (LUMO, + 2.779 eV) from a Ru orbital such as HOMO−3 (− 7.145 eV, Figure 6-8 top left) further activates H_2 toward heterolysis.

Analysis of the molecular orbitals for $[Ru(bMepi^{Me})(PPh_3)_2]^{2+}$, an alkylated Ru-complex with an increased positive charge, reveals lower energy orbitals when compared to $[Ru(bMepi)(PPh_3)_2]^+$. The orbitals available for σ- and π-interactions with H_2 are 1.5 and 0.95 eV lower in energy (LUMO+1, −4.421 eV and HOMO−4, −8.094 eV, Figure 6-8 middle) compared to that of $[Ru(bMepi)(PPh_3)_2]^+$. While the lower energy of the unoccupied *d*-orbital (LUMO+1) results in a stronger interaction with the HOMO of H_2, the π-backbonding ability with σ^*-H_2 also decreases due to the lower energy of the non-bonding *d*-orbital (HOMO−4). Despite these counteracting effects, the net increase in overlap for the σ-interaction will result in a more acidic Ru−(η^2-H_2) species for $bMepi^{Me}$ compared to bMepi complexes. Similarly, the cationic complex based on the neutral 2-Me-NCN ligand, $[Ru(2\text{-Me-NCN})(PPh_3)_2]^{2+}$ also exhibits lower energy *d*-orbitals. Again, a net increase in σ-overlap is calculated for the neutral 2-Me-NCN ligand (LUMO, −4.617 eV, Figure 6-8, bottom right) compared to the anionic bMepi ligand, despite a decrease in the π-backbonding ability (HOMO, −8.147 eV, Figure 6-8, top right). Thus, $[Ru(2\text{-Me-NCN})(PPh_3)_2]^{2+}$ is also expected to produce a more acidic Ru−(η^2-H_2) species compared to the bMepi ligand.

The situation changes when we evaluate *intra*molecular H^+ transfer between Ru−H and Ru−(η^2-H_2) intermediates. During inner-sphere H^+ transfer with amines, the inner-sphere electronic effects of the pincer ligand dominate over the overall charge of the complex. The

thermodynamic energies for intramolecular H^+ transfer was evaluated using the cationic [Ru(2-Me-NCN)(H)(PPh_3)($BnNH_2$)]$^+$ or neutral [Ru(bMepi)(H)(PPh_3)($BnNH_2$)] and their respective Ru–(η^2-H_2) complexes ($BnNH_2$ = benzylamine, Figure 6-9). Protonation of a Ru–H supported by the 2-Me-NCN ligand was calculated to be 19.8 kcal/mol, while the same analysis for the Ru(bMepi) complex required 23.6 kcal/mol.

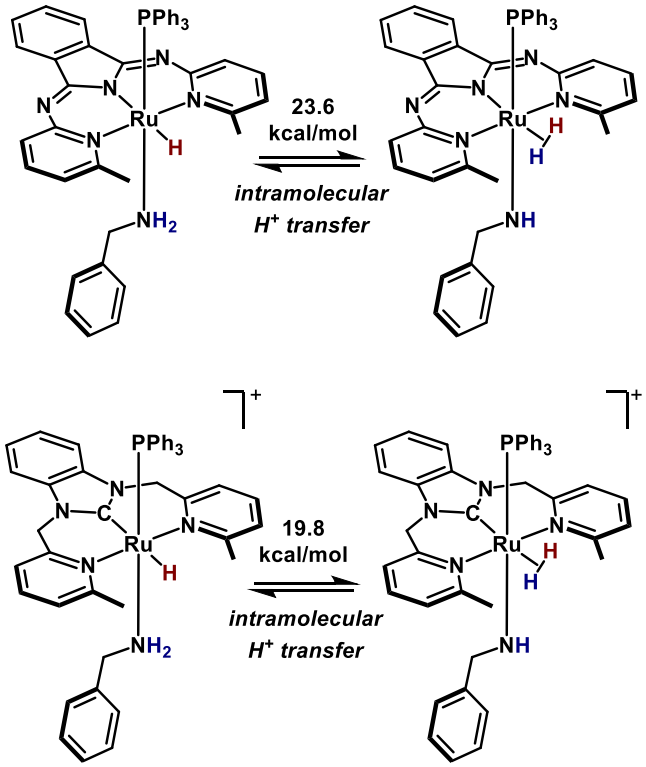

Figure 6-9. Intramolecular H^+ transfer between Ru–H and Ru–(η^2-H_2) complexes comparing the X-type bMepi and L-type 2-Me-NCN ligand

The lower energy required for intramolecular H^+ transfer directly contradicts the trends in hydricity and pK_a expected for [Ru(**L**)(H)(PPh_3)$_2$]$^{\mathbf{m}}$ and [Ru(**L**)(η^2-H_2)(PPh_3)$_2$]$^{\mathbf{m}}$ complexes, where the cationic complexes are predicted to have less hydridic (high ΔG_{H-}) Ru–H and more acidic (low pK_a) Ru–(η^2-H_2) units. Because the overall charge stays the same during an intramolecular proton exchange, the thermodynamic stabilities of the respective Ru–H and Ru–

(η^2-H_2) are not influenced by differences in charge. Thus, the relevance of overall charge to hydricity and pK_a are negligible and contributions from the *trans* σ-donor become significant. In the context of ionic (de)hydrogenations, this applies to inner-sphere processes occurring on the metal (i.e. when the coordination number does not change). Moreover, this dichotomy may extend to hydrogen transfer catalysts that operate *via* metal-ligand cooperativity, where intramolecular H^+ transfer is facilitated by a basic site in the secondary coordination sphere. However, it is important to recognize that the overall charge will affect elementary steps beyond H^+ transfer, such as ligand association or dissociation.

6.1.2.3 Monodentate NHC ligands

As a simple alternative to modifying the pincer-platform of Ru-bpi type catalysts, the axial PPh_3 ligands may be replaced with monodentate NHC or PR_3 ligands. The catalytic properties of [HRu(bMepi)(**L**$_{ax}$)$_2$] where **L**$_{ax}$ ≠ PPh_3 are underexplored. We previously evaluated HRu(bMepi)(**PMe**$_3$)$_2$ as a catalyst for amine dehydrogenation (Chapter 3), and found that the more electron donating PMe_3 hindered turnover compared to PPh_3 due to the high energy required for ligand exchange with the primary amine substrate. Thus, it is difficult to say whether an electron donating or withdrawing **L**$_{ax}$ is desirable for (de)hydrogenation based on a single data point using a complex that did not exhibit productive hydrogen transfer.

Monodentate NHC ligands are exceptional ligands for ruthenium mediated olefin metathesis and hydrogen transfer transformations. This section gives detailed computational analyses that indicate a more facile H^+ transfer to Ru–H for IMes analogs compared to PPh_3. Based on the data presented here, we hypothesize that HRu(bMepi)(IMes)(L) will exhibit improved rates of dehydrogenation for primary amines compared to the analogous PPh_3 catalyst.

The complexes ClRu(bMepi)(IMes) and ClRu(bpi)(IMes)$_2$ (IMes = 1,3-Bis(2,4,6-trimethylphenyl)imidazole) were synthesized from the respective ClRu(bMepi)PPh$_3$ and ClRu(bpi)(PPh$_3$) analogs. The effect of the IMes ligand compared to PPh$_3$ on intramolecular H$^+$ transfer was evaluated between Ru–H and Ru–(η^2-H$_2$) complexes Ru(bRpi)(H)(**L$_{ax}$**)(BnNH$_2$) and Ru(bRpi)(η^2–H$_2$)(**L$_{ax}$**)(BnNH$_2$) (R = CH$_3$ or H and **L$_{ax}$** = IMes or PPh$_3$) (Table 6-2). The energy needed for protonation of the Ru–H decreases for both bMepi and bpi complexes when **L$_{ax}$** = IMes. A decrease of 1 kcal/mol was calculated for Ru(bpi)(H)(**IMes**)(BnNH$_2$), while a decrease of 1.9 kcal/mol was calculated when *ortho*-CH$_3$ groups are included.

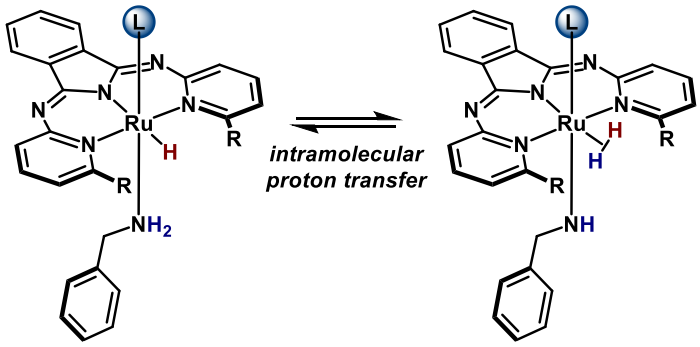

L$_{ax}$	**R**	**ΔG (kcal/mol)**
PPh$_3$	H	26.2
PPh$_3$	CH$_3$	23.6
IMes	H	25.2
IMes	CH$_3$	21.7

Table 6-2. Energy required for intramolecular H$^+$ transfer with PPh$_3$ or IMes as the axial ligand

Because IMes is more donating than PPh_3, we hypothesized that the decrease in energy required for protonation of the Ru–H using IMes may be a result of a stronger (more basic) Ru–H. The increased σ-donation of IMes over PPh_3 is exhibited in the complexes Ru(bMepi)(H)(**L**$_{ax}$)($BnNH_2$) with an increased length of the Ru–NH_2Bn bond (2.292 vs. 2.247 Å), shorter Ru–**L**$_{ax}$ bond length (2.059 vs. 2.320 Å), and a destabilization of the HOMO. However, the Ru–H bond length scarcely increases when PPh_3 (Ru–H = 1.602 Å) is replaced by IMes (Ru–H = 1.606 Å). Moreover, when an NBO analysis was performed on Ru(bMepi)(H)(IMes)($BnNH_2$) and Ru(bMepi)(H)(PPh_3)($BnNH_2$), the polarization coefficients found for each σRu–H NBO revealed equal distributions of Ru and H (Table 6-3). Regardless, the natural charge of each hydride indicates a slightly higher negative charge when **L**$_{ax}$ = IMes (– 0.073) compared to PPh_3 (– 0.056) (Table 6-3).

	L$_{ax}$ = IMes		**L$_{ax}$ = PPh$_3$**	
Atom	**NBO charge**	**polarization coefficient**	**NBO charge**	**polarization coefficient**
Ru	– 0.288	0.7040 (49.7%)	– 0.488	0.7104 (50.5%)
H	– 0.073	0.7102 (50.4%)	– 0.056	0.7038 (49.5%)

Table 6-3. Natural population analysis of Ru(bMepi)(H)(L$_{ax}$)($BnNH_2$) when L$_{ax}$ = IMes or PPh$_3$

The destabilization of the HOMO of Ru–H is an additional factor that may contribute to improved H^+ transfer using the IMes ligand. A large contribution to the thermodynamic stability of Ru(bMepi)(H)(**L**$_{ax}$)($BnNH_2$) is the charge transfer between the donor σRu–H orbital with the acceptor σ*Ru–**L**$_{ax}$ orbital (Figure 6-10). The charge transfer interaction between the donor and acceptor orbitals through the application of second-order perturbation theory gives insight on the origin of thermodynamic stabilization. The stabilization energy (E^2) due to charge transfer is

indicative of the extent of charge delocalization and bonding interaction between the occupied and acceptor orbital. The stabilization energy (E^2) due to donor/acceptor overlap is significantly greater for Ru(bMepi)(H)(**PPh$_3$**)(BnNH$_2$) (34.5 kcal/mol) compared to Ru(bMepi)(H)(**IMes**)(BnNH$_2$) (21.6 kcal/mol). Thus, H^+ transfer will occur more readily when $\mathbf{L_{ax}}$ = IMes due to the decreased stability of the Ru–H species.

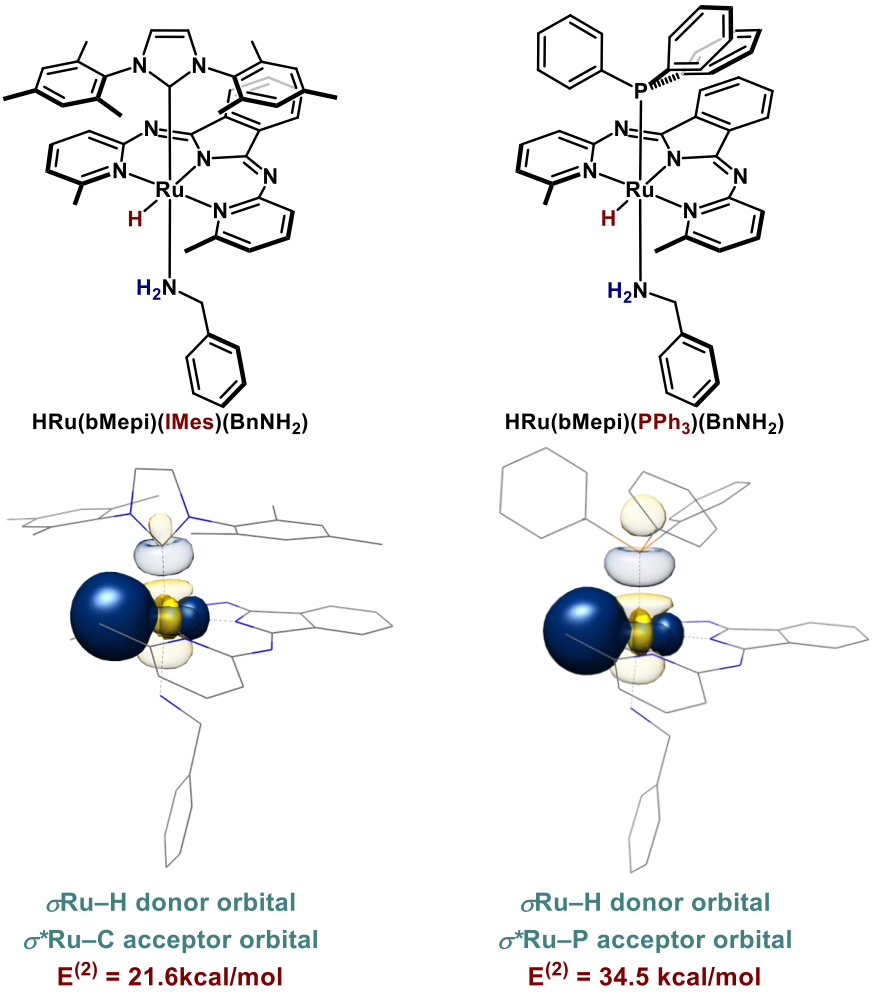

Figure 6-10. Increased donor/acceptor orbital overlap for HRu(bMepi)(PPh$_3$)(BnNH$_2$) (right) compared to HRu(bMepi(IMes)(BnNH$_2$) (left)

6.2 Beyond Dehydrogenation: monodentate cooperative ligands for Ru-bpi type catalysts

The advent of metal-ligand cooperative catalysts significantly transformed the field of hydrogen transfer chemistry. Exceptional catalysts that operate *via* ionic (de)hydrogenations manipulate H_2 to transfer H^+ and H^- equivalents to and from unsaturated and saturated C–C, C–O, and C–N bonds. A common motif in a metal-ligand cooperative system consists of a ligand with Brønsted acid/base functionality (i.e. group Y, Figure 6-11) which can increase catalyst turnover frequency through intramolecular H^+ transfer from the substrate (i.e. group X, Figure 6-11) and/or H_2. Additionally, a hydrogen bond network created between the protic ligand and a polar substrate can stabilize high energy transition states and intermediates. The capacity to facilitate fast H^+ transfer as well as enable access to high energy species are key factors that have contributed to the success of cooperative systems.

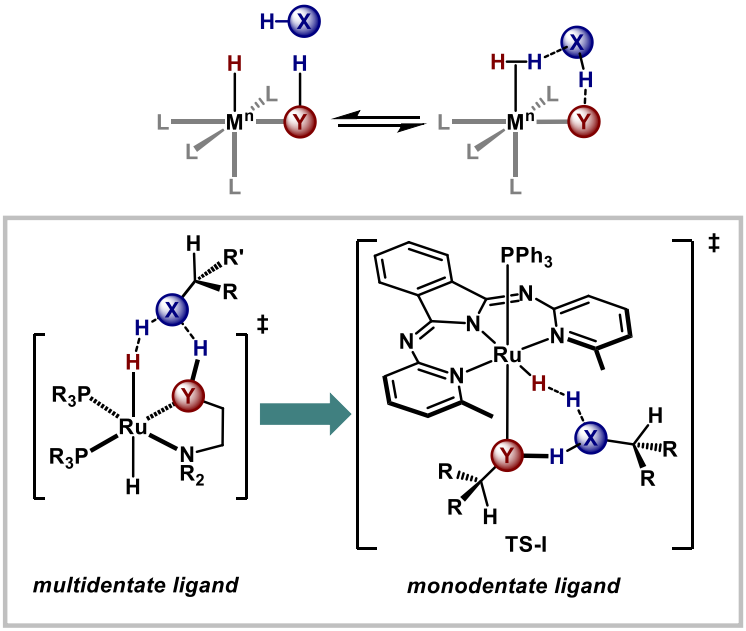

Figure 6-11. General motif for metal-Brønsted acid/base cooperativity

Because multidentate ligands provide stability to transition-metal complexes through the chelation effect, cooperative catalysts are often composed of bidentate bisphosphine or tridentate pincer platforms. However, the synthesis of multidentate scaffolds that incorporate appended acidic –OH, $–NH_2$, or $–CH_2$ groups can be time-consuming and costly. The limitations associated with intricate ligand designs has prevented the quick assessment of reactivity trends for various cooperative groups, and effective ligands are still largely found through trial and error. Moreover, the lack of cooperative ligand parameters is in stark contrast to the well-established trends of innocent primary-sphere ligands, such as the Tolman electronic and steric parameters. A catalyst that can easily incorporate different cooperative groups could provide a wealth of information for improving (de)hydrogenation chemistry across a broad range of substrates.

The ruthenium hydride catalyst, $HRu(bMepi)(PPh_3)_2$, is an excellent dehydrogenation catalyst for alcohols and amines. Mechanistic studies reported by our group revealed an important transition state for the formation of a Ru–(η^2-H_2) intermediate involving a 6-memebered proton shuttle between the $Ru–NH_2$ or Ru–OH group and the *cis*-hydride (Figure 6-11, bottom right). This transition state is fundamentally similar to known cooperative hydrogen transfer catalysts. Noyori-type hydrogenation catalysts facilitate H_2 heterolysis *via* a Ru–(η^2-H_2) and Ru–NH group aided by a 6-memebered proton shuttle formed with exogeneous substrate (Figure 6-11, bottom left). Based on the similarities between TS-I and known cooperative systems, we hypothesized that amine and alcohol additives could accelerate the hydrogenation for a broad range of unsaturated species using H_2. Overcoming TS-I (Figure 6-11, bottom right) for productive hydrogen transfer is dependent on the hydricity (basicity) and pK_a of Ru–H and Ru–(η^2-H_2) intermediates, in addition to the pK_a of Ru–YH (Y = O or NH) and the substrate. A beneficial affect with protic additives

may be observed during hydrogenation if 1) H^+ transfer to the substrate is faster with the amine or alcohol additive compared to H_2, and/or 2) H_2 heterolysis is faster from a Ru–NH or Ru–O species compared to H_2 heterolysis from the substrate.

The hydrogenation of α-phenylcinnamonitrile provided a test case for evaluating the effect of protic additives during hydrogenation with HRu(bMepi)$(PPh_3)_2$. The slow hydrogenation of the C=C bond, in addition to a well-defined Ru-ketenimine resting state prior to hydrogenation (Chapter 5 and Section 5.3) enabled detailed kinetic and spectroscopic analyses with and without protic additives. Because Ru-ketenimine **3a** is the resting state prior to hydrogenation, we hypothesized that H^+ transfer to C2 from a Ru–(η^2-H) species to form the saturated nitrile is a turnover limiting step. Thus, protic additives may influence both the rate of H_2 heterolysis, and additionally serve as an H^+ source for the anionic C2 carbon of the Ru-ketenimine.

The Gibbs free energy required for H_2 heterolysis across Ru–NH or Ru–O to form a hydrido Ru–NH_2 or Ru–OH species was evaluated using Density Functional Theory (DFT) with $BnNH_2$, 4-CF_3-$BnNH_2$, 4-OMe-$BnNH_2$, BnOH, and H_2O (Figure 6-12). All atoms underwent geometry optimization using the rb3lyp functional with the polarizable continuum model (PCM) solvent model for benzene, and 6-31G(d,p) basis set, with the exception of Ru, which was optimized using the SDD basis set. Computations revealed favorable conversion of basic amido ligands to amino ligands when protonated by H_2; formation of Ru–NH_2 from Ru–NH and H_2 was exergonic for the *para*-substituted benzylamines –CF_3 (− 5.05 kcal/mol), –OMe (− 3.81 kcal/mol), and –H (− 6.25 kcal/mol). Contrastingly, formation of Ru–OH complexes from Ru–O and H_2 was endergonic for both benzylalcohol (+ 8.37 kcal/mol) and water (+ 7.13 kcal/mol).

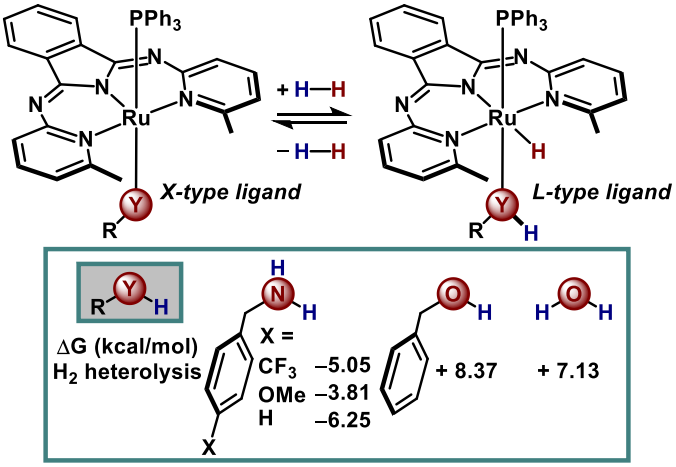

Figure 6-12. Gibbs free energy required for H_2 cleavage or formation between Ru–Y and Ru–YH species.

The Gibbs free energy for the protonation of Ru-ketenimine **3a** by amines, alcohols, and water was also evaluated by DFT (Figure 6-13). When H_2 is the H^+ source, formation of the saturated nitrile and HRu(bMepi)(PPh_3) is thermoneutral ($\Delta G = -0.16$ kcal/mol). Protonation of **3a** to form a saturated nitrile and 5-coordinate Ru–Y species is exergonic for benzylalcohol (− 6.60 kcal/mol) and H_2O (− 10.6 kcal/mol). In contrast, protonation of **3a** by benzylamine derivatives is endergonic by + 1.86, 1.89, and 2.63 kcal/mol for *para*–CF_3, –H, and –OMe, respectively.

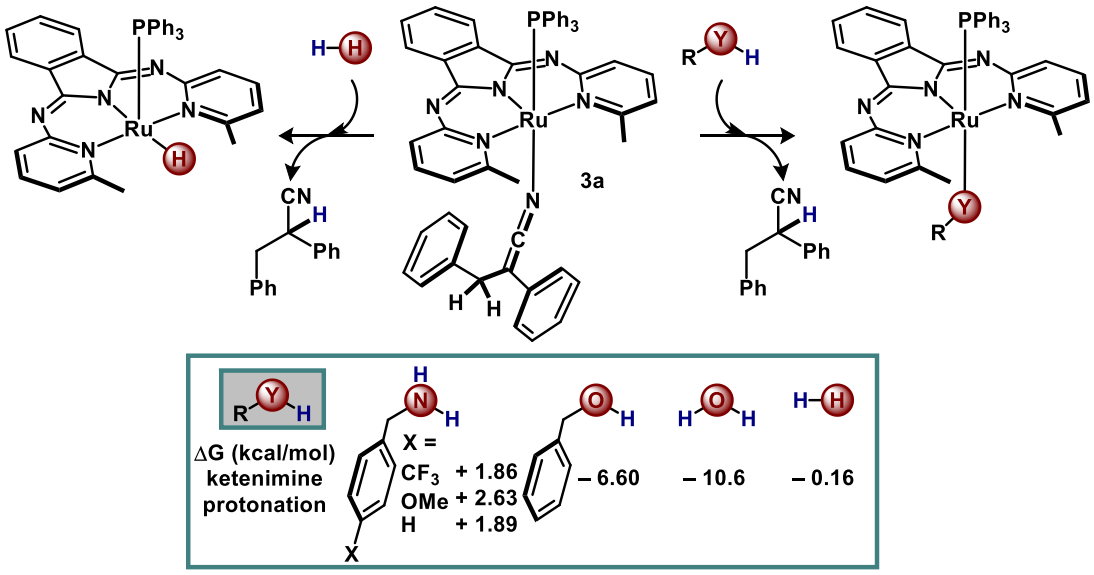

Figure 6-13. Gibbs free energy for the protonation of 3a **using amines, alcohols, water, or H_2. The protonation of** 3a **by H_2O results in the formation of Ru(bMepi)(OH)(PPh_3)·2H_2O**

A competition experiment supports the favorable protonation of **3a** by the more acidic benzylalcohol compared to benzylamine. When an equimolar ratio of benzylamine and benzylalcohol (5 equiv each) were added to **3a**, the Ru-alkoxide species was identified as the major product by ^{31}P NMR spectroscopy after 1 hour at 25 °C (Figure 6-14, top). Moreover, the addition of H_2O (5 equiv) to **3a** at 25 °C results in the Ru–hydroxide complex, Ru(bMepi)(OH)(PPh_3) (Figure 6-14, bottom). The 5-coordinate Ru–hydroxide species has a similar ^{31}P shift to Ru–alkoxide complexes previously isolated by our group (δ~ 40 ppm). However, unique to Ru(bMepi)(OH)(PPh_3) is a hydrogen bonding network formed between the Ru–OH unit, two exogeneous H_2O molecules, and the imine nitrogen atom (N1) within the backbone of the bMepi ligand. The hydrogen bonds between H3b–N1, H3a–O2, and H2a–O1 are 2.253, 1.862, and 1.843 Å, respectively. Computational analysis comparing Ru(bMepi)(OH)(PPh_3) (with no additional H_2O molecules) to Ru(bMepi)(OH)(PPh_3)·2H_2O, shows that two exogeneous water molecules provide 0.31 kcal/mol stabilization to the 5-coordinate complex. All-together, the increased acidity

and/or hydrogen bonding ability provided by more acidic additives enable more facile H^+ transfer to **3a**.

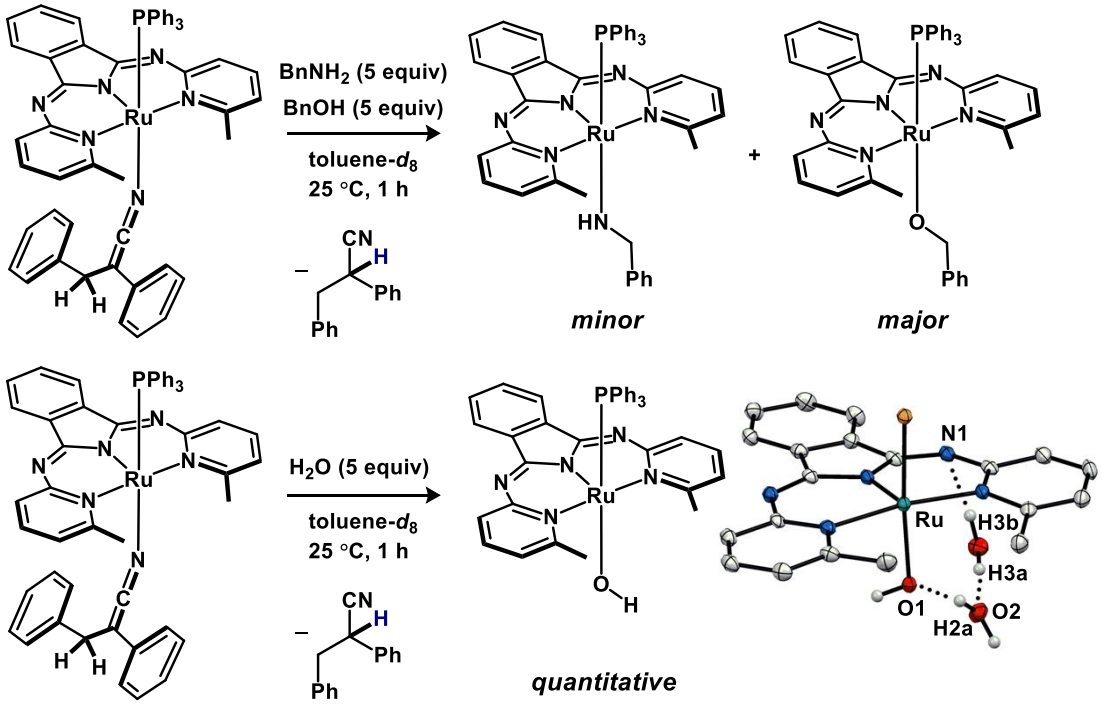

Figure 6-14. Competition experiment between benzylamine and benzylalcohol showing the favored formation of Ru-alkoxide species via protonation of 3a

The Gibbs free energy for the protonation of **3a** by alcohols and amines (Figure 6-13) shows an inverse trend compared to that calculated for H_2 heterolysis (Figure 6-12). However, the effect of protic additives during hydrogenation of α-phenylcinnamonitrile is a composite of both H_2 heterolysis and transfer of H^+ to the substrate (Figure 6-15). The net Gibbs free energy (ΔG_{net}) for each additive is the total energy required for the protonation of **3a** combined with the deprotonation of H_2. Benzylamine provides the most energetically favorable protonation/deprotonation sequence (− 4.36 kcal/mol), while benzylalcohol is overall uphill in energy (+ 1.77 kcal/mol) (Table 6-4).

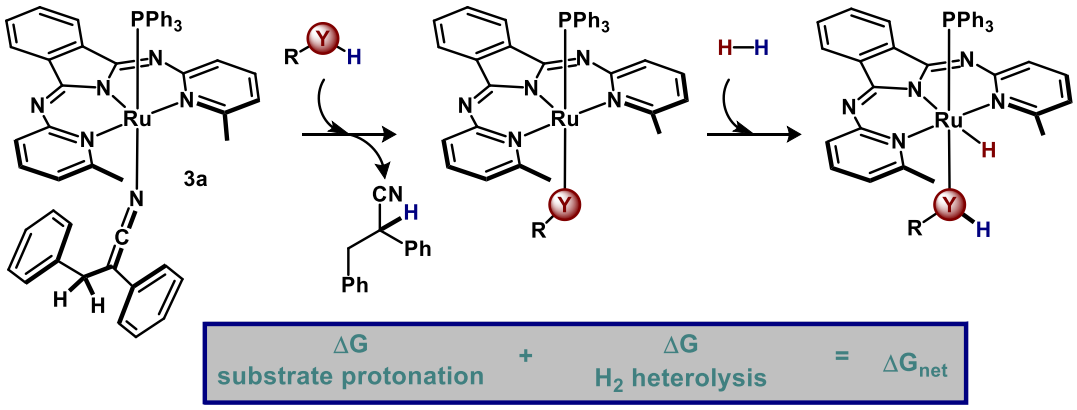

Figure 6-15. The additive affects both the protonation of substrate and deprotonation of Ru–(η^2-H$_2$). The net Gibbs free energy for both events dictate the experimentally observed trend

Additive	Net ΔG_{net} (kcal/mol)
BnNH$_2$	− 4.36
4-CF$_3$-BnNH$_2$	− 3.19
4-OMe-BnNH$_2$	– 1.18
BnOH	+ 1.77
H$_2$O	– 3.47

Table 6-4. Net Gibbs free energy (ΔG_{net}) for H^+ transfer to substrate and Ru–H

Based on the net downhill thermodynamics of the benzylamine additives, we hypothesized benzylamine derivatives would promote the hydrogenation of α-phenylcinnamonitrile. When α-phenylcinnamonitrile was subjected to 20 psi H_2 at 80 °C for 1 h in the presence of HRu(bMepi)(PPh$_3$)$_2$ (1 mol %), we observed only 15% GC yield of the saturated nitrile, corresponding to a turnover frequency (TOF) of 0.42(8) x 10^{-2} s^{-1} (entry 1, Table 6-5). When benzylamine and the derivatives with *para*-F and *para*-OMe groups (5 mol %) were added to the hydrogenation reaction, we observed an increase in TOF ranging from 1.42(7) x 10^{-2} s^{-1} to 1.62(6) x 10^{-2} s^{-1} (entries 2-4, Table 6-5). These results support a rate-limiting H_2 heterolysis step which

is promoted by the $BnNH_2$ additive. Work is ongoing in our group to establish the TOF values in the presence of benzylalcohol and water. Additionally, we anticipate that these studies will provide general trends of simple amine and alcohol additives for the hydrogenation of a broad range of unsaturated substrates.

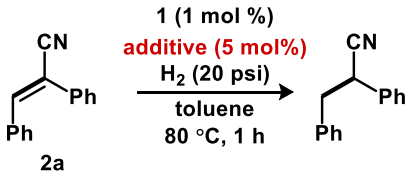

Entry	Additive	TOF (x 10^{-2} s^{-1})
1	None	0.42(8)
2	$BnNH_2$	1.44(6)
3	4-F-$BnNH_2$	1.62(6)
4	4-OMe-$BnNH_2$	1.42(7)

Table 6-5. Effect of benzylamine additives on TOF during the hydrogenation of α-phenylcinnamonitrile

6.3 Outlook for Hydrogen Transfer Catalysis with Ru-bpi type catalysts

The work outlined in this dissertation provides detailed analyses of Ru-bpi type complexes for ionic hydrogen transfer reactions. (De)hydrogenation occurs *via* reversible H^+/H^- transfer between the organic substrates and Ru–H and Ru–(η^2-H_2) intermediates. Two catalyst design principles are crucial for future hydrogen transfer catalysts with the bpi ligand scaffold: 1) the electronic parameters that influence the kinetic barriers toward transfer of H^+ and/or H^- between catalytic intermediates; and 2) the steric profile needed to stabilize coordinatively unsaturated Ru intermediates. This chapter outlined our efforts toward catalyst (re)design, and additionally provided new directions for hydrogen transfer with Ru-bpi type catalysts.

Future catalyst design for dehydrogenation chemistry should target increasing the hydricity and/or increasing the pK_a of Ru–H and Ru–(η^2-H_2) intermediates. However, as a prediction tool for HT with amines, hydricity should only be used to predict reactivity for complexes that maintain the same overall charge. Hydricity measurements characterize the ability to formally remove H^-, and thus may be more applicable to outer-sphere type mechanisms, rather than the inner-sphere mechanisms described in this work. The relevance of charge and hydricity becomes negligible when *intramolecular* H^+/H^- transfer occurs, such as that found for amine and alcohol dehydrogenation. Amine dehydrogenation by **1** occurs only when the $-NH_2$ group is coordinated *cis* to Ru–H. Following H^+ transfer to form a Ru–(η^2-H_2), an amido group remains coordinated to Ru. The overall charge of the complex does not change, and contributions from the *trans* σ-donor become significant.

In addition to targeting the parameters of Ru–H and Ru–(η^2-H_2) intermediates, catalyst (re)design may also target the stabilization of coordinatively unsaturated species. The addition of steric bulk in the equatorial plane and near the open coordination site promotes octahedral geometry. Incorporation bulky methyl or isopropyl groups into the bpi scaffold provides approximately 10 kcal/mol stabilization to coordinatively unsaturated intermediates, such as the Ru-amido and Ru-alkoxide species previously identified during the dehydrogenation of primary amines and alcohols.

An alternative route to changing the pincer platform to improve H^+ transfer involves replacing the axial PPh_3 ligand. IMes replaces PPh_3 from ClRu(bRpi)(PPh_3) pre-catalysts and is an underexplored supporting ligand for Ru-bpi type complexes. Computational analysis suggests that the more donating ligand decreases the thermodynamic energy required for H^+ to Ru–H in the case

of amine substrates. Additionally, monodentate NHC ligands may provide a route for producing chiral Ru-bpi analogs (Figure 6-16), however a general reproducible route is needed to incorporate axial NHC ligands beyond IMes.

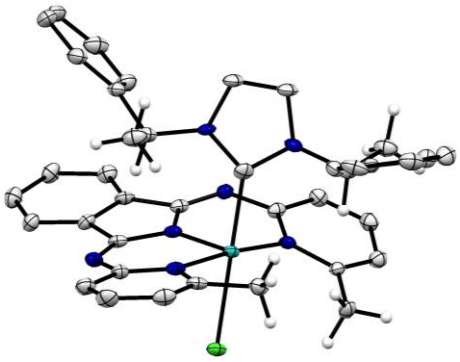

Figure 6-16. ClRu(bMepi) with a monodentate chiral NHC ligand in place of PPh_3

Finally, while hydrogenation chemistry may also be improved using analogous ligand modification strategies for modifying the pK_a of Ru–(η^2-H_2) species, utilizing protic additives to co-catalyze hydrogenations is an intriguing approach that warrants further exploration. Employing catalytic amounts of simple additives such as benzylamine, benzylalcohol, or even H_2O avoids the high cost and time required for complex ligand synthesis. We have currently explored the role of amine additives for chemoselective C=C hydrogenation of α,β-unsaturated nitriles, which increase the rate of H_2 heterolysis and thus act as co-catalysts with Ru(bMepi)(PPh_3). The combined Gibbs free energy required for H^+ transfer to substrate and from a Ru–(η^2-H_2) intermediate can be used to predict the effect of the additive. This strategy will be highly attractive if applicable to a broader range of unsaturated substrates.